ROYAL INSTITUTE OF TECHNOLOGY

Imaging 2010

Book of abstracts

Oral presentations

How X-ray optics gave us another image of the universe

Stephen S. Murray – Johns Hopkins University/Harvard-Smithsonian Center for Astrophysics

At low energies (below about 10 keV), X-ray can be reflected off of surfaces if they impinge at a shallow grazing angle. This property allows the construction of X-ray optics including X-ray telescopes that can focus incident X-ray radiation from celestial objects onto an appropriate imaging device to form images. Using X-ray telescopes in space, astronomers have been able to study the Universe in the 0.1 – 10 keV band revealing many new aspects of the cosmos. I will briefly describe a particular type of X-ray telescope, and then present some highlights from the past decade of high resolution X-ray imaging from space taken from NASA's Chandra X-ray Observatory and ESA's XMM-Newton X-ray Observatory, both of which are still in operation today. With the advent of these fairly large facilities, X-ray studies of the Universe have become an important element of modern multiwavelength astronomy. I will end my talk discussing some plans for the next generation of X-ray observatories and their current status.

Challenges in medical imaging, today and in the future

P. Aspelin

One of the important challenges in health care is to make an early diagnosis in order to implement an early treatment that may positively change the outcome of disease. Medical imaging is one of the most important tools in early diagnosis of diseases. Therefore the importance of imaging is increasing. The technical development has led to that today medical imaging is not only monitoring anatomy and function but also molecular and metabolic processes. The image is also increasingly important in image guided interventions. This has brought to us that imaging is part of prevention, diagnosis, treatment, monitoring of treatment and understanding of the pathogenesis of diseases.

The challenge today is to use and in the future to develop methods that both are cost effective, harmless, and results in a change in patient outcome. The tools are exploding in number and it is important that they are used with great care so that the sensitivity and specificity of the method is considered when using it. The technological advances are fast and promising, but they have to be proven in clinical practice to be balanced with the possible benefits for the patients.

So the challenge is not only to get better and more precise imaging methods but to perform clinical outcome studies where the different tools, advantages and disadvantages can be measured. Over-information and false positive results are almost equally as dangerous as false negative. The technical development in imaging is, however, one of the most promising tools in making a change in health care today and in the future.

Inverse Geometry CT

Norbert J. Pelc
Stanford University

Computed Tomography (CT) has had an enormous impact on medicine since its introduction, and many physicians consider CT (along with MRI) to be the most important recent technological innovation in medicine. Further technical improvements can be expected to have important clinical benefit. All commercial clinical CT systems use the so-called "third generation" system design comprising a single x-ray source that generates a fan or cone beam and a large detector that measures the intensity transmitted through the object. While this system design has been tremendously successful, it has some limitations. We are exploring an alternative approach that we call Inverse Geometry CT (IGCT). As the name implies, the geometry is inverted and uses a distributed array of many x-ray sources and a smaller (compared to a third generation system) array of x-ray detectors. IGCT promises to deliver wide volumetric coverage in a single rapid scan with no "cone-beam" artifacts, high spatial and temporal resolution, improved dose efficiency, and reduced radiation dose to the patient. Our results thus far provide evidence that these goals can be achieved. In a collaborative project between Stanford University and GE Global Research Center funded by the US National Institutes of Health and GE, we are building an experimental IGCT system.

In general, the noise in a CT image varies across the image and for each region depends on the detected x-ray intensity for all measurements that went through that region. Ideally, the distribution of incident radiation should be designed so as to guarantee sufficient image quality while minimizing the radiation dose to the patient. Clinical CT systems use "bowtie" filters to control the intensity across the fan beam and also modulate the x-ray intensity as a function of angle. However, since these systems illuminate the entire object being imaged all at once and the bowtie filter is fixed for the entire scan, the degree to which they can customize the x-ray field is limited. By comparison, the irradiation field of an IGCT system is composed of many smaller beams, each produced by one of the sources. The relative intensity of the sources can be adaptively controlled and also varied as a function of view angle to customize the radiation field to the specific imaging situation. This "virtual bowtie" technique can be used to ensure that the minimum amount of radiation is used for a particular study. Computer simulations predict that very significant dose reduction can be achieved while maintaining image quality. Other benefits of the IGCT approach include a more uniform spatial resolution across the imaged field of view and, if the source array is distributed in the axial direction, the ability to produce 3D images with a wide axial field of view in a single rotation without "cone beam" artifacts.

Arguably, the most critical and unusual component in an IGCT system is the source array. We have investigated two approaches, one using a scanned anode x-ray source and another composed of multiple discrete x-ray emitters. The system we are currently constructing will have 32 addressable x-ray sources and a 64x256 array of x-ray detectors. The components have been integrated into a rotating gantry and we have demonstrated the ability for the system to rotate in 1 sec. Initial CT images of small phantoms have been produced.

Seeing Dark Energy

A. Riess

Cosmologists are fortunate to have access to new, powerful and complex telescopes to image the Cosmos as never before. Most recently NASA astronauts have refurbished the Hubble Space Telescope with new instrumentation to allow astrophysicists to see the birth of galaxies shortly after the Big Bang and the exploding stars which are used to track the expansion history of the Universe. Yet the subjects of our greatest curiosity, dark matter and dark energy cannot be directly seen even with these incredible telescopes. Rather their existence and properties must be inferred by their gravitational influence on the luminous material we can see. I will review how cosmologists haven recently "seen" the presence of dark energy through the accelerating expansion of the Universe and how we continue to try and unravel the deep mystery of its existence.

Recent developments in imaging system assessment methodology

Dev P. Chakraborty, University of Pittsburgh, USA, dpc10ster@gmail.com

Search is a ubiquitous task in everyday life. There is interest, especially at this conference, in optimizing specialized search tasks such as finding targets in a background of false targets, e.g., a face in a crowd, contraband in luggage, cancer in the breast, enemy in the battle field, etc., while not finding false targets. There are costs associated with missing targets and finding false targets and the two types of errors are interrelated and need to be minimized. This work addresses assessing performance in a search task of a new imaging modality vs. an existing modality. The new modality could be a novel detector or a new screening device for airport security, etc. The observer (the "searcher") could be a radiologist or a computerized algorithm. The observer finds suspicious regions, some of which are marked, and for each mark a rating or confidence-level that the marked region is actually a target, is available. A mark close to a real target is classified as true target localization and otherwise it is classified as false target localization. This type of data describes the free-response receiver operating characteristic (FROC) paradigm.

While the FROC paradigm is clearly relevant to several real-life applications until recently a satisfactory method for analyzing FROC data did not exist (analysis software is now available). The receiver operating characteristic (ROC) paradigm is currently widely used to assess imaging modalities. In ROC the observer assigns a single rating to the whole image. The location(s) of the region(s) that influenced the rating is not recorded. Because it ignores location information one may suspect that ROC analysis is less precise than FROC and more prone to missing a true modality improvement. Simulation testing and clinical FROC/ROC studies have confirmed this expectation. If a true modality improvement is missed the designer may abandon a promising algorithm design approach and progress in the field is delayed. Additionally, it is possible that the suspicious region that influenced the rating was not the true target. ROC analysis ignores this possibility which could have serious repercussions: an enemy position is missed and an air strike is called at an incorrect location causing collateral damage. FROC analysis penalizes a modality that is prone to such mistakes.

Models of observer performance can yield insight into the observer's perception process which could be used to optimize performance. A number of models for ROC data have been developed but their parameters do not have a clear correspondence to search performance. A recently proposed search-model for FROC data has parameters corresponding to the ability to find targets, the ability to avoid finding false targets, and the ability to assign higher ratings to true targets than to false targets. For example if the observer is finding too many false-targets more training with target absent images is indicated. If the observer is missing targets more training with target containing images is indicated. If the observer is finding targets but fails to report them, training aimed at recognizing features of true targets that distinguish them from false targets is indicated. Estimation of the search model parameters will be illustrated.

The subjectivity of the human observer, the cost and time needed to conduct such studies sometimes discourages scientists/engineers from performing observer performance studies. Fourier measurements (MTF, SNR, DQE, etc.) are often used to optimize imaging hardware. The major advantages of observer performance measurements are: they include the task for which the imaging system was designed; they include the entire imaging chain: detector, image processing, image display and, most importantly, the observer who makes the critical final decision (e.g., patient has cancer); and the evaluation is performed on real-life (not synthetic) images. Fourier measurements are usually conducted on uniform background images with unrealistic targets. They allow ready optimization of detector performance but the effect of the improvement on overall performance is not known (the weak-link could be elsewhere). After the detector and other components have been optimized by conventional methods an observer study should be conducted to assess net improvement.

In summary, ROC measures classification performance between target-present and target-absent images. FROC measures search performance: finding and reporting targets at the correct locations while minimizing the number of false target reports. Significant recent advances in FROC methodology and search task modeling may benefit imaging scientists and engineers in various fields.

Computer-aided detection and diagnosis for breast imaging

R. Nishikawa

Screening mammography has been proven to be effective in reducing breast cancer mortality. However, there are limitations to the ability of screening mammography to detect breast cancer at a low false positive rate. Computer-aided detection (CADe) and computer-aided diagnosis (CADx) are being developed to improve radiologists' accuracy in screening mammography and in diagnostic breast imaging. There are a number of technical, methodological, and clinical barriers to the widespread implementation of CADe and CADx. The clinical results so far appear on the surface as ambiguous. However, careful analysis reveals that CADe can increase radiologists' sensitivity by approximately 10% with a minimal decrease in positive predictive value. The current paradigm for CADe is a second reader to help radiologists avoid overlooking a cancer, but the possibility for using CADe as a first reader seems technologically possible in the next few years. I will provide an overview of the development of CADe and CADx, their current performance levels, and how they might be used in the future.

The MAGIC-5 CAD System for Lung Nodule Detection in Thorax CT Images

Giorgio De Nunzio[1*]

[1] Dept of Materials Science, University of Salento, and INFN (Istituto Nazionale di Fisica Nucleare) (Lecce, Italy)
* on behalf of the MAGIC5 Collaboration

Lung cancer is one of the main causes of death among both men and women. The 5-year survival rate is strictly related to the stage in which the disease is diagnosed: early detection and subsequent resection of the lung cancer can significantly improve the prognosis. The development of 'computer-assisted detection' (CAD) techniques to automatically locate nodules can help in managing the large number of CT scans coming from screening programs, and improve diagnosis in the usual clinical practice.

This work is part of the development of a CAD system for the detection of pulmonary nodules in chest CT scans, carried out in the framework of the "Medical Applications on a Grid Infrastructure Connection" (MAGIC-5) Collaboration, an experiment of the Italian INFN ("Istituto Nazionale di Fisica Nucleare").

Different kinds of tumor nodules may be found in the lung parenchyma: shape, size, position may vary considerably, so that no unique detection approach can exist. In particular, dense pulmonary nodules may be found in contact with the pleura, because either the nodule grew near, or originated from, the pleural sheet. A nodule with these features can easily be excluded from the segmented lung volume due to its high density, outside the range that defines the parenchyma tissue. Segmentation algorithms that do not explicitly provide a correct treatment of such structures fail in returning correct lung borders, with all the nodules included: in this case, juxta-pleural nodules appear as small border concavities of quite strong curvature.

In this work we describe the overall structure of the CAD system developed by the MAGIC-5 Collaboration, describing the details of the segmentation procedure, and various approaches to internal nodule searching.
We then focus on the problem of efficiently locating juxta-pleural nodules: we compare the success of several concavity-patching methods in: (1) preserving juxta-pleural nodules within the border of the segmented lung, (2) minimizing the amount of extra-pulmonary tissue erroneously included in the lung border, which may give false positive findings, (3) discriminating juxta-pleural nodules from other structures.

Imaging using the Medipix chips family

Michael Campbell on behalf of the Medipix2 and Medipix3 Collaborations.

The recent members of the Medipix family of single photon counting chips each contain arrays of 256 x 256 pixels at a pitch of 55um. The chips have the flexibility to be combined with different semiconductor sensors or with other sensitive devices based on charge amplification. This paper reviews the imaging performance of the chips in different applications.

The Medipix2 chip contains 2 thresholds per pixel and has been used extensively in a large variety of applications. The successor Timepix chip has only one threshold per pixel but is capable of operating at a lower minimum detectable signal. Moreover, the each pixel can be programmed to record either the total number of hits (like Medipix2), or Arrival Time, or Time over Threshold. This opens up new areas by providing either time resolution at the 10ns level or improved spatial resolution based on centroiding using the Time over Threshold information. Imaging applications extend over a significant part of the electromagnetic spectrum from visible light to gamma rays but also include charged particles and neutrons. Examples of each will be demonstrated.

With the Medipix3 chip inter-pixel communication is implemented on an event by event level at the front-end. This permits charge summing to be performed prior to the discrimination process and the pixel hit allocation. 2 thresholds and counters are available per pixel. There is also the option of connecting one front end in 2 in both x and y permitting single large pixels to use all of the 8 discriminators and counters available. First results from chips connected to Si sensors will be shown.

Title

NEMA NU1-2001 performance tests of four Philips Brightview cameras.

Author

A. Seret, Experimental Medical Imaging, Université de Liège, Liège, Belgium.

Abstract

Introduction. The Brightview is the latest generation dual-head SPECT and SPECT-CT camera from Philips. It is equipped with two large field of view digital Anger detectors for γ-rays and with a flat panel detector for X-rays.
Methods. All primary and some secondary NEMA NU1-2001 performance tests were conducted on four (two SPECT and two SPECT-CT) recently installed Brightview systems mainly with ^{99m}Tc and the low energy high resolution (LEHR) collimators. The intrinsic uniformity for four other isotopes (^{67}Ga, ^{123}I, ^{131}I, ^{111}In) and the system uniformity with the medium (ME) and high (HE) energy collimators was also measured on two (^{131}I, HE) or three cameras. The NEMA procedures for acquiring and processing the data were carefully followed except for the energy window width that was set at 20% as recommended by the manufacturer. Only mean value ± standard deviation obtained in the UFOV are reported here but all values will be presented.
Results. For ^{99m}Tc, the following values were obtained for intrinsic tests: energy FWHM = 9.22±0.17 %, spatial FWHM = 3.16±0.09 mm, absolute (differential) linearity = 0.27±0.09 (0.05±0.09) mm, integral (differential) uniformity = 2.25±0.47 (1.48±0.13) %. The integral (differential) intrinsic uniformity was 3.07±0.38 (1.68±0.19) % for ^{67}Ga, 2.49±0.36 (1.66±0.29) % for ^{123}I, 3.43±0.90 (2.29±0.64) % for ^{131}I, 3.33±0.61 (1.95±0.23) % for ^{111}In. The multiple window spatial registration was 0.55±0.19 mm with ^{67}Ga. With ^{99m}Tc and LEHR, the mean sensitivity was equal to 73.49±1.48 cp/MBq/s and the mean FWHM values (after Astonish processing) for system resolution without scatter were as follows. Planar: 7.22±0.11 (4.98±0.07) mm; whole body: 7.03±0.16 (4.81±0.10) mm perpendicular and 7.58±0.05 (5.19±0.11) mm parallel to the bed motion; SPECT: 9.76±0.06 (4.00±0.28) mm central transaxial, 10.40±0.34 mm (4.43±0.13) mm central axial, 9.76±0.05 (3.74±0.26) mm peripheral radial, 8.12±0.52 (3.38±0.23) mm peripheral tangential and 9.26±0.49 (3.93±0.65) mm peripheral axial. With ^{99m}Tc, system integral (differential) uniformity were: 3.66±0.36 (1.91±0.33) % for LEHR collimator, 4.14±0.74 (1.92±0.29) % for ME collimator and 3.77±0.75 (1.79±0.14) % for HE collimator. System alignment could not be processed according to NEMA due to a file writing problem when performing 360° rotation per head. However, the COR test recommended by Philips was performed for both head configurations (180° and 90°) and was found satisfactory. Moreover, the spatial co-registration between SPECT and CT images was also checked using the Philips procedure. The mean average distance was (1.34±0.57) mm and the maximum difference distance was (1.93±0.58) mm. A one year follow-up of the intrinsic uniformity and of the COR test will also be presented.
Conclusions. The measured parameters were almost identical for all tested systems and they all were within the manufacturer specifications.

Study of the stability of CT-Based Positron Range Correction in High Resolution 3D PET Imaging

J. Cal-González[1], J. L. Herraiz[1], S. España[2], M. Desco[3], J.J Vaquero[3], J. M. Udías[1]

[1] Grupo de Física Nuclear, Dpto. Física Atómica, Molecular Nuclear, UCM, Madrid, Spain

[2] Department of Radiation Oncology, Massachusetts General Hospital and Harvard Medical School, Boston, MA, USA.

[3] Unidad de Medicina y Cirugía Experimental, Hospital GU "Gregorio Marañón", Madrid, Spain

Positron range limits the spatial resolution of PET images [1]. It has a different effect for different isotopes and positron propagation materials. Therefore it is important to consider it during image reconstruction, in order to obtain optimal image quality.

Positron range distributions for most common isotopes used in PET in different materials, were computed using Monte Carlo simulations with PeneloPET [2]. PeneloPET models positron trajectories and computes the spatial distribution of annihilation coordinates with respect to positron emission point. These range profiles were introduced into the 3D-OSEM image reconstruction software FIRST [3], and employed to blur the image either in the forward projection or in the forward and backward projection. The blurring introduced takes into account each material in which the positron is propagated. Information on these materials can be obtained for instance from a segmentation of a CT image.

Acquisitions of an Image Quality phantom [4] filled with different isotopes (^{68}Ga or ^{18}F) have been simulated for the ARGUS small animal PET scanner [5] and resolution and noise properties of the images reconstructed, with and without CT-based material specific information positron range modelling, have been compared. Results using high positron energy isotopes show significant improvement in the spatial resolution of the reconstructed images, compared with reconstructions without positron range modelling [6]. Also the effect of the use of different shapes of positron range profile in the quality of the reconstructed images with positron range correction was studied.

Introducing positron blurring in both the forward and backward projection steps was compared to using it only during forward projection. The results obtained show that positron blurring in the backward projection smoothes out the reconstructed image, delaying the appearance of high resolution details to further image updates, but otherwise looks very similar in terms of resolution versus noise.

SUPPORTING DATA

Figure 1 shows the Image Quality Phantom filled with ^{68}Ga, with and without positron range corrections in the reconstruction algorithm.

Figure 2 shows a comparison between results obtained in a test case where a reconstruction including positron blurring in both forward and backward projection operations, with results obtained when range it is only included during forward projection. Images were reconstructed using 20 iterations of 10 subsets and results of each iteration are compared, using the resolution – noise plot, obtained for the IQ phantom, filled with ^{68}Ga isotope. We can see that the use of the positron blurring in the backprojection smoothes out the reconstructed image, making the iterative algorithm to converge more slowly, but otherwise yielding similar results, only that for different number of image updates.

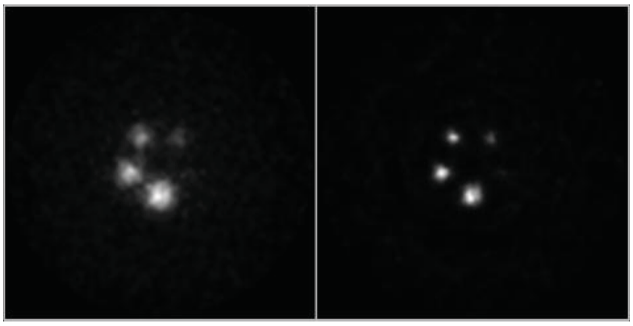

Figure 1: IQ phantom filled with ^{68}Ga reconstructed with 3D OSEM with (Right) and without (Left) range corrections. *In both cases, 10% noise images are compared*

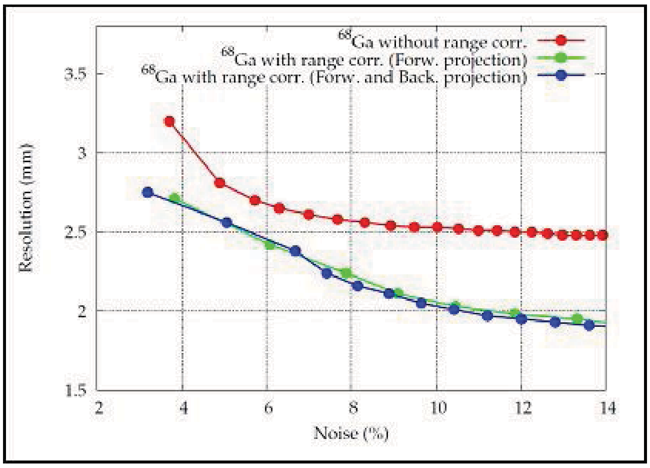

Figure 2: Resolution-noise curves obtained for the 3 mm rod IQ phantom filled with ^{68}Ga and reconstructed using 3D-OSEM with and without range corrections. Each point corresponds to 10 updates of the image.

REFERENCES

[1] C.S. Levin and E.J. Hoffman, Phys. Med. Biol., 44:781-99, 1999.

[2] S. España et al., Phy Med Biol, 54, 1723-42.

[3] J. L. Herraiz et al., IEEE Trans. Nucl. Sci., 2003, vol. 50, pp. 398-404.

[4] NEMA N-2008 Performance Measurements for Small Animal Positron Emission Tomographs.

[5] W. Yuchuan et al., J. Nucl. Med. Vol. 47 No.11 1891-1900

[6] J. Cal-Gonzalez et al., IEEE Nucl. Sci. Symposium Conference Record, 2009.

Design of a high resolution scintillator based SPECT detector (SPECTatress)

K. Deprez, S. Vandenberghe, S. Staelens

Medical Signal and Image Processing group, Ghent University-IBBT, Ghent, Belgium

INTRODUCTION:

In traditional clinical SPECT systems the system resolution is mainly determined by the collimator (in most cases parallel hole collimators are being used) so the detector intrinsic spatial resolution is of minor importance.

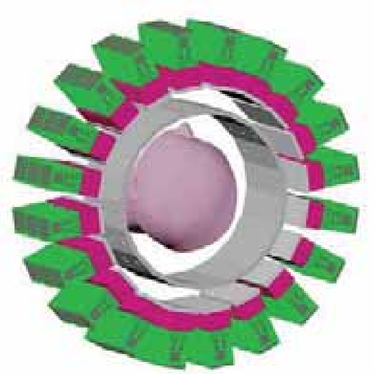

Figure 1: Multi-pinhole brain SPECT scanner with multiple high resolution gamma detector modules. Each pinhole has its own dedicated detector module.

Multi-pinhole collimators for organ-specific and small-animal SPECT systems however benefit more from a better spatial intrinsic detector resolution. Indeed, a better intrinsic detector resolution requires less magnification and results in a system that makes it possible to use more pinholes (resulting in an increased sensitivity). Such a system is drawn in figure 1.

The aim of this project is to build a detector with a better intrinsic spatial resolution and with depth-of-interaction capabilities by optimizing the detector components and by optimizing the positioning algorithms while maintaining an acceptable component cost.

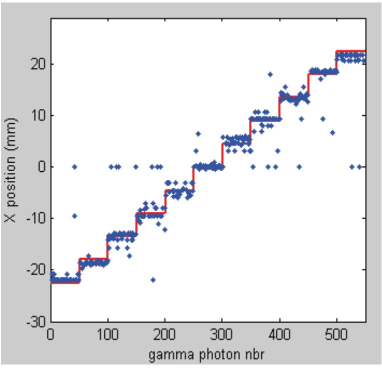

Figure 2: Gate simulation of the scintillator that is scanned from left to right by a beam source in 11 intervals. (red=beam source position / blue=detected position using Anger logic)

The construction of the detector is optimized by using optical Gate simulations (figure 2). The simulations enabled us to derive several design guidelines for the scintillator and the light sensor to optimize the spatial and energy resolution of the detector. These guidelines made us select a 5mm thick NaI(Tl) scintillator (with rough finish and reflecting sides) and a Hamamatsu H8500 PSPMT.

This detector will be used to study several positioning algorithms so all anode data should be available for further processing. All the anodes of the PSPMT have their own dedicated amplifier and ADC. The amplifier is an op-amp based circuit which limits the bandwidth of the PMT pulses and which has a differential output. Multi-channel high-speed ADCs with serial LVDS outputs have been selected to minimize the size of the PCB and to avoid signal-integrity problems. These ADCs are connected to an FPGA, which takes care of the charge integration and sends all the anode data to a PC using a 1Gbit Ethernet link.

Figure 3: SPECTatress detector module

At present we have mounted the scintillator on the PSPMT and are currently optimizing the readout electronics (figure 3).

ProSPECTus: Next Generation Single Photon Emission Computed Tomography

LJ Harkness[1], AJ Boston[1], HC Boston[1], JR Cresswell[1], DS Judson[1], PJ Nolan[1], JA Sampson[1], DP Scraggs[1], I Burrows[2], K Cheung[2], J Groves[2], J Headspith[2], IH Lazarus[2], J Simpson[2], WE Bimson[3], GJ Kemp[3], and D Gould[4]

1. Department of Physics, The University of Liverpool, UK
2. STFC Daresbury Laboratory, UK
3. MARIARC, The University of Liverpool, UK
4. Royal Liverpool University Hospital, Liverpool, UK

Single Photon Emission Computed Tomography (SPECT) [1] is an established imaging technique used in the diagnosis and monitoring of cancer and neurological conditions. However, the design of current systems results in only a very small fraction of the patient dose being used to generate an image. The ProSPECTus project aims to demonstrate a highly sensitive alternative to traditional SPECT systems by replacing the gamma camera with a Compton camera [2]. The main benefits of this technology include improved image quality, shorter data acquisition times and the potential for lower patient doses. Geant4 [3] simulated data has shown the potential increase in sensitivity is up to 100 times that of current systems [4]. The prototype system has also been designed to operate simultaneously with a standard clinical Magnetic Resonance Imaging (MRI) scanner in collaboration with the Magnetic Resonance and Image Analysis Research Centre (MARIARC).

Conventional SPECT systems utilise a gamma camera to locate the distribution of a radioactive tracer which has been administered to a patient to study specifically targeted biological processes. The gamma camera is typically composed of NaI scintillation detectors coupled to a mechanical collimation device. The purpose of the collimator is to allow the distribution of the radiation to be inferred and is a necessary component in the current design. However, the collimator inherently results in an undesirable compromise between efficiency and image resolution. The ProSPECTus system aims to alleviate this compromise through optimising the arrangement of two semiconductor detectors in Compton camera configuration, removing the need for mechanical collimation. A Compton camera provides information on the location of a radiation source through detecting at least two interactions from each incident gamma ray. The system will have excellent solid angle coverage, resulting in a vast increase in the fraction of radiation which is used to generate an image.

Validated simulations have been used to design the optimum Compton camera configuration for a gamma ray energy of 141keV, emitted from the most commonly used SPECT radioisotope, ^{99m}Tc. Determining the optimum configuration required an assessment of imaging efficiency and resolution, whilst considering the performance of the system in the vicinity of an MRI scanner [5]. The chosen configuration of a Si(Li) scatter detector coupled to a HPGe absorber detector is currently being built. An assessment of imaging performance, together with initial results of overall performance of the ProSPECTus system, will be presented.

References

[1] Y. Du et al., Med. Phys. 2007: 34 (9): 3530
[2] RW Todd, JM Nightingale, DB Everett Nature, 1974: 251: 132-134
[3] S. Agostinelli, et al., NIM A 2003: 506: 250-303
[4] L. Harkness, et al., NIM A 2009: 604: 351-354
[5] L. Harkness, et al., NIM A: to be submitted

Single Photon Emission Imaging With A Multi-Layer Detector (PEDRO)

M.R. Dimmock, J.M.C. Brown, C. Hall, R. Lewis and J.E. Gillam

In Single Photon Emission Imaging (SPEI), sensitivity is often sacrificed in order to increase the spatial resolution of the reconstructed image. Multiplexing [1] in the measurement domain can relax the sensitivity-resolution relationship at the expense of a further reconstructive step. Electronic collimation, such as is used in a Compton camera [2], offers increased sensitivity, however the resolution is limited by the detector performance and Doppler broadening. In order to address the deficiencies in both mechanical and electronic collimation systems, a hybrid imaging device has been proposed - The Pixelated Emission Detector for RadioisOtopes (PEDRO) [3].

The experimental PEDRO prototype, currently under development, consists of a mechanically collimating device in front of a stack of Silicon (Si) detectors and a Cadmium Telluride (CdTe) detector. The aperture array has been designed to accommodate pinholes, slats or open-areas, as the optimal mechanical modulation for hybrid imaging between the above spectral extents is as yet uncertain. A Geant4 simulation of this setup has been developed to fully describe the detector, collimator, RF housing and emission source and optimize this geometry over a broad range of photon emission energies (30 keV $\leq E_\gamma \leq$ 511 keV).

There are many advantages to a hybrid SPEI system including Region of Interest (RoI) selection and multitracer studies. In this work we present the findings from PEDRO where the collimator incorporates three pinholes spaced at the corners of an equilateral triangle with 10.0 mm spacing. The multi-layer structure of the Compton camera allows for different magnification projections of the collimator to be acquired simultaneously, each with different image resolutions and levels of multiplexing. Data were simulated for a single projection angle and processed with consideration of Compton information for ordering when multiple interactions were measured. Maximum Likelihood Expectation Maximization [4] reconstructions were performed for two test cases. For the first simulation, 140keV photons were emitted from a triple intensity source (1:20:50) shown in *Figure 1a*. *Figures 1b* and *1c* show the reconstructed source, 60.0 mm from the collimator, after 1 and 10 iterations, respectively. For the second simulation, a two layer version of the same source was studied. The two planes had relative rotations of 90^o and were separated by 30.0 mm in depth. *Figures 1d* and *1e* show the reconstructed slices through the volume that correspond to locations at 45.0 mm and 75.0 mm and are also those with the maximum intensity. Although the statistics, sampling and number of iterations were limited, these data demonstrate the PEDRO's ability to perform single projection angle tomography. This work is currently being extended to increase the event statistics and push to higher incident energies.

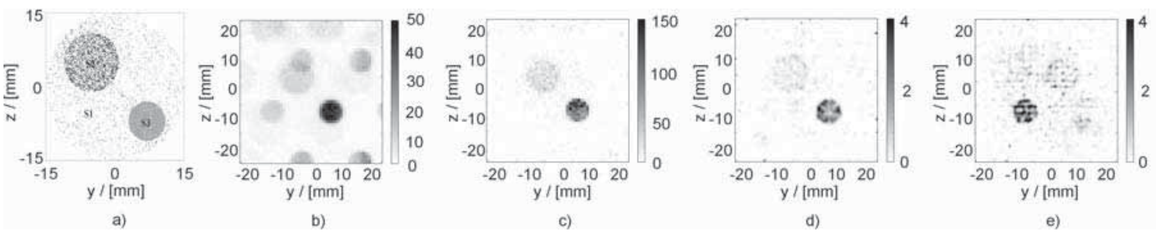

Figure 1: a) Representation of a triple intensity source simulated with Geant4. b) and c) MLEM reconstructions of the triple intensity source after 1 and 10 iterations. Geant4. d) and e) MLEM reconstructions of the two maximum intensity planes of the reconstruction volume for two triple intensity sources simulated simultaneously with a separation of 30.0 mm in depth and a 90^o rotation, after 10 iterations.

References

[1] J. Qian, et al. Nucl. Instr. and Meth. A 594 (2008) 102

[2] S. Motomura, et al. IEEE Trans. Nucl. Sci. 54 (2007) 710

[3] M.R. Dimmock et al., Nucl. Instr. and Meth. A. 612 (2009) 133

HICAM: development of a high-resolution Anger Camera for nuclear medicine

P.Busca[1,2], R.Peloso[1,2], C.Fiorini[1,2], A.Gola[1,2], A.Abba[1,2], C.Bianchi[3], G.L.Poli[3], B.F.Hutton[4], K.Erlandsson[4], L.Ottobrini[5], P.Lechner[6], L. Strüder[7], A.Pedretti[8]

[1]Politecnico di Milano, Dipartimento di Elettronica e Informazione, Milano, Italy
[2]INFN, Sezione di Milano, Milano, Italy
[3]Ospedali Riuniti di Bergamo, Bergamo, Italy
[4]Institute of Nuclear Medicine, University College London, London,UK
[5]Università degli Studi di Milano, Milano, Italy
[6]PNSensor GmbH, München, Germany
[7]MPI für Extraterrestrische Physik Halbleiterlabor, München, Germany
[8]L'accessorio Nucleare S.R.L. – L'ACN, Cerro Maggiore, Italy

ABSTRACT

A new compact and high-resolution Gamma Camera is under development in the framework of the HICAM (HIgh resolution CAMera) project, supported by European Community. The proposed Gamma camera, based on the well-established Anger architecture, offers a high intrinsic resolution (~1mm). Thanks to the camera compactness the distance between the collimator and the imaged target could be reduced and this factor, joined to the high intrinsic resolution, leads to an overall improvement of imaging performance of ~ 2.5 mm spatial resolution @ 5cm. This camera will be employed in applications in cancer research and diagnosis where the mentioned performances will produce a valuable benefit with respect to the results achievable with the presently used instrumentation.

The performances of the HICAM camera are based on the use of Silicon Drift Detectors (SDDs), which have recently demonstrated to be competitive devices for the readout of scintillators. The detection unit of the HICAM camera has a modular structure, based on monolithic linear arrays of five square shaped SDDs of 1cm^2 of active area each. The new Anger camera will be composed by 100 SDDs of 1cm^2 active area each, in a 10x10cm^2 format, representing the biggest gamma-ray imaging device based on SDD in use. A drawing of the detection head is shown in Fig.1. The system is moderately cooled by Peltier elements, necessary to achieve excellent performances in terms of electronics noise. A custom designed ASIC implements all the electronic necessary for the proper filtering and transmission to the acquisition module of the signals read from the sensors. An appropriate data acquisition module processes these signals and provides an estimation of the spatial distribution of emission events in form of an image on a display.A smaller prototype of HICAM camera, composed by 25 SDD with a 5x5cm^2 FOV, coupled to a CsI(Tl) scintillator, and using a parallel hole collimator (hole diameter 1.2mm, septal thickness 0.2mm, length 45mm, NUFI, Holland), offers a spatial resolution of about 1.5 mm at the collimator surface. Fig. 2 shows the image of a grid with holes of 0.5mm diameter and pitch 2mm, irradiated with a ^{99}Tc source at 87 cm from the detector. Fig . 3 shows the image of a phantom of a thyroid with hot and cold nodules. Significant experiments of small animal imaging were carried out with the smaller prototype. In particular, measurements have been performed to explore new techniques to label cells and to study their migration towards sites of interest An image that shows the migration of dendritic cells, labelled with ^{111}I, toward two lymph nodes in a mouse is reported in Fig.4.The small HICAM camera will be incorporated in systems for both planar and SPECT acquisition in small animals studies, while the bigger one will be dedicated to clinical studies on humans, as planar studies of small bones, parathyroid and thyroid, infant kidney and intra-operative imaging of breast cancer and melanoma.

Due to the compatibility of the SDDs to magnetic fields, a SDD-based camera, as HICAM, has also potentialities to be used in combination with MRI. Thus, this category of gamma camera opens new and important possibilities for the research and for future projects.

The current development of HICAM camera as well as the results of its performances in gamma-ray imaging are presented in this work.

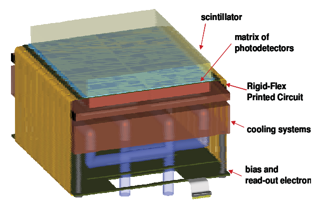

Fig. 1 – Drawing of the detection module of HICAM camera, based on 20 monolithic arrays of 5 SDDs each .

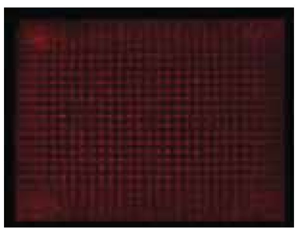

Fig. 2 – Distribution of the ^{99}Tc irradiation points obtained with a grid of holes of 0.5mm of diameter, pitch 2mm

Fig. 3 – Acquisition of a thyroid phantom simulating a 30-40 g thyroid with hot and cold nodules, filled with 2mCi of ^{99m}Tc.

Fig. 4 – Image of the migration of radiolabeled cells from the injection site (upper-left corner) to two lynphonodes. The radioactive source is ^{111}I.

CZT and ASIC Technology for Molecular Imaging Applications

Dirk Meier(1), Douglas J. Wagenaar(1), James W. Hugg, James(1), , Rex A. Moats(2), Kevin Parnham(1), Joshua Li(1), Gunnar Maehlum(1), Samir Chowdhury(1), Bradley E. Patt(1)

Gamma Medica-Ideas (1) Canada/Norway/USA, Children's Hospital of Los Angeles, USA (2)

The development of ionizing radiation detectors based on CdTe and CdZnTe (also known as CZT) began in the 1950s, and first pixellated detectors were reported in the 1970s for imaging applications. Parallel and collaborative efforts in the fields of CZT crystal growth and application specific integrated circuits (ASICs) over the past 30 years have lead to numerous prototype instruments for applications in physics and astronomy, and to first commercial instruments with applications in molecular imaging, industrial scanning, and homeland security.

We present our radiation detector module and its applications. We have developed the radiation detector module based on CZT and ASICs for molecular imaging applications [Figure 1]. The CZT crystal has 256 electrodes (pixels) which are read out by application specific integrated circuits (ASICs). Up to one hundred of these CZT modules are assembled inside molecular imaging systems which are typically used for bio-medical research (pre-clinical animal imaging), and recently for clinical breast imaging. The modular concept allows us to design planar and curved imaging systems which are relatively small and light weight compared to imaging hardware based on NaI scintillators and photomultiplier tubes (PMTs). Our modules have an intrinsic spatial resolution of 1.6 mm and an average energy resolution 5keV FWHM at 140 keV. These figures allow us to design imaging systems with improved sensitivity, higher contrast-to-noise and better spatial resolution than NaI/PMT-based systems. The improved image quality ultimately reduces radiation dose, shortens the acquisition time and enables new imaging applications.

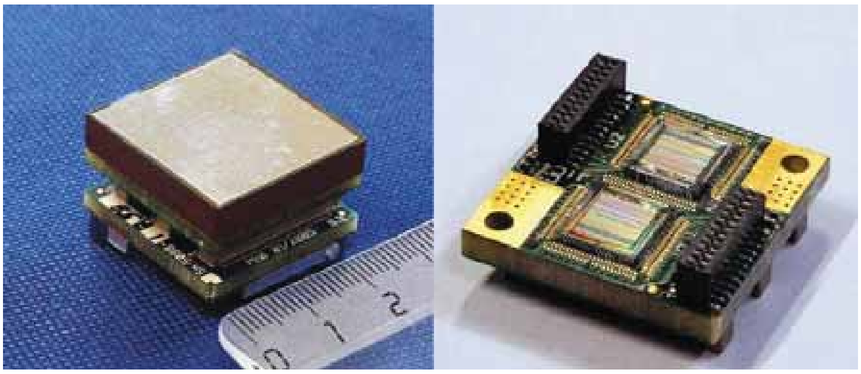

Figure 1: Ionizing radiation detector module with CZT (left) and ASICs (right).

The very high intrinsic *spatial resolution* of CZT-based detectors combined with multi-pinhole radiation collimators dramatically increases the system sensitivity. We observe very high sensitivity in our pre-clinical SPECT imaging systems (Triumph™) and in our "12-cm dia., small-barrel" SPECT camera for mice (>10cps/kBq). An intrinsic resolution in the CZT of less than 1.6 mm is quite possible with smaller pixel pitch and improved methods of readout and signal processing in the ASIC. Our module can be configured with essentially no dead space among pixels and modules. This feature can be exploited in the future for planar systems where collimator septa can be registered to pixels, but also for curved and ring systems that enable dynamic SPECT without a moving gantry. The very high *energy resolution* of CZT-based detectors improves image contrast through scatter rejection and enables imaging of multiple isotopes simultaneously. For example a cocktail with three isotopes (^{201}Tl, ^{111}In and ^{99m}Tc) allows one to visualize a mouse heart, thyroid and bones, simultaneously. Like multiple-isotopes, we demonstrate the multiple modalities of SPECT+MRI. We have operated our modules in 3Tesla magnetic fields which enables SPECT inside an MRI system and perfect registration of images from both modalities in space and time. Advances in our ASIC design have lowered the power consumption of the module by a factor of five. Lower power consumption now allows for stable operation at room temperature with heat dissipation through Peltier devices instead of water circulation. The low-power option is important for mobile, hand-held and battery powered spectroscopic imaging devices. Our presentation will summarize the benefits of CZT with integrated readout.

3D SPECT Renal Imaging Quantitative Evaluation

Lyra Maria[1], Gavrilelli Maria[2], Chatzigiannis Christos[2], Charalabatou Paraskevi[1], Fytros Stavros[1], Roussou Irène[1] and Lyra Vasiliki[3]

[1]Radiation Physics Unit, A' Radiology Dep., University of Athens

[2]"Medical Imaging" Athens Nuclear Medicine Center

[3]Nuclear Medicine Dep., Attikon Hospital, University of Athens

Our aim is to get an accurate estimation of the volume of the kidneys for dosimetric calculations as well as to obtain 3D images of the kidneys' at various spatial views for quantization of scars.This study attempts to give further than SPECT slices of the kidneys, high quality 3D volume surface images, carrying useful qualitative and quantitative diagnostic details. Total and partial volume data for the calculation of indices have also been extracted, useful in renal scars classification.

Data sets of 32 cases were obtained by a GE Starcam AT-4000 interfaced with a GE Xeleris-2 processing system. Tomographic imaging was carried out with data acquisition 15 sec at each of 32 posterior positions over 180 degrees. Data reconstructions were completed by ramp, FBP and OSEM filters. The computational scheme includes a method for compensation of attenuation and scatter, performed as part of the iterative reconstruction method. 3D images were generated by using a special threshold % of max for each patient (range 25%-50%) and a gradient factor of 15.

Angular measurements of renal parenchyma, analysis and quantification of 3D images of the kidneys' were made. Segmentation process has been used to partition the images into classes and subsets that were homogeneous with respect of tissue texture. Volumetric estimations and geometric data measurements are extracted. Images sets were evaluated for qualitative assessment of renal scarring and quantitative analysis of renal size and parenchyma function. Scarring was quantified using a 10 point scale. Relative ratios between kidneys' volumes indicate a threshold of the renal function.

This figure shows a 3D image of kidneys with scars. A scarring point of 7.2 for left kidney, 2.4 for right kidney and right to left relative ratio is equal to 3.1.

Maria Lyra, Assoc. Professor, A Radiology Dep., University of Athens
76, Vas. Sophias Ave, Aretaeion Hospital, Athens 11528, Greece
Email:mlyra@med.uoa.gr, Fax:0030-210-9827768

Direct imaging of three-dimensional atomic arrangement by stereophotography using two-dimensional photoelectron spectroscopy

H. Daimon[1], F. Matsui[1], T. Matsumoto[1], K. Goto[1], Y. Kato[1], T. Matsushita[2]
[1] *Nara Institute of Science and Technology (NAIST), 8916-5 Takayama, Ikoma, Nara 630-0192 Japan*
[2] *SPring-8/JASRI, Kouto 1-1-1, Mikazuki, Sayo, Hyogo 679-5198, Japan*

We have developed a new imaging method to take a stereo photograph of the three-dimensional atomic arrangement around specific atomic species, with which one can view the three-dimensional atomic arrangement directly by the naked eyes [1]. The azimuthal shifts of forward focusing peaks [2] in a two-dimensional photoelectron intensity angular distribution pattern excited by left and right helicity light are the same as the parallax in a stereo-view as shown in Fig. 1(d). Taking advantage of this phenomenon of circular dichroism in photoelectron intensity angular distribution, one can take a stereo photograph of atomic arrangement. A display-type spherical-mirror analyzer [3] installed at BL25SU in SPring-8 is used to take stereoscopic photographs directly on the screen without any computer-aided conversion process.

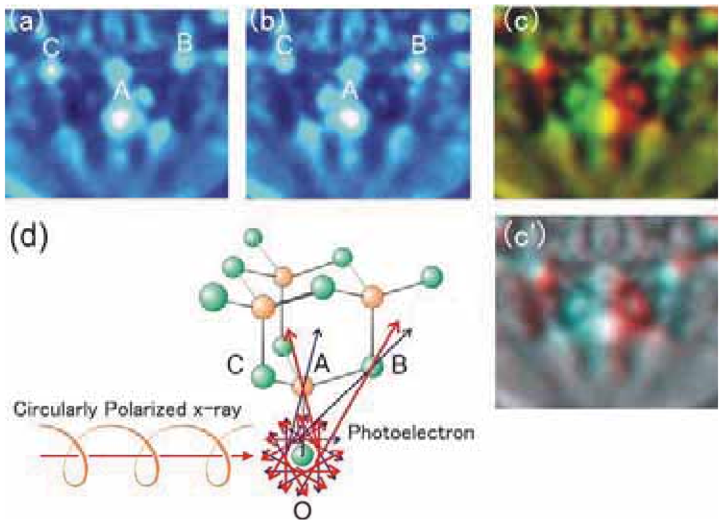

Fig. 1 (a) and (b) are stereo photograph of atomic arrangement around In atom in InP(001) for left eye and right eye, respectively. (c) and (c') are those for red-and-blue glasses (if printed in color). (d) explains the principle and arrangement of the emitter O and the scatterers A, B,.and C.

Recent results of stereo photograph of atomic arrangement around In atoms in InP(001) [4] are shown in Fig. 1. Figure 1(a) and (b) are stereo photograph for left eye and right eye, respectively. Figure 1 (c) and (c') are those for red-and-blue glasses (Blue glass is for right eye). (d) explains the principle and arrangement of the emitter O and the scatterers A, B,.and C. "A" atom looks closer to the observer than B and C atoms.

References

[1] H. Daimon, Phys. Rev. Lett. 86, 2034 (2001). [2] H. Daimon, T. Nakatani, S. Imada, S. Suga, Y. Kagoshima, and T. Miyahara, Jpn. J. Appl. Phys. 32, L1480 (1993). [3] H. Daimon, Rev. Sci. Instrum. 59, 545 (1988). [4] T. Matsumoto, F. Matsui, T. Matsushita, K. Goto, Y. Kato, H. Daimon, e-J. Surf. Sci. Nanotech. 7, 181 (2009).

The X- ray spectrometer onboard Chang'E-1 Lunar Orbiter and Its operation Status

Huanyu WANG* Chengmo ZHANG* Jinzhou WANG* Xiaohua LIANG* Min GAO*
Xuelei CAO* Wenxi PENG* Xingzhu CUI* Jiayu ZHANG* Jiawei YANG*
Chunlai LI** Yongliao ZOU** Jian zhong LIU** Ziyuan OUYANG**
* Institute of High Energy Physics of Chinese Academy of Sciences
** National Astronomy Observatory of Chinese Academy of Sciences

Abstract

Chang'E-1 is the first Chinese Lunar exploration satellite, which is an orbiter with eight scientific payloads circling the moon 200km above the moon surface. The satellite was successfuly launched on 24 October 2007, and finished its operation on 1 March 2009. On 20 November 2007 the stereo camera instrument was switched on, henceforth all the instruments were successfully switched on one by one. After a period of parameter adjustment and initial check out, all scientific instruments were in their normal operating phase. The X-ray spectrometer (XRS) is one of the eight scientific payloads onboard. It consists of a lunar X-ray detector, a solar X-ray monitor and an electronics box. The main goals of XRS are to detect the fluorescent X-ray from the lunar surface and provide abundance distribution of the major rock-forming elements as Mg, Al, Si, etc on the Moon. The system construction and principle of the X-ray spectrometer and its priliminary observation results will be presented in this paper.

Imaging Physics for Astronomy and Bio-Medicine

Zdenka Kuncic
Institute of Medical Physics, School of Physics, University of Sydney, Australia
zdenka.kuncic@sydney.edu.au

Astronomy and medicine share many similar demands for increasingly sophisticated and diverse imaging techniques as well as associated cutting-edge instrumentation technologies and advanced software tools for multi-dimensional data storage, manipulation and processing. In addition, there is a less obvious, but equally important need for fundamental physics in modeling radiation transport and radiation detection. In this talk, I will present an overview of these synergies, identifying along the way opportunities for knowledge diffusion and technology transfer across the two disciplines. I will compare and discuss imaging tools and techniques in astronomy and biomedicine, including tomography, reconstruction and 3D visualization, as well as meta-data handling and analysis. I will also discuss radiation transport modeling in both fields. Finally, I will briefly discuss efforts towards an intradisciplinary research initiative in astronomical and biomedical imaging at the University of Sydney.

Ground-Based Very High Energy Gamma Astrophysics by Means of Imaging Atmospheric Air Cherenkov Telescopes

In recent years the Imaging Atmospheric Cherenkov Telescopes (IACT) have proven to be a remarkably successful technique for the detection of very high energy gamma rays from astro-physical sources above few hundred GeV. The 3rd generation IACT installations VERITAS, H.E.S.S., MAGIC and CANGAROO, located in 4 different continents, are delivering highly interesting science results.

The number of discovered sources continues to steadily increase and probably during this year it will cross the line of 100 sources. Many researchers believe that the puzzle of the origin of cosmic rays is close to being largely resolved in the next few years.

The birthday of modern ground-based gamma-ray astrophysics is considered to be the first measurement of a strong signal from the Crab Nebula by the Whipple team working with the 10m diameter telescope on mount Hopkins in Arizona. Important milestone was the use of multi-pixel imaging camera of 0.5° pixel size, producing relatively crude images of air showers in Cherenkov light in the observation field of view of ~3°. Two years after the first detection a camera of half-pixel size of 0.25° has been used that significantly enhanced the sensitivity. Later on researchers from other collaborations started using imaging cameras with pixel sizes in the range of 0.10° - 0.16° in their telescopes. These enhanced the sensitivity even further up allowing one to perform source measurements also in the sub-100 GeV energy range.

One of the current ground-based gamma-ray efforts has been concentrated primarily on improving the sensitivities to lower energies ($E_\gamma \leq$ 300-100 GeV, down to 30 GeV) so as to provide overlapping observations with satellite-born detectors and potentially find new classes of sources. Gamma ray images in the lower energy range are becoming progressively smaller in size and irregular in shape. They start heavily overlapping in size with those of orders of magnitude more intense background of hadrons. To provide better signal to noise ratio one needs to move towards smaller pixel sizes and higher resolution.

Now the fourth generation telescopes are under planning. It seems that the new type of semiconductor sensors, namely the SiPM, could offer serious advantages over traditionally used in IACTs classical PMTs. The main advantage could be the anticipated about two times higher photon detection efficiency. But also their naturally small physical size calls for the use in the high resolution imaging cameras. Already now first SiPM-based mini-cameras are under tests. Obviously one will need to modify the trigger and the data acquisition concepts for maximising the advantages offered by the new sensor. Simultaneously new and important questions are arising concerning the optimum imaging under the condition of a relatively strong backgrounds and a limited number of signal photons.

In our presentation we would like to discuss the main developments during the last 20 years as well as we will try to tackle the sensitive questions about the limits of IACT technique for very high energy gamma astrophysics.

Spectral CT in Medical Imaging

Presenter: Anders Persson MD, PhD, Assoc. Professor, Director Center for Medical Image Science and Visualization (CMIV), Linköping University, SWEDEN.

Abstract: The practice of medical image diagnosis is currently undergoing a fast transformation. Vast amounts of data can be generated in standard examination and focus is shifting from improving the collection of relevant data for diagnosis to development of effective methods to analyze, visualize, navigate, and interact with medical information.

In general X-ray imaging technology typically detects whether an X-ray comes through the object or not, i.e. only absolute density is detectable. Despite the fact that different organs and materials absorb different parts of the X-ray spectrum (measured in KeV) in different ways there has been no technology to discriminate the spectral beams whilst maintaining a reasonable radiation dose for the patient.

Historically, the only way to create Spectral (colour) X-ray Imaging has been to use multiple X-ray sources and several exposures. This is a costly and time consuming process. Despite this, the market is moving rapidly towards Spectral (colour) X-ray Imaging. This development may provide a whole new range of imaging possibilities although the current market standard uses only two "colours", made with two different X-ray tubes – Dual Energy Computed Tomography, e.g. Siemens Somatom Definition Flash.

Since the introduction of this Dual-Energy Computed Tomography (DECT) four years ago, added clinical value has been proven. The potential of DECT to differentiate elements within body tissue makes CT an even more powerful clinical tool. The trend now is not to restrict the technique to just two X-ray energies. New methods promise to identify materials being imaged with greater precision. While conventional systems often fail to differentiate between contrast between plaque and contrast on the counting of individual photons reveals a strong contrast between plaque and contrast agent in a coronary vessel. Initial experience is promising and warrants further exploration of multi-energy CT as a possibly feasible single imaging investigation for the comprehensive diagnosis of coronary stenosis and myocardial ischemia. Coronary artery disease is the main cause of death in the western world and only one example of a diagnostic problem that this new technique can solve.

Multi-energy CT takes advantage of the variations in attenuation when composite materials are imaged by X-rays of differing energies. Dual-energy scanning with two separate X-ray energies will yield two data sets with quite different attenuation profiles. A comparison of these will yield information on the average atomic number of the material being examined and its density. The above method could be used clinically to distinguish between elements with a high atomic number, such as calcified arterial plaques or iodinated contrast media, and bodily tissues with a lower atomic number. Dual-energy imaging cannot, however, separate several individual elements from each other. This higher level of discrimination requires attenuation information from more than two X-ray energies. Detectors working in Photon Counting mode can potentially measure the energy of every detected X-ray photons and achieve better image contrast sensitivity for a given dose. Unfortunately, most current X-ray detectors suffer from limited count rate capability, due either to a long charge migration time in semiconductor and gas detectors, or to a slow decay time in ceramic scintillators. A current drawback with Photon Counting detectors is that photon efficiency is maximised in the span of 50-90kVp and today's CT scanners acquire data in the range of 80-140kVp.

This talk will take its starting point in state-of-the-art Dual-Source CT scanners and then discuss the need for a research agenda that focuses on the development of the next generation of scanners based on early clinical results, emphasizing the fact that these scanners must be based on medical user requirement and workflow studies as well as on new technical developments.

Evaluation of the image transfer properties of a flat-panel based microCT scanner prototype

A. Martínez-Dávalos, J. Kikushima and M. Rodríguez-Villafuerte

Instituto de Física, Universidad Nacional Autónoma de México, A.P. 20-364, 01000 México D.F., México

A microcomputed tomography scanner prototype based on a CMOS flat panel detector (FPD) has been developed at Instituto de Física, UNAM, and is currently being characterised. The tests include measurements of the energy spectra and uniformity of the X-ray beam, and the determination of the image transfer characteristics of the flat panel detector, such as linearity of response, MTF, noise and DQE. The alignment of the system is carried out with a specially build phantom using 1 mm diameter Al markers. Tomographic image reconstruction is performed with in-house developed programs based on the Feldkamp algorithm, and calibration in Hounsfield Units is carried out by means of a tissue-equivalent phantom. The dose performance of the system has been evaluated using TLD-100 chips, and the results have been compared with Monte Carlo simulations.

The microCT system uses an Oxford Instruments X-ray tube (Apogee XTG5011) with a nominal focal spot size of 35 µm, 50 kVp maximum voltage, 1.0 mA maximum anode current, 22° cone beam angle, fixed tungsten anode and a thin beryllium exit window. The performance of the microCT system has been evaluated with the tube operating between 30 and 50 kVp, up to 1.0 mAs and filtered with 1 mm high purity Al**.** The uniformity of the beam was evaluated using EBT GafChromic film. The detector is a Rad-icon Shad-o-Box 2048 flat panel with four CMOS photodiode arrays coupled to a Min-R 2190 scintillator screen. This detector has 2048×1024 pixels at 48 µm pitch, and it has 12 bits per pixel resolution depth. The samples are mounted on a Standa 8MR150-1 rotational stage (0.01°/step) which is in turn attached to a Standa 8MT175-50 linear stage (2.5 µm/step) for alignment along the transverse axis of the system. X-ray output, sample movement and image acquisition are computer controlled with a National Instruments PCI-6024E I/O board and in-house developed LabVIEW programs.

The linearity of the system was evaluated from flat image acquisitions under different kVp's in the range 02-0.9 mAs by varying the mA for a constant integration time (500 ms) in order to avoid variations in the dark noise contributions. The noise characteristics have been obtained from the same images after dead pixel interpolation and fixed-pattern noise corrections. The MTF was measured using the slanted edge technique from images of a 1.0 mm thick Ta sheet (2.5×2.5 cm^2), carefully machined and placed on top of the entrance window of the flat panel. Tomographic acquisitions of the calibration and dosimetry phantoms were taken in a 360° circular orbit with 1° steps. Image reconstruction was performed using cone-beam FBP. In this work an overview of the main system characterisctics is presented, with an emphasis on image quality and dose performace.

Monte Carlo simulation of iodine-based contrast agent dosimetry in microCT

M. Rodríguez-Villafuerte and A. Martínez-Dávalos

Instituto de Física, Universidad Nacional Autónoma de México, A.P. 20-364, 01000 D.F., México

In the last years there has been an increasing interest in generating high quality microCT images in terms of high spatial resolution, high contrast and low noise. It is well known that achieving these three characteristics in a single study has a direct impact in the dose imparted to the animal: the better the quality of the image, the larger the dose. A promising method to increase the contrast in microCT studies is the use of iodine-based contrast agents with concentrations of the order of 10 mg/mL. This technique may allow to achieve contrast enhancement while at the same time lowering the x-ray tube current, and even increasing the kVp. However, due to the high Z of iodine, it is unclear whether the new exposure conditions would affect the absorbed dose to the animal.

Dose measurements represent a difficult task in objects as small as a mouse, as it requires the use of high precision dosimeters with relatively high spatial resolution. An alternative method to determine dose is to use Monte Carlo (MC) techniques. In this work, a MC program was developed based on the PENELOPE code that simulates a cone-beam microCT system to calculate spatial dose distributions in different cylindrical geometries. The MC simulation was first validated using thermoluminescent dosimetry, and the validated code was then used to calculate spatial dose distributions in a cylindrical water phantom containing an inset with different iodine concentrations.

In order to compare the Monte Carlo results with experimental data we closely followed the design geometry of a prototype microCT scanner prototype build in our laboratory, which uses an Oxford Instruments Apogee XTG5011 x-ray tube operating in the 20-50 kVp range and has a 1 mm Al additional filter. Experimental dose measurements were carried out using LiF:Mg,Ti (TLD-100) thermoluminescent 1×1×1 mm^3 dosemeters placed within a cylindrical solid water phantom (3 cm diameter, 6 cm height). For the simulations the contrast phantom was assumed to be a water cylinder of 30 mm diameter, 60 mm height with a cylindrical inset containing iodine contrast with different concentrations. Two different diameters for the inset were considered, 1.0 and 0.3 cm, and different x-ray beam qualities were used, with effective energies ranging from 18 to 37 keV. Results show, as expected, a large dose increase in the cylinder containing different concentrations of iodine.

Title: Sensor for simultaneous spectral photon counting/standard CT and combined PET/CT based on SiPM technology

A. Persson, A. Khaplanov and B. Cederwall
The Royal Institute of Technology, Department of Physics, SE-106 91 Stockholm, Sweden

Abstract
Recent developments make it possible to utilize SiPMs for quantifying high radiation fluxes in current mode as well as for pulse mode measurements for counting and characterizing individual gamma-ray or X-ray photons when coupled to scintillators. This enables the construction of medical imaging systems that combine different imaging modalities in a common detector system.
There is an increasing clinical need for low-dose photon counting CT for certain applications. In this work we present a novel detector design making it possible to combine photon counting CT with standard current mode CT. In photon counting mode the sensor has excellent energy resolution, and can therefore provide energy discriminatory data, enhancing the image information content and adding imaging power to the use of contrast agents. Currently, two separate detector systems are required for combined PET/CT. The advantages of a unified PET/CT system include increased patient throughput, higher image fusion accuracy due to perfect PET-CT sensor alignment and reduced system cost. The new detector concept would enable the combination of PET and CT imaging in a single detector system.

A silicon PET probe

A. Studen[1], E. Chesi[2], V. Cindro[1], N. H. Clinthorne[3], E. Cochran[2], B. Grošičar[1], K. Honscheid[2], H. Kagan[2], C. Lacasta[4], G. Llosa[4], V. Linhart[4], M. Mikuž[1,5], V. Stankova[4], P. Weilhammer[2] and D. Žontar[1]

[1] *Jožef Stefan Institute, Ljubljana, Slovenia,* [2] *The Ohio State University, Columbus, OH, USA,* [3] *The University of Michigan, Ann Arbor, MI, USA,* [4] *IFIC/CSIC-UVEG, Valenica, Spain,* [5] *The University of Ljubljana, Ljubljana, Slovenia.*

Abstract

PET scanners with high spatial resolution offer a great potential in improving diagnosis, therapy monitoring and treatment validation for several severe diseases. One way to improve resolution of a PET scanner is to extend a conventional PET ring with a small probe with excellent spatial resolution. The probe is intended to be placed close to the area of interest. The coincidences of interactions within the probe and the external ring provide a subset of data which, combined with data from external ring, greatly improve resolution in the area viewed by the probe.

Our collaboration is developing a prototype of a PET probe, composed of high-resolution silicon pad detectors. The detectors are 1 mm thick, measuring 40 by 26 mm^2, and several such sensors are envisaged to either compensate for low stopping power of silicon or increase the area covered by the probe. The sensors are segmented into 1 mm^3 cubic voxels, giving 1040 readout pads per sensor. A module is composed of two sensors placed in a back-to-back configuration, allowing for stacking fraction of up to 70 % within a module. The pads are coupled to a set of 16 ASICs (VaTaGP7.1 by IDEAS) per module and read out through a custom designed data acquisition board, allowing for trigger and data interfacing with the external ring.

This paper presents an overview of probe requirements and expected performance parameters. It will focus on the characteristics of the silicon modules and their impact on overall probe performance, including spatial resolution, energy resolution and timing resolution. We will show that 1 mm^3 voxels will significantly extend the spatial resolution of conventional PET rings, and that broadening of timing resolution related to varying depth of photon interactions can be compensated to match the timing resolution of the external ring. The initial test results of the probe will also be presented.

A Triple-Modality SPECT-OT-CT Small Animal Imaging Instrument with Axially Superimposed Fields-of-View

Jörg Peter & Liji Cao

German Cancer Research Center · Div. Medical Physics in Radiology · Heidelberg · Germany

Objective

To build a trimodal tomographic small animal imaging instrument for simultaneous non-contact data acquisition of in vivo bio-distributions involving radio-labeled probes (SPECT) and optical markers (bioluminescence imaging, BLI; fluorescence mediated tomography, FMT), both of which being fused with information about the imaged object's anatomy.

Methods

All imaging parts (Fig. 1) are mounted within a light-tight and radiation-protected housing on a common rotatable gantry. The γ-camera used for SPECT imaging incorporates a 2×2 array of Hamamatsu H8500 position sensitive photomultiplier tubes (PSPMTs) that are optically coupled to an array of 66×66 NaI(Tl) scintillator elements (St. Gobain Crystals and Detectors), each with a size of $1.3\times1.3\times6\ mm^3$, composing a total detector array size of approx. $10\times10\ cm^2$. The detector parts are housed within a tungsten (Densimet, Plansee AG) body providing a mounting for changeable pinhole and slit-slat collimators with focal lengths of 7.5 cm, respectively. Electrical output signals from the 16×16 anode pads of the four PSPMTs are summed in each direction reducing the number of output channels from 256 to 32. These signals are used for energy determination and for a truncated center of gravity calculation for event positioning forming a final raw data image grid of 66×66 bins (electronics provided by Jefferson Nat. Acc. Fac.). Because of the consequentially rather low intrinsic spatial resolution the camera's best performance is obtained with a pinhole diameter / slit widths of 1mm, respectively.

The implemented x-ray tube is embodied by an Apogee 5000 (Oxford Instruments) which is operated with an anode current of up to 1mA at an anode target voltage in the range of 4 to 50 kV (50W continuous maximum power). A 500 µm aluminum foil is used for beam filtration. The beam is operated using filament current triggering. A Shad-o-Box 2048 (Rad-Icon Imaging corp.) flat panel x-ray detector having a sensitive area of $5\times10\ cm^2$ is mounted opposite to the tube with respect to the axis of rotation. It consists of a Gd_2O_2S scintillator screen rated for photon energies within the range of 10 to 50 keV that is glued to a CMOS sensor made of a 512×1024 silicon photodiode matrix with 48 µm pixel pitch.

A commonly used ORCA AG cooled CCD camera (Hamamatsu Photonics) is used for the optical detector sub-system. The camera is equipped with a near infrared corrected lens (CNG compact, Schneider). Various light sources (e.g. a 670nm diode laser (LG Laser-Technologies)) can be substituted for respective fluorochrome excitation. By use of additional mirrors the light camera has full circumferential view of the imaged object at every projection angle.

All involved imaging parts are (co-)calibrated yielding intrinsically fused submodal projection data. The following image reconstruction algorithms are implemented: ordered subset maximum likelihood (SPECT), Feldkamp-Davis-Kress (CT), Bayesian finite element (FMT).

Results

All three sub-modalities operate at their highest performance capabilities, respectively, without being affected by the adjacent modalities (except that the SPECT camera is being switched of while the x-ray tube is operating due to scatter contribution). The most significant advantage of this instrument is expected for the optical modality because tomographic optical imaging is not yet been solved for heterogeneous objects with unknown geometry. Given the presented approach, the crucial boundary conditions for FMT effectively can be provided by the CT data set whereas further prior information can be incorporated by the SPECT data, particularly when chemically linked probes are imaged in which case quantitative optical imaging seems possible. A number of phantom experimental studies have already been performed (Figs. 2, 3).

Fig. 1 *Photograph of the trimodal imager: SPECT γ-camera (12 o'clock), x-ray tube (10 o'clock), laser (7 o'clock), light camera (6 o'clock), x-ray detector (4 o'clock). γ-camera and x-ray control units are mounted beneath the imaging compartment.*

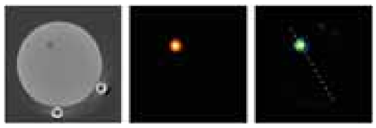

Fig. 2 *Imaging results of a cylindrical phantom with tissue-like optical properties containing a 2mm cylindrical inclusion filled with a dilution of Tc^{99m} and Cy5.5; CT (left), SPECT (ctr.), FMT (right).*

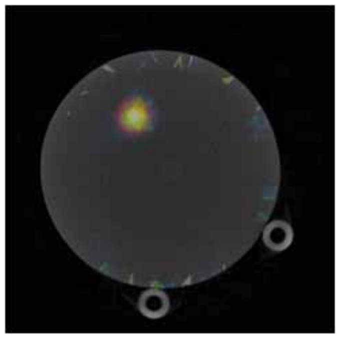

Fig. 3 *Intrinsically fused transversal slice incorporating SPECT, CT, and FMT.*

Clinical Aspects of Photon Counting CT

R. Levinson

Photon Counting Detectors enable multi-energy data acquisition capabilities not available with current state-of-the-art CT systems. Multi-energy data acquisition opens the possibility of material-specific imaging: anatomic and physiological imaging of targeted tissues, organ systems and disease processes in the human body.

This paper will describe work done at the GE CT Engineering group in Haifa, Israel that developed and built a prototype, medical photon-counting CT system. The system was installed in Rabin Medical Center and two clinical trials: carotid angiography and adrenal perfusion were performed with the scanner.

Technical challenges of integrating a photon counting detector in a clinical CT system will be reviewed. The main obstacles were achieving fast temporal response for the detectors and the design and implementation of a multi-energy detector calibration protocol for single and dual energy scanning.

The goal of photon counting CT detectors is to provide superior imaging performance for conventional, single energy CT imaging and enable multi-energy CT imaging. Both single and dual energy imaging were performed in the clinical studies. The imaging performance of the photon-counting system was compared to conventional CT systems. Dual energy imaging was performed for angiographic and organ perfusion imaging. The clinical results of single and dual energy imaging will be presented.

Statistical Behavior Of Energy Resolving Photon Counting Detector at High Count Rates

Vladimir A. Lobastov and J.Eric Tkaczyk

GE Global Research,
1 Research Circle, KW C424
Niskayuna, NY12309, USA

ABSTRACT

Imaging applications with X-rays such as CT-tomography, dental radiography, mammography, will potentially benefit from photon counting detectors with multi-bin energy resolving capability. However, the degradation of the statistical information at high photon flux rate due to pile-up limits the useful dynamic range, energy resolution and dose efficiency. In this study, we measure the response of photon counting CdTe detectors to intense x-ray flux density and quantify statistical metrics as a function of increasing X-ray flux rate. The mean and variance is shown to be consistent with a model for the non-paralyzable case and parameterized by the maximum periodic rate parameter. In order to assess detector spectral performance and its potential for medical diagnostics, multi-bin CT images were also obtained from an iodine contrast agent phantom. Evaluation of the image quality, counting statistics and detector performance at CT-relevant X-ray flux rates was performed in the image domain. The contrast-to-noise ratio (CNR) is calculated as a function of count rate. The impact of CNR degradation on CT image quality is demonstrated. The spectral response of the detector is measured as a function of flux density.

CT imaging of the internal human ear: test of an high resolution scanner.

M.Bettuzzi[1], R.Brancaccio[1], M.P.Morigi[1], A.Gallo[2], F.Casali[1]

[1] Department of Physics University of Bologna and National Institute of Nuclear Physics Section of Bologna
[2] Department of Physics University of Catanzaro

ABSTRACT

In the course of year 2009, in the framework of a project supported by the National Institute of Nuclear Physics, a number of tests have been carried out at the Department of Physics of the University of Bologna in order to achieve a good quality CT scan of the internal human ear. The work has been done in collaboration with the local Hospital "S.Orsola" in Bologna and a company (CEFLA) already involved in the production and commercialization of a CT scanner dedicated to dentistry. A laboratory scanner with a simple concept detector (CCDcamera-lens-mirror-scintillator) has been used to see to which extent it was possible to enhance the quality of a conventional CT scanner when looking to the internal human ear. To test the system, some conventional measurements have been done as the spatial resolution calculation with the MTF and dynamic range evaluation. Different scintillators have been compared to select the more suitable for the purpose. With 0.5mm thick structured Cesium Iodide and a field of view of 120x120 mm2 a spatial resolution of 6.5lp/mm at 5% MTF has been obtained. The CT of a couple of human head phantoms has been done at an energy of 120kVp. The first phantom was a raw representation of the human head shape, with soft tissue made of coarse slabs of Lucite. Some inserts, like small aluminium cylinders and cubes, with 1mm diameter drilled holes, have been used to simulate the channels that one finds inside the human inner ear. The second phantom is a plastic PVC fused head with inside a real human cranium. The bones in the cranium are well conserved and the inner ear features, as the coclea and semicircular channels, are clearly detectable. After a number of CT tests we obtained good results for what concerns structural representation and channel detection. A couple of images of the 3D rendering of the CT volume are shown below. Satisfaction has been expressed by the doctors of the local hospital who followed our experimentation. The CT was compared to a virtual endoscopy and judged really useful for a clinical pre-surgery diagnostics. The experimentation goes on with a faster scanner now under development in our laboratories. We believe this work has a certain relevance for the medical imaging world.

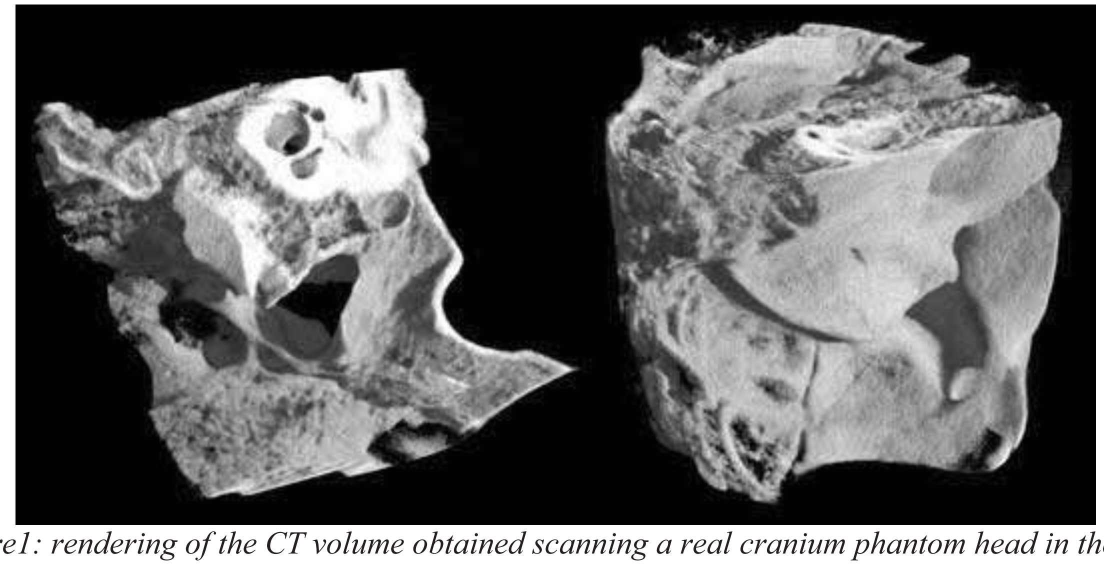

Figure1: rendering of the CT volume obtained scanning a real cranium phantom head in the area of internal ear. Coclea and semicircular cannels are clearly detected.

X-Ray Phase Contrast Imaging

Christian David, Paul Scherrer Institut, CH-5232 Villigen-PSI, Switzerland

We report on a hard x-ray interferometry technique based on diffraction gratings fabricated using microlithography techniques [1]. It allows to record separate phase and absorption images of an object simultaneously. By taking data sets under many viewing angles, a tomographic reconstruction of both the real part and the imaginary part of the objects complex refractive index distribution can be obtained [2]. In addition, the local small-angle scattering power of the sample can be visualized [3]. This dark-field signal gives information about the structure on length scales below the detector resolution.

Compared to other x-ray phase-contrast imaging methods, the grating interferometer only has very moderate requirements in terms of coherence. It can accept a wide spectral band width, and virtually no spatial coherence is required when a third grating is placed close to the radiation source [4]. This makes it possible to use the method with standard x-ray tubes, which opens up a huge range of applications e.g. in medical imaging [5]. We have obtained phase contrast radiographs and tomographs of biomedical samples at photon energies of up to 60keV [6].

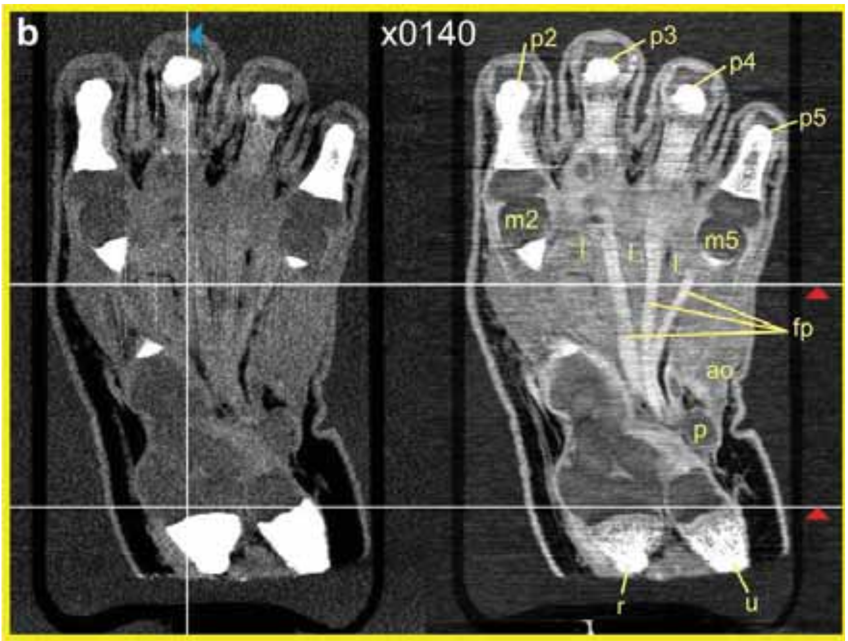

Comparison of conventional slices through the tomographic data-set of an infant hand obtained in conventional attenuation contrast (left) and phase contrast (right). The phase image shows strongly enhanced contrast of soft tissue regions. The images were acquired with a standard x-ray tube source.

References:

[1] C. David et al. *Microelectronic Engineering* **84** (2007) 1172

[2] T. Weitkamp, A. Diaz, C. David, F. Pfeiffer, M. Stampanoni, P. Cloetens, and E. Ziegler, *Optics Express* **13** (2005) 6296

[3] F. Pfeiffer, T. Weitkamp, O. Bunk, and C. David, *Nature Physics* **2** (2006) 258

[4] F. Pfeiffer, M. Bech, O. Bunk, C. Grünzweig, E.F. Eikenberry, Ch. Brönnimann, C. David, *Nature Materials* **7** (2008) 134

[5] T. Donath et al. accepted in: *Investigative Radiology* (2010)

[6] T. Donath et al. *Review of Scientific Instruments* **80** (2009) 053701

Liquid-metal-jet-anode x-ray tubes for phase-contrast imaging

H.M. Hertz, U. Lundström, P. Skoglund, P. Takman, U. Vogt, T. Tuohimaa*, M. Otendal*, and O. Hemberg*

Biomedical and X-Ray Physics, Department of Applied Physics,
Royal Inst. of Technol./Albanova, SE-106 91 Stockholm, Sweden,
E-mail: *hans.hertz@biox.kth.se*

**) Excillum AB, Finlandsg. 14, SE-164 74 Kista, Sweden*

We recently introduced the electron-impact liquid-metal-jet anode x-ray source.[1,2] This laboratory source has potential for >100× higher brightness than present micro-focus sources while still producing high power. The source was originally designed for operation at a few tens of keV with a tin jet[1] but has since been extended to several different jet materials. Figure 1 shows the 9 keV-dominated spectrum of a gallium-jet source[3] , and we have also demonstrated operation with a non-metal (methanol) jet[4]. The source is presently operated with a 5-20 µm focus and 50-200 W e-beam power on a room-temperature GaInSn jet.[5] This corresponds to more than an order of magnitude higher e-beam power density than is possible on other microfocus sources.

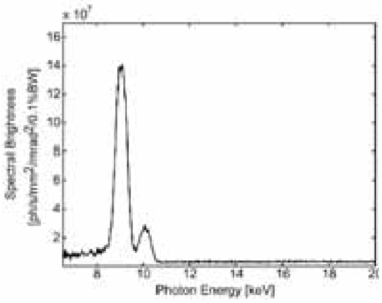

Figure 1. Source spectrum from electron-impact liquid-gallium-jet anode microfocus source.

X-ray imaging based on phase contrast shows promise to reveal improved detail[6]. However, the method requires spatially coherent illumination and therefore present work is primarily performed at high-brightness synchrotron sources. Unfortunately, available laboratory sources have too low brightness and flux to allow phase-contrast imaging with reasonable exposure times. The high brightness/flux operation of the liquid-metal-jet sources enables high-resolution phase-contrast x-ray imaging with adequate exposure times in the laboratory or clinic.

We have demonstrated laboratory phase-contrast imaging in an in-line-arrangement with few-µm detail and excellent contrast both at 25 kV[7] and at 9 kV. Figure 2 shows phase imaging of latex beads with the Ga-jet source. Note that in classical absorption imaging none of these beads are visible due to lack of contrast. Note also that beads as small as 10 microns are clearly visible in phase contrast, indication very high detectability. Present work is focused on detailed numerical modelling of the imaging process, imaging of whole-body-thickness objects and preliminary experiments on small-animal imaging aimed at tumour detection.

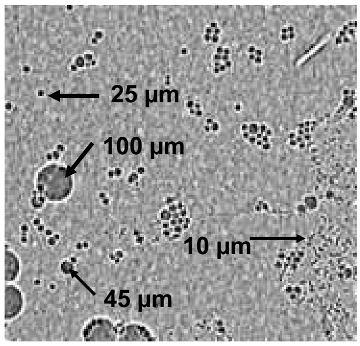

Figure 2. Phase-contrast image of latex beads.

References

[1] O. Hemberg et al, Appl. Phys. Lett. **83**, 1483 (2003)
[2] M. Otendal et al, J. Appl. Phys. **101,** 026102 (2007)
[3] M. Otendal et al, Rev. Sci. Instr. **79**, 016102 (2008)
[4] T. Tuohimaa et al, Appl. Phys. Lett. **92**, 233509 (2008).
[5] www.excillum.com
[6] R.A. Lewis, Phys. Med. Biol. **49**, 3573 (2004)
[7] T. Tuohimaa et al, Appl. Phys. Lett. **91**, 074104 (2007)

Carbon Nanotube based X-ray Sources: Applications in Pre-Clinical and Medical Imaging.

Yueh Z. Lee, MD/PhD[1,2]; Laurel Burk[2]; Guohua Cao, PhD[2]; Xin Qian, PhD[2]; Guang Yang, PhD[2]; Shabana Sultana, PhD[2]; Xiomara Calderon, PhD[3]; Jianping Lu, PhD[3]; Otto Zhou, PhD[2,3].

1 Department of Radiology, University of North Carolina at Chapel Hill,
Chapel Hill, NC 27599, USA
2 Department of Physics and Astronomy, University of North Carolina at Chapel Hill,
Chapel Hill, NC 27599, USA
3 Curriculum in Applied Science and Engineering, University of North Carolina at Chapel Hill, Chapel Hill, NC 27599, USA

Carbon nanotube (CNT) based x-ray sources generate electrons based on field emission with a cathode of vertically arranged nanotubes. The high aspect-ratio and near atomic sharpness of CNT tips allows them to serve as near optimal field-emission cathodes. The application of an electric field across the nanotube creates electron emission at 5 V/μm or lower, with stable current densities of 1500 mA / cm^{-2} or higher. Source stability at high currents has been demonstrated to be in excess of 30 continuous hours, with focal spots as small as 50 microns. We have demonstrated the utility of these sources for a number of applications, including pre-clinical small animal imaging of mice, solid-state breast tomosynthesis and other uses.

Field emission cathodes allow for simple modulation of the x-ray source by controlling the gate voltage. For preclinical small animal imaging applications, this allows straightforward respiratory or cardiac gated imaging at high physiological rates (300 beats per minute or more). We have demonstrated successful cardiac and respiratory gated imaging at 12 and 30 msec x-ray pulses, respectively, allowing functional imaging of mouse models of pulmonary and cardiac disease. Minimum imaging time of our system is 8 minutes, primarily limited by the detector. Physiological parameters, such as tidal lung volume and ejection fraction, can be readily derived from the CNT μCT images. No intubation of the animals was required. In contrast to other published systems, the CNT micro CT system enables rapid prospectively gated imaging with a straightforward control system.

The inherent focusing of CNT sources enables close placement of the x-ray sources, allowing the creation of individually addressable x-ray sources. We have demonstrated this application for stationary digital breast tomosynthesis, where minimizing motion reduces the apparent focal spot and reduces imaging time. Tomosynthesis allows more depth resolution and improves separation between overlying objects. Additional advantages include reduced imaging time, thereby reducing patient discomfort. The addressable arrays may also be utilized for other novel volumetric imaging in complex geometries, such as the ongoing development for radiotherapy and interventional applications.

CNT based x-ray sources have allowed the development of new imaging techniques and geometries not previously attainable using conventional sources. New detector technologies will further enhance the possibilities of the CNT sources.

ChromAIX: Fast Photon-counting ASIC for Spectral Computed Tomography

Roger Steadman[1], Christoph Herrmann[1], Oliver Mülhens[1]

[1]Philips Research Europe, Weisshausstr. 2, 52066 Aachen, Germany

roger.steadman@philips.com

Abstract

X-ray attenuation properties of matter (i.e. human body in medical Computed Tomography) are energy and material dependent. This dependency is largely neglected in conventional CT techniques, which require the introduction of correction algorithms in order to prevent image artefacts. The exploitation of the inherent energy information contained in the x-ray spectrum allows distinguishing the two main physical causes of energy-dependent attenuation (photo-electric effect and Compton effect). Currently a number of methods exist that allow assessing the energy-dependent attenuation in conventional systems. These methods consist of using two distinct spectra (kVp switching or dual source) or by discriminating low and high energy photons by means of stacking two detectors. Further improvements can be achieved by transitioning to direct-conversion technologies and counting-mode detection, which inherently exhibits a better signal-to-noise ratio. Further including energy discrimination, enables new applications, which are not feasible with dual-energy techniques, e.g. the possibility to discriminate K-edge features (contrast agents, e.g. Gadolinium) from the other contributions to the x-ray attenuation of a human body. The capability of providing energy-resolved information with two or more independent measurements is referred as Spectral CT.

A new proprietary photon counting ASIC (ChromAIX) has been developed to provide high count-rate capabilities while offering energy discrimination. The ChromAIX consists of a pixel array with an isotropic pitch of 300 µm. Each pixel contains independent discriminators which enable the possibility to discretize incoming photons into a number of energy levels. Extensive electrical characterization has been carried out to assess the performance in terms of count-rate performance and noise. Observed rates exceeding 10 Mcps/pixel (Poissonian, mean incoming rates > 27 Mcps). The energy resolution is better than 4.1 keV FWHM and has been shown to be consistent with simulations. Pile-up behaviour and count-rate dependency have also been evaluated. Electrical crosstalk among pixels in terms of count-rate activity and threshold position has been assessed and show no measureable influences across the array.

X-ray tests have also been performed on samples directly flip-chip bonded to CdTe and CZT crystals. The pulse shape and spectrum obtained from a ^{241}Am source is consistent with simulations.

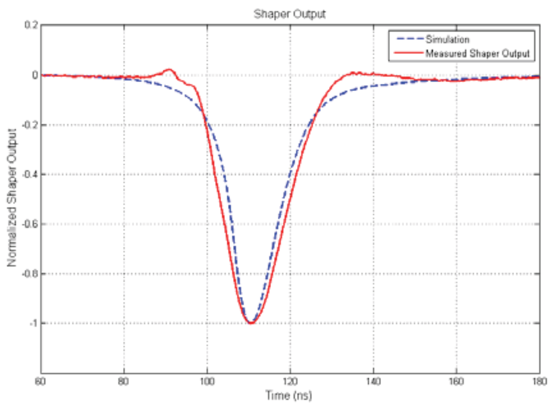

Figure 1. Measured and simulated shaper output at the same input equivalent energy of 100 keV, measured input injection circuit

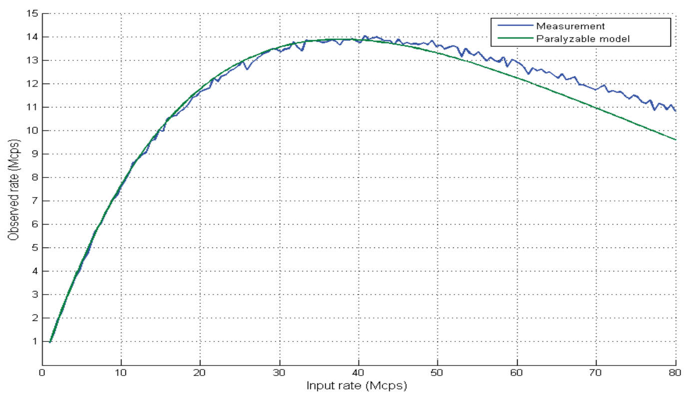

Figure 2. Count-rate performance at an input equivalent energy of 62 keV at a 40 keV threshold. Measured by injection of poisson distributed pulses

PIXELIZED M-π-n CDTE DIODE COUPLED TO MEDIPIX2 READ OUT CHIP

J. Kalliopuska[1], S. Nenonen[2], R. Penttilä, H. Pohjonen[1], A. Gädda[1], I. Vanttaja[1], H. Andersson[2], P. Laakso[1], J. Likonen[1], L. Tlustos[3]
[1] VTT Micro and Nanoelectronics, Tietotie 3, Espoo, PO. Box 1000, FI-02044 VTT, Finland
[2] Oxford Instruments Analytical Oy, Espoo FIN-02631, Finland
[3] CERN, PH/ESE, CH-1211 Geneva 23, Switzerland
email: juha.kalliopuska@vtt.fi

We have realized a simple method for patterning an M-π-n CdTe diode with a thick diffused junction, such as Indium anode on the CdTe. The method relies on removing semiconductor material on the anode side until the physical junction has been reached, as shown in Fig. 1. The pixelization of the p-type CdTe diode with an Indium anode has been demonstrated by patterning perpendicular trenches with a high precision diamond blade and laser. In this way, the pixelization or microstrip pattering can be done on both sides of the diode, also to the cathode side. Interstrip resistances of 100-200 GΩ on the anode side and 10-25 GΩ on the cathode side have been measured and published earlier [1].

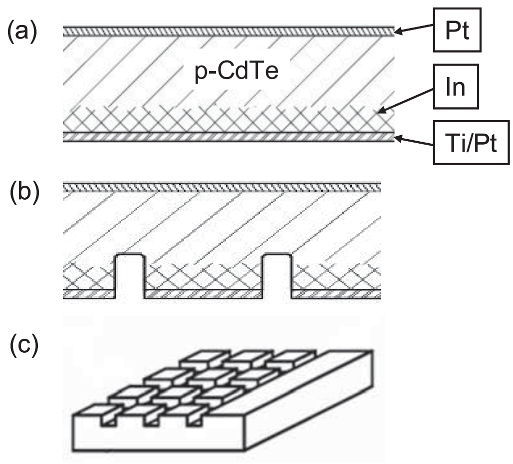

Fig. 2 (a) M-π-n CdTe diode with special metallization on the anode side. (b) Patterned anode side (c) Pixelized M-π-n CdTe diode.

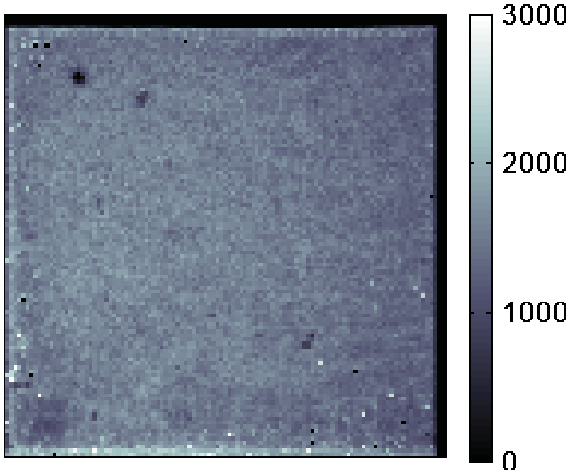

Fig. 1 Pixelized M-π-n CdTe diode, with 55 µm pitch, flip chip bonded to the Medipix2 ROC. Am-241 X-ray source image with acquisition time of 300 s.

The presentation compares the patterning quality of the diamond blade saw, picosecond and femtosecond lasers. New leakage current and inter-strip resistance measurements are presented and compared with the earlier ones. SIMS-characterization has been done for a diode to define the pn-junction depth and to see the effect of the thermal loads of the flip-chip bonding process. The anode side of a 6x6 mm^2 diode was patterned with a diamond blade and flip-chip bonded to the Medipix2 readout chip (ROC). First imaging results with the X-ray and electron sources are presented. Fig. 2 shows the first Am-241 X-ray image taken with a CdTe detector with a patterned pn-junction side.

[1] J. Kalliopuska, et al., *Patterning thick diffused junctions on CdTe*, Nucl. Instr. Meth. in Phys. Res. A, Volume 607, Issue 1, 1 August 2009, Pages 98-102, doi:10.1016/j.nima.2009.03.243.

Design and Feasibility Studies of a Stationary Digital Breast Tomosynthesis System

G. Yang[a], X. Qian[a], F. Sprenger[b], S. Sultana[c], X. Calderon-Colon[c], B. Kearse[b], D. Spronk[b], J. Lu[a], O. Zhou[a,c,d]

a: Department of Physics and Astronomy, University of North Carolina at Chapel Hill, Chapel Hill, NC, USA
b: XinRay Systems LLC, Research Triangle Park, NC, USA
c: Curriculum in Applied Sciences and Engineering, University of North Carolina at Chapel Hill, Chapel Hill, NC, USA
d: Lineberger Comprehensive Cancer Center, University of North Carolina at Chapel Hill, Chapel Hill, NC, USA

Digital breast tomosynthesis (DBT) is a three dimensional imaging technique which reconstructs slice images using projection images from a certain angular range. DBT can potentially improve the tumor conspicuity over conventional mammography by reducing tissue overlapping. Current prototype DBT scanners are based on single x-ray source full-field digital mammography (FFDM) systems. To acquire projection images from different angular positions, the x-ray gantry rotates during patient scanning. The total scan time is much longer than conventional mammography. The prolonged imaging time introduces more patient motion blur. The effective x-ray focal spot size is enlarged due to the x-ray source movement during exposure, which also degrades the image quality. To obtain three dimension reconstruction images while maintain the high image quality of conventional mammography, we proposed a prototype stationary digital breast tomosynthesis system (s-DBT). The proposed s-DBT system acquires projection images without mechanical movement, and the scan time can be significantly shorter than the regular DBT scanners. The core component of the s-DBT system is a specially designed distributed multi-beam x-ray tube based on the carbon nanotube field emission x-ray source technology. The multi-beam x-ray source array replaces the x-ray gantry of a commercial mammography system. The performance of the multi-pixel x-ray tube is characterized, including focal spot size, output, variation and lifetime. The control interface of x-ray tube, detector, and electronics is customized, and these system components can be controlled and synchronized through a work station.

Latest Developments in Micro and Nano Tomography at PETRA III

A. Haibel, F. Beckmann, T. Dose, M. Ogurreck, F. Wilde, M. Müller, A. Schreyer

Institute of Materials Research, GKSS Research Centre, Max Planck-Str. 1,
21502 Geesthacht, Germany

Developments of novel materials and production technologies are significantly linked by fundamental understanding of the materials characteristics, especially the three dimensional inner structures. Characteristic length scales, which influence these structural properties, are often in the range of some micrometers down to a few nanometers.

The unique beam characteristics of the new storage ring PETRA III at DESY in Hamburg promote novel applications of tomographic techniques enabling high speed in-situ measurements with highest density resolutions and spatial resolutions down to the nanometer range. Additionally, the highly coherent beam enables the application of phase contrast methods in an exceptional way.

Therefore, the Imaging Beamline IBL will be equipped with a micro and a nano tomography endstation, as well as with a smart X-ray and light optics concept. The energy range is tunable between 5 and 50 keV. The technical specifications of the tomographic endstations aim for spatial resolutions from the (sub-) micrometer range down to 50 nm.

We will present the tomography instrumentation including the implementation of sample adjustment units which minimize tilt errors, first nanometer resolution tests obtained by using X-ray lenses, the sample changer concept, the slip ring concept for the rotation stage, and the concept to combine of tomographic techniques with diffraction.

Singular-value decomposition of a tomosynthesis system

Anna Burvall,[1] Harrison H. Barrett,[2] Kyle M. Myers,[3] and Christopher Dainty[4]

[1] *Biomedical and X-Ray Physics, Royal Institute of Technology, SE-10691Stockholm, Sweden*

[2] *College of Optical Sciences and Dept. of Radiology, Univ. of Arizona, Tucson, AZ 85724*

[3] *NIBIB/CDRH Laboratory for the Assessment of Medical Imaging Systems, Rockville, MD 20850*

[4] *Applied Optics, Dept. of Experimental Physics, National University of Ireland, Galway, Ireland*

Tomosynthesis [1] is an emerging technique for breast and chest screening, where the two-dimensional (2D) x-ray projection of e.g. mammography is replaced by a number of images taken at a varying but limited angle. Sometimes referred to as "lightweight tomography", it provides partial three-dimensional (3D) information on the object in question. Prototype tomosynthesis systems have already been developed and pilot clinical trials performed [2]. We present an analytical singular-value decomposition (SVD) of a tomosynthesis system, which provides the measurement component of any given object [3]. The method, which is similar to an earlier 3D system analysis [4], is demonstrated on an example object. The measurement component can be used as a reconstruction of the object, and can also be utilized in future observer studies of tomosynthesis image quality.

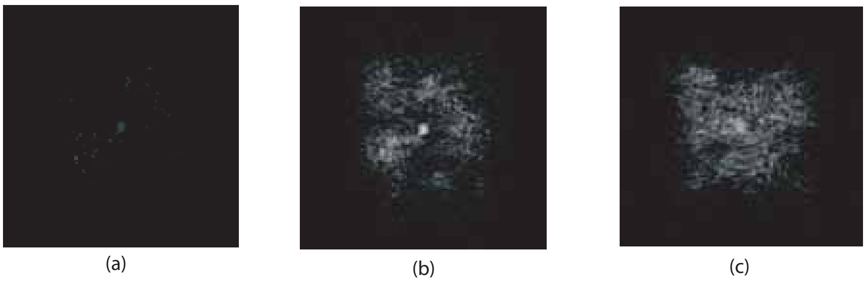

Figure 1: (a) Transverse slice of object, (b) the same transverse slice of its measurement component, and (c) 2D projection of object.

Figure 1 shows a transverse slice through an example object, its measurement component, and its 2D projection. The object is a clustered lumpy background (CLB) with an overlapping designer nodule. The CLB has been extended from 2D to 3D by redistributing the functions in 3D, an approach that is obviously not sufficient since the result is much too sparse for breast tissue. Still, it is interesting to notice how the measurement component is a hybrid between the object and its projection. This is because the object is in full 3D and the projection in 2D, while the measurement component in tomosynthesis contains partial 3D information. More results are readily obtained from our SVD model.

[1] J.T. Dobbins III, "Tomosynthesis: at translational crossroads," Med. Phys. **36**, 1956–1967 (2009).

[2] G. Gennaro, A. Toledano, C. di Maggio, E. Baldan, E. Bezzon, M. La Grassa, L. Pescarini, I. Polico, A. Proietti, A. Toffoli, and P.C. Muzzio, "Digital breast tomosynthesis versus digital mammography: a clinical performance study," Eur. Radiol. 10.1007/s00330-009-1699-5 (2009).

[3] H.H. Barrett and K.J. Myers, *Foundations of Image Science* (John Wiley, Hoboken, New Jersey, 2004).

[4] A. Burvall, H.H. Barret, C. Dainty, and K.J. Myers, "Singular-value decomposition for through-focus imaging systems," J. Opt. Soc. Am. A, **23**, 2440–2448 (2006).

From Image Science to Image-Guided Surgery

Jeffrey H. Siewerdsen, Ph.D.
Department of Biomedical Engineering, Johns Hopkins University
Baltimore MD USA 21205

The development of large-area flat-panel x-ray detectors (FPDs) has spurred investigation in a spectrum of advanced medical imaging applications, including high-performance dual-energy (DE) imaging, tomosynthesis, and cone-beam CT (CBCT). Recent research has extended image quality metrics and theoretical models to such applications, providing a quantitative foundation for the assessment of imaging performance as well as a powerful framework for the design, optimization, and translation of such technologies to new applications. For example, cascaded systems models of Fourier domain metrics, such as noise-equivalent quanta (NEQ), have been extended to each of these advanced modalities to describe the propagation of signal and noise through the imaging (and image reconstruction) chain and to quantify the factors that govern spatial resolution, image noise, and detectability. Moreover, such models have demonstrated agreement with human observer performance for a broad range of imaging conditions and imaging tasks. These developments in image science have formed a strong foundation for the development and translation of new imaging technologies – for example: high-performance DE imaging of the chest that transcends conventional dose / detectability limitations of radiographic lung nodule detection; and CBCT implemented on a mobile surgical C-arm for intraoperative 3D imaging. (See Figure 1.) The ability to acquire high-quality 3D images on demand during surgical intervention overcomes conventional limitations of surgical guidance in the context of preoperative images alone. A prototype mobile C-arm demonstrates CBCT with low radiation dose, sub-millimeter spatial resolution, and soft-tissue visibility approaching that of diagnostic CT. Integration of the 3D imaging system with real-time tracking, registration, endoscopic video, and 3D visualization offers a promising addition to the surgical arsenal in interventions ranging from head-and-neck surgery to spine, orthopaedic, thoracic, and abdominal surgeries. Cadaver studies show the potential for significant boosts in surgical performance under CBCT guidance, and early clinical trials demonstrate feasibility, workflow, and image quality within the surgical theatre.

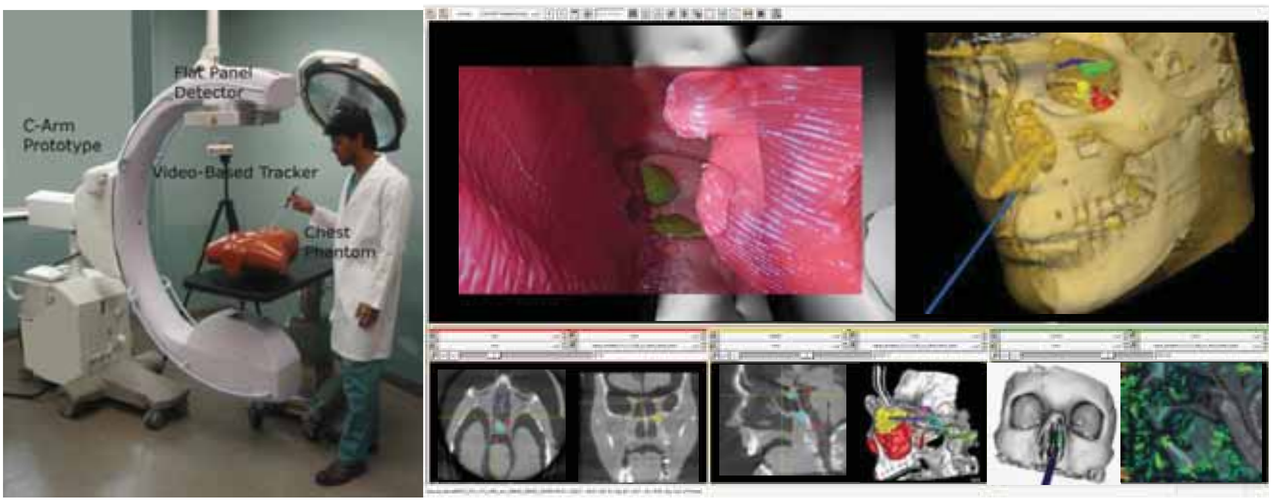

Figure 1. Cone-beam CT for image-guided surgery. (left) Photograph of a prototype mobile C-arm developed to provide intraoperative 3D images with sub-millimeter spatial resolution and soft-tissue visiblity. (right) Example "screenshot" illustration of intraoperative information available to the surgeon, including: (top left) real-time video endoscopy registered to CBCT and planning data; (top right) volumetric display of image data, planning data (target and normal structures highlighted in colors), and real-time tracking (blue line indicating the position of a tool inserted in the sinuses); (bottom row) 3D slice and surface views of CBCT with target and normal anatomy segmented in surgical planning; and (bottom right) deformable registration of preoperative CT, MR, and planning data to the most up-to-date intraoperative CBCT image.

Regularized versus Non-Regularized Statistical Reconstruction Techniques

N.V. Denisova

Institute of Theoretical and Applied Mechanics,
630090, Novosibirsk, Russia

An important feature of Positron Emission Tomography (PET) and Single Photon Emission Computer Tomography (SPECT) is the stochastic property of real clinical data. Statistical algorithms such as Maximum Likelihood – Expectation Maximization (ML-ME) and Maximum a Posteriori (MAP) are a direct consequence of the stochastic nature of the data [1-2]. The principal difference between these two algorithms is that ML-EM is non-regularized approach, while the MAP is regularized algorithm. From the theoretical point of view, reconstruction problems belong to the class of ill-posed problems and should be considered by using regularization. Regularization introduces an additional unknown *regularization* parameter into the reconstruction procedure as compared with no regularized algorithms. However, a comparison of non-regularized ML-EM and regularized MAP algorithms has shown very minor difference between results of reconstructions [3-4]. This problem is analyzed in the present paper. We have shown that using of empirical constant regularization parameter equalized the MAP algorithm with ML-ME approach. To improve reconstruction quality, a new numerical strategy based on the spatially adaptive regularization parameter is developed. The MAP algorithm with adaptive regularization was tested in reconstruction of the Hoffman brain phantom.

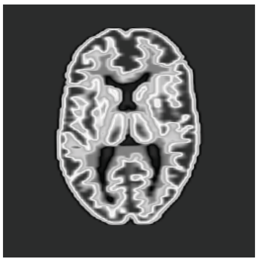

Fig.1. A slice of the Hoffman brain phantom.

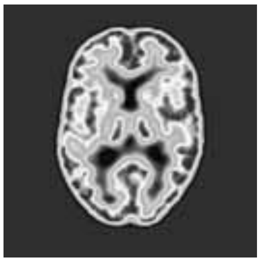

Fig.2. Reconstruction with the MAP algorithm using adaptive regularization parameter.

1. N.V. Denisova Bayesian Reconstruction in SPECT With Entropy Prior and Iterative Statistical Regularization // IEEE Trans. on Nuclear Science. 2004. V.51 P.136-141.
2. N.V.Denisova Reconstruction of heart images using emission tomography // Mathematical modeling 2007. V. 19. №1. C. 104-116.(in Russian)
3. Lalush, D. S., E. C. Frey, and B. M. W. Tsui Fast maximum entropy approximation in SPECT using the RBI-MAP algorithm // IEEE Trans. Med. Imag. 2000. V. 19. P. 286-294.
4. Nuyts J., J.A. Fessler. A penalized-likelihood image reconstruction method for emission tomography, compared to post-smoothed maximum-likelihood with matched spatial resolution // IEEE Trans. Med. Imag. 2003. V. 22. P. 1042-52

Partial volume correction in SPECT reconstruction with OSEM

Kjell Erlandsson, Ben Thomas, John Dickson and Brian F Hutton
The Institute of Nuclear Medicine, University College London, London, UK

Background: SPECT images suffer from poor spatial resolution which leads to partial volume effects due cross-talk between different anatomical regions. By utilizing data from a high-resolution structural imaging modality (CT or MRI) it is possible to compensate for these effects. Traditional partial volume correction (PVC) methods suffer from various limitations, such as assuming a stationary point spread function (PSF), limited number of regions or returning only regional mean values.

Aims: We recently presented a novel method (1) in which PVC was combined with the reconstruction process, based on filtered backprojection (FBP), in order to take into account the distance dependent PSF in SPECT. We now present a new method in which PVC is incorporated into the OSEM reconstruction algorithm, which has advantageous noise-properties compared to FBP. We also present results obtained with SPECT data from brain studies on healthy volunteers.

Methods: SPECT studies were performed with a GE Infinia/Hawkeye scanner on 10 healthy subjects after injection of the dopamine transporter tracer ^{123}I-FP-CIT (DATSCAN). Each subject also had a T1-weighted MRI scan which was realigned to the SPECT image-space using the SPM co-registration tool and segmented into 32 anatomical regions using the Freesurfer software. The SPECT data were reconstructed using OSEM, and PVC was applied at each iteration in the projection domain. The PVC factors were calculated by forward projection of a piece-wise constant pseudo-image with and without distance-dependent resolution modelling, as described in (1). The pseudo-image was generated from the segmented MRI where each region contained the mean value from the current image estimate. Images were also reconstructed using standard OSEM with and without resolution recovery (RR) for comparison. All reconstructions were done using 10 subsets of 12 projections each. 8 iterations were used for OSEM and OSEM-PVC, and 16 iterations for OSEM-RR. A Butterworth smoothing-filter was applied to all images.

Results: Reconstructed images from one of the subjects are shown in figure 1 for the different reconstruction methods. The OSEM-RR image has higher intensity in the basal ganglia as compared to the OSEM one, but the structural definition is poor. On the other hand, the OSEM-PVC image has both higher intensity and improved structural definition. The mean binding potential in the basal ganglia increased by 37% with OSEM-RR and by 45% with OSEM-PVC as compared with standard OSEM.

Conclusions: Our new method, OSEM-PVC, results in images with visually improved structural definition as well as higher quantitative uptake values as compare to standard techniques.

Reference: 1) Erlandsson K, Hutton BF (2010) *Tsinghua Sci Techn*, **15**(1):50-55.

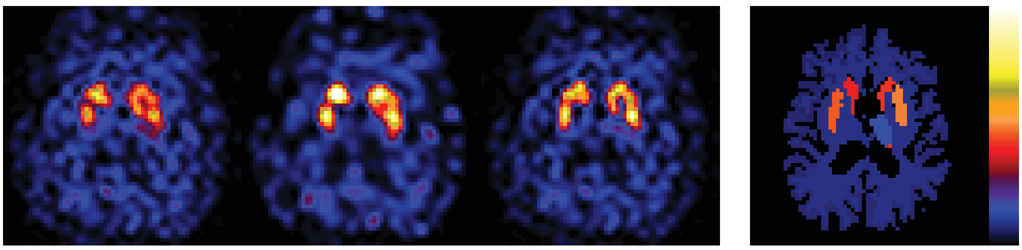

Figure 1: The three pictures on the left show reconstructed SPECT images from a healthy volunteer using (from left to right) OSEM, OSEM-RR and OSEM-PVC. The picture on the right shows the segmented MRI with regional mean values from the OSEM-PVC image, for comparison.

Theory and algorithms for phase-contrast tomography with synchrotron and laboratory sources

Andrei V. Bronnikov

Bronnikov Algorithms
P.O. Box 77 6800AB Arnhem The Netherlands

Keywords: phase contrast, micro CT, image reconstruction, high resolution, cone-beam CT

Recent developments in detectors and x-ray sources have led to emergence of a new imaging modality: phase-contrast imaging. Unlike conventional x-ray imaging, phase-contrast imaging is based not on attenuation of the x rays in the medium, but on the information of the phase shifts of the beam penetrating through the object. This type of imaging can be implemented at third generation synchrotron radiation sources or by using a laboratory source. In the first case, phase contrast is observed because of high spatial coherence of synchrotron radiation; in the latter case, the necessary level of spatial coherence is achieved due to geometrical characteristics of the microfocus source and high-resolution detector. In both cases, by rotating the sample in the propagating beam, a tomographic data set can be acquired, and a 3D image of the sample can be reconstructed. However, the lack of a mathematical theory comparable to that of conventional attenuation-based tomography has substantially limited the progress in this field. In the series of papers, the author has suggested such a theory and proved a fundamental theorem that plays the same role in phase-contrast tomography as the Fourier slice theorem does in conventional tomography. The fundamental theorem establishes a straightforward relation between the three-dimensional Radon transform of the object function and the two-dimensional Radon transform of its phase-contrast projection and allows one to derive image reconstruction algorithms in the form of filtered backprojection (FBP). The FBP algorithms are the fast image reconstruction algorithms, which makes them ideally applicable for processing huge volumes of high-resolution phase-contrast data. The suggested approach requires no phase retrieval and provides a closed-form solution to the problem of exact quantitative reconstruction of the refractive index from the intensity measurements. Purely phase objects can be reconstructed from tomographic data acquired in a single plane in the near field region. Reconstruction of the mixed phase and amplitude objects requires additional information of absorption, which can be obtained experimentally or generated numerically; both approaches are discussed in the paper. The theory is also extended to cone beams such as produced by microfus tubes, which allows developing algorithms for cone-beam phase-contrast tomography with laboratory sources. The author makes the overview of all existing approaches to acquire and reconstruct phase-contrast data in parallel beams (at synchrotrons) and cone beams (laboratory sources). A number of novel developments in increasing quantitative accuracy of phase-contrast tomography are addressed. An overview and comparison of all existing methods of inline-mode phase-contrast tomography is presented. The results of reconstruction of computer-generated and experimental data are discussed.

1. A.V. Bronnikov, "Reconstruction formulas in phase-contrast tomography," Optics Communications, vol. 171, pp. 239 –244, 1999.
2. A.V. Bronnikov, "Theory of quantitative phase-contrast computed tomography," J. Opt. Soc. Am. A, 19, pp. 472-480, 2002.
3. A.V.Bronnikov, Phase contrast CT: Fundamental theorem and fast image reconstruction algorithms, Developments in X-Ray Tomography V. Edited by Bonse, Ulrich. Proceedings of the SPIE, Volume 6318, pp. 63180Q (2006).
4. www.bronnikov-algorithms.com

Reproducibility Evaluation of I-123 ADAM SPECT Imaging Using SPM Software and AAL ROI Methods

Bang-Hung Yang[1,2], Shyh-Jen Wang[1,2], Yuan-Hwa Chou[3], Chen Chia Jay[4], Jyh-Cheng Chen[1,5]

[1] Department of Biomedical Imaging and Radiological Sciences, National Yang-Ming University, Taipei, Taiwan, R.O.C

[2] Department of Nuclear Medicine, Taipei Veterans General Hospital, Taiwan, R.O.C

[3]Department of Psychiatry, Taipei Veterans General Hospital, Taipei, Taiwan, R.O.C

[4]Institute of Nuclear Energy Research, Longtan , Taiwan, R.O.C

[5]Department of Education and Research, Taipei City Hospital, Taipei, Taiwan, R.O.C

Abstract

The level of serotonin is regulated by serotonin transporter (SERT), which is a crucial protein in regulation of serotonin neurotransmission system. Many psychiatric disorders are also related to serotonin in human brain. I-123 ADAM is the novel radiopharmaceutical to image SERT in brain. The aim of this study was to measure test-retest variability of SERT densities by anatomical automatic labeling (AAL) method. Furthermore, we also used statistic parameters mapping (SPM) on a voxel by voxel analysis to find difference between test and retest of I-123 ADAM single photon emission computed tomography (SPECT) images.

Twenty-four healthy volunteers were scanned twice with SPECT four hours after intravenous administration of 185 MBq of ^{123}I-ADAM. The image matrix size was 128×128 and pixel size was 3.9 mm. All images were obtained through filtered back-projection reconstruction algorithm. Region of interest (ROI) definition was performed based on AAL brain template in PMOD version 2.95 software package. ROI demarcations were placed on midbrain, pons, cerebrum, and striatum. SPM integrated the general linear model to create the statistical map and the theory of Gaussian fields to derive regional effect from statistical inference. All images were spatially normalized to the SPECT MNI (Montreal Neurological Institute) templates supplied with SPM2. And each image was transformed into standard stereotactic space which was matched to the Talairach and Tournoux atlas. Then differences across scans were statistically estimated on a voxel by voxel analysis using paired t-test (Population main effect: 2 cond's, 1 scan/cond.) which was applied to compare concentration of SERT from the test and retest cerebral scans.

The specific uptake ratio (SUR: target/cerebrum-1) of ^{123}I-ADAM binding to SERT in midbrain was 1.87, pons was 1.81, and striatum was 0.98. The test-retest SUR variability was -1.62±1.32. Besides, there was also no significant statistical finding in cerebral area using SPM2 analysis. This finding might help us to understand reliability of I-123 ADAM SPECT imaging and further develop new strategy for the treatment of psychiatric disorders.

Attenuation correction without transmission scan for the MAMMI breast PET.

A.Soriano[1], A.Orero[1], L.Moliner[1], M.Carles[1], F.Sánchez[1], JM.Benlloch[1], AJ.González[2], C.Correcher[2], V.Carrilero[2], M.Seimetz[2]
[1]IFIC (Universitat de València – CSIC), Valencia (SPAIN)
[2]ONCOVISION (GEM-Imaging group), Valencia (SPAIN)

Abstract
Breast cancer is the most prominent form of cancer diagnosed in women [1], although death rates have been decreasing since 1990. Treatment advances, earlier detection through screening, and increased awareness, are responsible for this decrease. Positron emission tomography (PET) scanning is routinely used in assessing therapy response, staging and restaging of breast cancer [2, 3]. However, whole-body PET scanners are limited by low geometric sensitivity, low spatial resolution and signal loss due to attenuation in the body. These factors reduce their utility in detecting small lesions (< 1 cm) and/or those with low tracer uptake [4]. Since breast cancer patients frequently present lesions smaller than 1 cm in size, this is a significant limitation in the management of primary breast cancer.
In this work we present the design and preliminary results obtained with the MAMMI Breast PET. MAMMI is a dedicated breast PET scanner which consists of 12 detector modules shaping a dodecagon with a scanner aperture of 186 mm. Each detector head contains a single monolithic scintilliating LYSO crystal, a position sensitive photomultiplier (PSPMT) and the readout and high voltage power supply electronics [5]. By measuring the widht of light distribution collected in the PSPMT we determine Depth of Interaction (DOI) [6], thus making possible the correct identification of LORs with large incidence angles. A 170 mm diameter transaxial FOV is available in the scanner. Dead time, scatter and random events are compensated in the MLEM 3D reconstruction. The new and dedicated MAMMI Breast PET has demonstrated to acquire images with a spatial resolution near 1.5 mm. This scanner has been successfully tested at the pre-clinical level, and a clinical validation is under progress at the Netherlands Cancer Institute in Amsterdam (NKI-Amsterdam).
PET data attenuation originated by the loss of true events due to scatter and absorption, produces overall count losses, thus reducing the data signal-to-noise ratio (SNR) and worsening the quantification of radioactivity concentration. The increased noise effects can not be solved, while the quantitative accuracy of radioactivity distribution can be recovered with attenuation correction (AC). Another effect of attenuation is to introduce non-uniformities into reconstructed images. This will produce images showing artificially depleted radioactivity deeper in the body, while a “bright” outer contour of the body is observed.
In dedicated, high resolution breast cancer, AC correction would improve the proper diagnosis in early disease stages. In whole-body PET scanners, AC is usually taken into account by means of transmission scans, either by external radioactive rod sources [7] or by Computed Tomography (CT) [8]. Since a transmission scan significantly increases the radiation dose to the body, and adds considerable time in the case of rod sources, calculated AC methods have been proposed. The calculated methods are foreseen to work properly well in the case of imaging organs with almost constant tissue density and regular geometric body outline, producing accurate noise-free attenuation factors [9]. For the above reasons these methods seem to be more suitable than the transmission methods for breast PET studies. In this work we propose a method for breast shape identification, by means of PET image segmentation. The breast shape identification will be used for the determination of the AC. For the case of a specific breast PET scanner the procedure we propose should provide AC similar to that obtained by transmission scans as we take advantage of the breast anatomical simplicity. The main advantage of the attenuation correction proposed is an important dose reduction since the transmission scan is not required.

References
[1] Ferlay J et al. (2007) *Annal. Oncol.*, 18(3):581-592
[2] Linden HM et al. (2006) *Journal of Clinical Oncology*, 24(18):2793-2799
[3] Eubank WB et al. (2005) *Seminars in Nuclear Medicine*, 32(2):84-99
[4] Avril N et al. (2000) *Journal of Clinical Oncology*, 18(20):3495-3502
[5] Benlloch JM et al. (2007) *Nuclear Instruments and Methods in Physics Research A*, 571:26-29
[6] Lerche ChW et al. (2005) *IEEE Transactions on Nuclear Science*, 52(3):560-572
[7] Yu KS et al. (1995) *Physics in Medicine and Biology*, 40:1255-1266
[8] Beyer T et al (2000) Journal of Nuclear Medicine, 41:1369-1379
[9] Siegel S et al (1992) IEEE Transactions on Nuclear Science, 32(4):1117-1121

On the Limitations and Optimisation of High-Resolution 3D Medical X-ray Imaging Systems

Shu-Ang Zhou* and Anders Brahme
Karolinska Institutet, Department of Oncology-Pathology
Box 260, SE-171 76 Stockholm, Sweden

Abstract --- X-ray imaging has played a dominating role in medical imaging and diagnostics over more than one hundred years. Despite of technology progresses during the past century, we are still limited in our ability to detect tumors in their earliest stages, monitor tumor phenotype, quantify early invasion and metastasis, and to visualize *in vivo* the effectiveness of anticancer treatments in real-time. Great challenges remain in detecting small sub-clinical malignant tumors of sizes less than 1–2 mm, which are mostly localized at its early stage when significant angiogenesis has not yet been initiated. Unfortunately, at present, no clinical imaging modalities are available to obtain 3D medical images of these tumors with sufficient resolution (< 0.1 mm) and good diagnostic accuracy in humans. This is mainly due to intrinsic limitations of conventional attenuation-based X-ray imaging techniques, planar or CT. Other commonly used imaging modalities, such as PET, magnetic resonance imaging and ultrasound have similar limitations in detecting arbitrarily located small tumors with sufficient image contrast, resolution and clinical specificity for human patients.

Here, based on a quantitative analysis of both attenuation and refractive properties of X-ray propagation in human body tissues and introduction of a mathematical model for image quality analysis, some issues on limitations and optimisation in developing high-resolution 3D medical X-ray imaging techniques are studied. In this paper, a comparison is made of conventional attenuation-based X-ray imaging with the recent phase-contrast X-ray imaging modalities. The results indicate that it is possible through optimal design of the X-ray imaging system to achieve high image resolution (< 0.1 mm) in 3D medical X-ray imaging of human body at a clinically acceptable dose level (< 10 mGy) by using the phase-contrast stereoscopic X-ray imaging technique. With such a high image resolution, it should then become possible to differentiate early-stage tumors of sizes around 1 or 2 mm, resolve their geometrical shapes, and improve significantly our diagnostic capability in detecting early-stage cancers, and therefore, hopefully increase cure rates and significantly reduce the risk of patients to get metastatic diseases if these early-stage tumors could be identified and eliminated. At present, although large synchrontron radiation facilities can be utilized to implement and test high-resolution 3D medical X-ray imaging techniques and systems for human body imaging, further research and development of innovative compact X-ray sources with high spatial coherence are required to generate sufficiently high fluxes of hard X-ray photons in order to achieve high-resolution 3D medical X-ray imaging with the wide diagnostic range desirable in hospital care.

Key words: High-resolution tumor imaging; Phase contrast; Stereoscopic imaging; X-ray imaging

Acknowledgement: Support from Cancer Society in Stockholm is gratefully acknowledged.

*Email: shu-ang.zhou@telia.com

A new iterative algorithm for position calculation for scintillating gamma-ray detector

A.Fabbri[1,2], V.Orsolini Cencelli[1,3], P. Bennati[1,2], F. de Notaristefani[1,3], T.Baroncelli[1], F.Petullà[1,2], E.D'Abramo[1,2], G. Moschini[4,5], F. Navarria[6,7], M.N. Cinti[8,9], R.Pellegrini[8,9], R.Pani[8,9].

[1]INFN Roma3; [2]EDEMOM PhD school of Electronics, "Roma Tre" University; [3]Physics Dept., "Roma Tre" University, Rome Italy; [4]LNL-INFN, Padua; [5]Physics Dept., Univ. Padua, Italy; [6]INFN Bologna; [7]Physics Dept, Bologna University, Italy; [8]INFN Roma1; [9]Dept. of Experimental Medicine, "Sapienza" University, Rome Italy.

In recent years a great deal of attention was given to the Hamamatsu Position Sensitive photo tubes (PSPMT), due to their suitability for building compact and high spatial resolution gamma cameras. In order to improve image performances from the PSPMT, a readout electronics that reads each channel individually could be chosen, but a great care must be also taken in designing and tuning the calculation of the scintillation point in which the photon has actually interacted within the crystal. The use of a standard center of gravity (CoG) based algorithm limited the diffusion of continuous crystal due to a strong image compression, but also scintillation crystal in array configuration could be impaired.
In this work, a mean square estimation (MSE) based algorithm for the interaction position calculation is presented. The performances analysis take into account different scintillation crystals pixelated and continuous shape, coupled to an Hamamatsu H8500 PSPMT with 8x8 segmented anodes. The readout electronics presents 64-independent channels each reading simultaneously the 64 anodes of the PSPMT. An array of NaI(Tl) with 1.8mm pixel and 2.0 mm pitch, one of CsI(Tl) with 1.6 mm pitch, and two YAP with 2.0 mm and 0.6 mm pixel size and continuous crystal of $LaBr_3$(Ce) and NaI(Tl), this study encompass also crystals in integral line assembly with the detector. The LaBr3(Ce) crystal was also coupled to an H8500-MOD8 PS-PMT equipped with a super-bialkali photocatode (38% QE at 380nm). Energy and spatial resolution were analyzed with a Co57 radioactive source and the scintillation points are calculated both with MSE and CoG algorithm for comparison. The MSE algorithm expands the useful field of view (UFOV) of the gamma camera up to almost the dimension of the PSPMT detector, giving a great advantage with respect to the CoG algorithms also with continuous crystal where a relevant reduction of the UFOV is present due to the truncation of the light distribution. With pixilated crystals, the MSE improve pixel identification with the array of CsI(Tl) and NaI(Tl) crystals where they were about 0.8 mm and 0.6mm, respectively. The new algorithm identifies all the 25 pixels of the NaI(Tl) one corresponding to the overall detector area. LaBr and NaI continuous crystals have shown a very good response, it must be pointed out that the new H8500-MOD8 coupled with $LaBr_3$ crystal shows an impressive spatial and energy resolution of 0.85 mm and 7.0% respectively, at 140 keV photon energy.
The iterative method was optimised by means of convergence techniques that allow the calculation of the interaction point at the speed of thousands of event per second on a standard PC. The study of the different light shapes obtained by different crystals, continuous and pixellated, has shown the need of adapting the fit function to the different crystal types in order both to maximise the spatial resolution and minimize the computation times. This study pointed out several problems to which a solution has been suggested. In addition, a Montecarlo simulation of the gamma photon and crystal interactions were very useful in this respect, with the aim to separate the different sources of distortion. The distortion due to the uneven anodic gain, the distortion due to the crystal edge reflection (in the case of continuous crystals) and, particularly for the low amplitude signals found in the last generation devices, the distortion introduced by the pre-charge of the feedback capacitor. Correction procedures were adopted that take into account these distortions and give better images. A final study took into account the computation times and the errors at the convergence point that are also available at the end of the computation, giving further improvements to the image quality for double hits, pile up events, and a malformed light distribution can be identified and excluded from the image.

High-Resolution Compton Imaging: From Concept to Applications

K.Vetter
Department of Nuclear Engineering, UC Berkeley, Berkeley, CA 94720
Nuclear Science Division, Lawrence Berkeley National Laboratory, Berkeley, CA 94720

Advances in the fabrication and the readout of segmented semiconductor detectors have enabled the development and demonstration of high-resolution Compton-scattering based gamma-ray imaging systems, so-called Compton cameras.
Our efforts focus on the development of high-resolution Si and Ge detectors enabling high-efficiency and high resolution. We have developed the Compact Compton Imager which consists of 2 large-volume Si(Li) and 2 large-volume HPGe detectors, all in double-sided strip configuration. We have continued to refine the signal shape analysis to improve the identification and localization of multiple interactions in the detectors as well as data processing and image reconstruction schemes to enhance the performance of the spectroscopic imaging capabilities. Examples are combination of spectral and image data, the ability to reconstruct radioactivity distributions in three dimensions in the near and far field, and the combination of gamma-ray image and complementary information, e.g. from laser mapping instruments. We are currently evaluating the feasibility of measuring the track of the Compton-scattered electron in high-resolution and fully depleted CCD systems. We were able - for the first time – to measure electron tracks in Si devices down to 100 keV and to reconstruct gamma rays based on the obtained information.
Preliminary results indicate a significant gain in detection and imaging capabilities.
We will provide an overview on the different aspects of our program in gamma-ray imaging and will discuss their applications in homeland security, nuclear safeguards, and biomedical imaging.

Acknowledgements
This material is based upon work supported by the U.S. Department of Homeland Security under the Grant Award Number 2008-DN-077-ARI-001-02.

Compton imaging with the PorGamRays detector

D S Judson[1], A J Boston[1], P J Coleman-Smith[2], D M Cullen[3], A Hardie[4], L J Harkness[1], L L Jones[4], M Jones[1], I Lazarus[2], P J Nolan[1], V Pucknell[2], S V Rigby[1], P Seller[4], J Simpson[2], M Slee[1], and the PorGamRays collaboration

1 The University of Liverpool, UK

2 STFC Daresbury Laboratory, UK

3 The University of Manchester, UK

4 STFC Rutherford Appleton Laboratory, UK

The PorGamRays project aims to develop a portable, hand-held, battery operated radiation detection system with both spectroscopic and imaging capabilities for a range of gamma-ray energies between 60 and 2000 keV. The system is designed to utilise a stack of thin (2 mm) cadmium zinc telluride (CZT) detectors. The imaging capability utilises the Compton Camera principle. Each of the detectors is segmented into 100 pixels which are read out through custom designed Application Specific Integrated Circuits (ASICs). This system has potential applications in the security, decommissioning and medical fields.

The work presented here focuses on the near-field imaging performance of lab-based demonstrator consisting of two 100-pixel CZT detectors bonded to two NUCAM II ASICs [1]. Measurements have been made with ^{133}Ba and ^{57}Co sources located ~ 40 mm from the absorber detector surface. Images have been generated using an analytical back projection algorithm. Position resolution of ~ 20 mm FWHM in the x and y-plane has been demonstrated along with the ability to distinguish multiple gamma-ray sources in a single measurement. A typical image is shown in figure 1. Geant4 simulations have been performed to validate and evaluate these results. This simulated data will also be discussed.

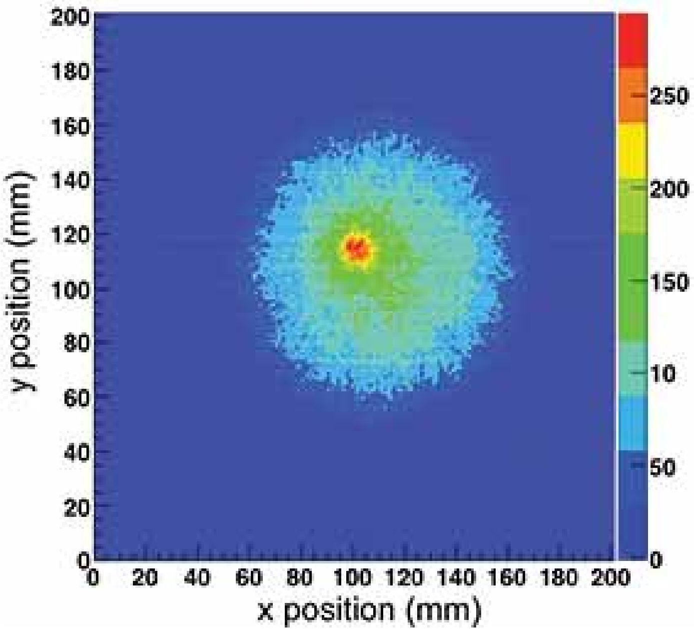

Figure 1. A typical experimental Compton image generated from the PorGamRays test system. The image was acquired using a ^{133}Ba point source located 40 mm from the face of the absorber detector.

[1] P Seller et. al. IEEE Nuclear Symposium Conf. Rec., vol 6, pp. 3786-3789, 2006

Compton Imaging Capabilities of AGATA with planar detectors for Background Rejection in DESPEC

M. Doncel[a], B. Quintana[a], A. Gadea[c,d], F. Recchia[b], and E. Farnea[b]

[a]*Laboratorio de Radiaciones Ionizantes, Universidad de Salamanca, Spain*
[b]*INFN sezione di Padova, Padova, Italy*
[c]*IFIC Valencia, Valencia, Spain*
[d]*INFN Laboratori Nazionali di Legnaro, Legnaro, Italy*

In this work, we present the results obtained by MC simulations when the background suppression algorithm developed for AGATA [1] it is applied to the DESPEC experiment [2]. The aim is to characterize the capabilities of the system made up by AGATA and an array composed of planar Ge detectors to discriminate between different γ source locations. AGATA segmented-contact Ge detectors and stripped-contact planar detectors are position sensitive to the interaction points through Pulse Shape Analysis allowing location of the γ sources simply by using a reconstruction algorithm based on the Compton formula.

The geometry considered for the analysis has been implemented in a MC simulation and is based on the system composed by AGATA 1π and a set of planar Ge detectors of dimensions 70*70*20 mm^3 placed between the sources and the AGATA detectors. AGATA, where the most interactions points are located, is placed in its nominal position at 23 cm from the target. The planar array is placed close to the emitting source for the first interaction to have a higher probability to occur in one of the planar detectors. In this configuration the distance between the first and second interaction points is large enough to perform imaging.

The algorithm is based on the comparison of the scattering angle of the photon as it is obtained from the kinematic of the Compton scattering with the value which is obtained from geometrical considerations. Only events with two interaction points, being the first one in a planar detector with 1 mm position resolution [3,4], are taken into account. The first interaction is considered as a Compton scattering and the second as a photoelectric interaction in AGATA, with 5 mm position resolution [5]. At this stage, the algorithm can separate properly the different spectra corresponding to each source location, being the γ transitions clearly assigned to different sources.

[1] M. Doncel et al,. "Experimental test of the background rejection through imaging capability of a highly segmented AGATA germanium detector". Not published yet.
[2] http://personal.ph.surrey.ac.uk/~phs1zp/Home.html
[3] A. Khaplanov et al., Nucl. Inst. and Meth. A 592 (2008) 325–333.
[4] C.S. William et al., IEEE Transactions on Nuclear Science, Vol 57 (2010) 860-869.
[5] F. Recchia et al., Nucl. Inst. and Meth. A 604 (2009) 555.

Compton Camera development for the imaging of high energy gamma rays

M. JONES[1], A.J. Boston[1], H.C. Boston[1], R.J. Cooper[1*], M.R. Dimmock[1+], A.N. Grint[1], L.J. Harkness[1], D.S. Judson[1], J. McGrath[1], P.J. Nolan[1], D.C. Oxley[1], B. Pietras[1], C. Unsworth[1], A. Sweeney[1]

M.J. Joyce[2], R.O.Mackin[2], B. D'Mellow[2], M. Aspinall[2], A.J. Peyton[3], R. Van Silfhout[3], G. Zhang[3].

(1) Department of Physics, University of Liverpool, Liverpool, UK, L69 7ZE.

(2) Department of Engineering, Lancaster University, UK, LA1 4YR

(3) School of Electronic & Electrical Engineering, University of Manchester, Manchester, UK, M60 1QD.

(*) Presently at: Joint Institute for Heavy Ion Research, Oak Ridge National Laboratory, Oak Ridge, TN, 37831-6371, USA.

(+) Presently at: Monash Centre for Synchrotron Science, Monash University, Clayton, Victoria, 3800, Australia.

The Distinguish collaboration is developing a system capable of detecting and imaging hidden illicit substances such as explosives or narcotics in luggage and vehicles in transit [1]. To this end there is a requirement for a detection system that is highly sensitive.

The Pulsed Fast Neutron Analysis (PFNA) technique [2] can be used to stimulate the emission of characteristic gamma rays, allowing the light elements (Oxygen – gamma-ray energy 6.13MeV, Carbon – gamma-ray energy 4.43MeV, Nitrogen – gamma-ray energies 1.64, 2.31 and 5.11MeV), that are normally used as primary components of explosive materials, to be investigated. This work also applies the Compton Camera principle [3] to produce a 3D image of the gamma-ray source. Compton Camera measurements are currently underway using two planar, double-sided, strip, High-purity Germanium (Ge) detectors. The characteristic fingerprint of the emitted gamma rays will be identified by the spectroscopic response of the detectors and the location of the source will be resolved using Compton kinematics.

The Geant4 simulation toolkit has been used to optimise the detector setup and will produce simulated Compton images for a direct comparison between simulated and experimental data in the energy range of 0.5 – 5.5MeV. The status of the project, including the Geant4 simulated Compton images and some experimental Compton images will be presented.

[1] M. Farahmand et al. "Detection of explosive substances by tomographic inspection using neutron and gamma-ray spectroscopy", NIMB 261 (2007) 396-400

[2] Brown, D.R., Gozani, T., Loveman, R., Bendahan, J., Ryge, P., Stevenson, J., Liu, F., Sivakumar, M., 1994. "Application of pulsed fast neutrons analysis to cargo inspection", Nucl. Instr. and Meth. A 353, 684-688

[3] D. B. Everett, J. **S.** Fleming, R. W. Todd, and J. M. Nightingale, "Gamma-radiation imaging system based on the Compton effect," *Proc. ZEE,* Vol. 124, pp. 995-1000, 1977.

Measurements of astrophysical polarization using Compton scattering

M. Kiss on behalf of the PoGOLite Collaboration

The Polarized Gamma-ray Explorer (PoGOLite) is a balloon-borne instrument designed to measure polarization in the energy range 25-80 keV from many classes of astronomical objects, including pulsars, accretion discs and astrophysical jets. Using coincident detection of Compton scattering and photoelectric absorption in an array of 217 detector cells, the modulation in scattering angles can be determined. By this technique, the instrument will be able to measure as low as 10% polarization from a 200 mCrab source in a six-hour flight at an altitude of 40 km.

The maiden flight of a 61-unit “pathfinder” instrument is scheduled to take place from the Esrange ballooning facility in northern Sweden in August 2010. This flight will focus on measuring polarization from the Crab nebula and possibly Cygnus X-1, as well as to study the in-flight background caused by cosmic ray particles, X-ray and gamma-ray photons, and albedo neutrons. In order to reject such background, the instrument features a combination of active and passive shielding, as well as both active and passive collimation of the incident photons.

Here, the design and status of the PoGOLite pathfinder instrument will be reviewed. Pre-flight calibration and performance tests will also be presented.

Design of a silicon stack Compton camera for prompt-γ imaging during ion beam therapy: a Monte Carlo simulation study

M.-H. Richard[a], F. Roellinghoff[a], M. Chevallier[a], D. Dauvergne[a], N. Freud[b], P. Henriquet[a], F. Le Foulher[a], J.M. Létang[b], G. Montarou[c], C. Ray[a], E. Testa[a], M. Testa[a], A.H. Walenta[d]

[a] *Université de Lyon, Université Lyon 1 and CNRS/IN2P3, IPNL, France*
[b] *INSA-Lyon, CNDRI, France*
[c] *LPC CNRS/IN2P3, Clermont-Ferrand University, France*
[d] *Uni-Siegen, FB Physik, Emmy-Noether Campus, Siegen, Germany*

In order to take advantage of the assets of ion irradiation, the position of the Bragg peak has to be monitored accurately. It was recently shown that the detection of the prompt-γ emitted quasi-instantaneously during the nuclear fragmentation processes with a collimated scintillator detector makes it possible to locate the Bragg peak during proton or carbon ion irradiations. It was also shown that the time of flight technique can be applied to discriminate γ-rays from the neutron background. Here, the use of a Compton camera in combination with a beam tagging device is investigated to improve the detection efficiency. For the Compton camera, we investigate the use of a stack of 2 mm silicon strip detectors as a scatterer and one pixellated LYSO detector as an absorber. We reconstruct analytically the prompt-γ emission points by intersecting the ion trajectories given by the hodoscope and the Compton cones reconstructed with the camera. The reconstructed points are weighted by a factor calculated as a function of the uncertainty on the scattering angle.

The performances obtained when reconstructing events with energy deposits in either two or three detectors are studied in detail, as is the influence of pair creation. We analyze the camera response to a photon point source by means of Geant4 simulations. Different geometrical configurations of the camera are tested, varying parameters such as the distance between the detectors and the number of layers in the stack.

In the current configuration, for a prompt-γ spectrum typical of a carbon ion irradiation, the spatial resolution of the camera is about 6.5 mm FWHM after weighting (8.5 mm without) and the detection efficiency 5×10^{-3} (reconstructible photons/emitted photons in the direction of the first detector). Finally, the clinical applicability of our system is considered.

A Coded-Aperture Based Method Allowing Non-Interferometric Phase Contrast Imaging with Incoherent X-Ray Sources

A. Olivo*, K. Ignatyev, P. R. T. Munro and R. D. Speller

Department of Medical Physics and Bioengineering, UCL, London WC1E 6BT, UK

X-Ray Phase Contrast imaging (XPCi) has been one of the hottest research topics in x-ray imaging for a number of years. Being able to exploit refraction/interference effects instead of purely x-ray absorption allows a much greater contrast to be extracted from details that would produce virtually no contrast if imaged with conventional absorption methods. The transformative power that this would have on a range of diverse applications (medicine, biology, material science, etc) has been widely demonstrated primarily by means of synchrotron radiation (SR) experiments.

For many years, XPCi has been restricted to SR facilities, due to the extreme requirements it imposes upon source coherence, the only exception being implementations with microfocal sources which, however, do not provide sufficient x-ray output to enable real-world applications.

Over the recent years, however, new techniques have emerged that enable XPCi to be performed with extended sources. Most of these approaches are based on the use of fine gratings with a pitch of a few microns, either exploiting the Talbot self-imaging effect by alternating phase and absorption gratings, or by exploiting the object-caused modification of Moire fringes generated by a combination of absorption gratings. This class of techniques, however, still requires the source to be coherent, and in fact implementations with large sources were obtained by modifying the source itself in order to make it sufficiently spatially coherent, normally by collimating and/or aperturing the source output. This collimation/aperturing, however, suppresses the source output, and may therefore lead again to exposure times excessively long for real-world applications.

We propose a different approach based on the use of coded apertures, which produces phase contrast images by exploiting the edge-illumination effect, i.e., illuminating only the edges of the detector pixels. This means that only approximately 50% of the detector area is covered by the solid parts of the apertures, so that 50% of the emitted radiation beam can be effectively exploited. This requires a factor of ~2 increase in exposure time, thus leading to exposure times compatible with real-world applications. The technique is non-interferometric and only exploits refraction effects, while maximizing them: as a consequence of this, it works with source sizes of up to 100 μm (compatible with state-of-the-art mammography sources, for example), without any need to collimate/aperture the source.

The talk will describe the working principles of the method, emphasizing the basic differences with grating-based approaches, and present preliminary results in the field of homeland security and material science, where it has been shown that features completely invisible by means of x-ray absorption are effectively detected by the proposed technique. Furthermore, it will show XPCi results obtained at tube voltages as high as 100 kV, which again is something that other methods do not allow at present. This allows a much higher penetration of the X-ray beam, therefore enabling both imaging previously inaccessible samples, and chances to reduce the x-ray dose in medical examinations.

Grating interferometer for phase-contrast imaging in materials science

J. Herzen[1,2], F. Beckmann[2], T. Donath[3,5], C. David[3], F. Pfeiffer[1], M. Ogurreck[2], J. Mohr[4], E. Reznikova[4], and A. Schreyer[2]

[1]Technische Universität München, Munich, Germany, [2]GKSS Research Centre, Geesthacht, Germany, [3]Paul Scherrer Institut, Villigen-PSI, Switzerland, [4]Karlsruhe Institute of Technology, Karlsruhe, Germany, [5]Dectris AG, Baden, Switzerland

To increase contrast in x-ray imaging of weakly absorbing materials the recently developed grating interferometer is successfully used, especially for medical and biological applications [1-4]. The method provides several contrasts simultaneously, the differential phase, the absorption and the dark-field contrasts that makes it very interesting for materials characterisation and can be used with both highly brilliant synchrotron radiation sources and laboratory x-ray tubes. By combining the information from the different contrasts more information about the microstructure of the specimens can be obtained by a single measurement.

Here, we present the results of radiography on laser-welded magnesium and aluminium joints (as used in civil aircraft or automotive production), and of tomography on biological samples (mouse brain and heart) imaged using the newly installed grating-based setup at the second-generation synchrotron radiation storage ring DORIS at DESY (Hamburg, Germany). In cooperation with PSI (Villigen-PSI, Switzerland), TU München (Munich, Germany), and KIT (Karlsruhe, Germany) the high energy beamline HARWI II operated by GKSS (Geesthacht, Germany) [5] has been equipped with the grating interferometer. Now, it combines the advantages of monochromatic radiation with high flux and a sufficient large field of view for imaging centimetre sized objects.

[1] C. David, B. Nöhammer, H. H. Solak, and E. Ziegler (2002), Applied Physics Letters 81 (17), 3287-3289.

[2] A. Momose, W. Yashiro, H. Maikusa, and Y. Takeda (2009), Optics Express 17 (12), 12540-12545.

[3] F. Pfeiffer, T. Weitkamp, O. Bunk, and C. David (2006), Nature Physics 2, 258.

[4] J. Herzen, T. Donath, F. Pfeiffer, O. Bunk, C. Padeste, F. Beckmann, A. Schreyer, and C. David (2009), Optics Express 17 (12), 10010.

[5] F. Beckmann, T. Donath, J. Fischer, T. Dose, T. Lippmann, L. Lottermoser, R. Martins, and A. Schreyer (2006), Proc. of SPIE 6318, 631810, 1-11.

Measurements and simulations analysing the noise behaviour of grating-based X-ray phase-contrast imaging

T. Weber[*,a], P. Bartl[a], J. Durst[a], W. Haas[a,b], T. Michel[a], A. Ritter[a], G. Anton[a]

[a] *University of Erlangen-Nuremberg, ECAP - Erlangen Center for Astroparticle Physics, Erwin-Rommel-Str. 1, 91058 Erlangen, Germany*
[b] *University of Erlangen-Nuremberg, Pattern Recognition Lab, Martensstrae 3, 91058 Erlangen, Germany*

Abstract

The last several years, it has been shown, that phase-contrast imaging using a grating interferometer is possible even with a low brilliance X-ray source and has the potential of increasing soft-tissue contrast [3]. Therefore, we concentrated on measurements regarding the noise behaviour of the differential phases. We will present the results gained by measurements and related simulations on this topic. These measurements were done using a microfocus X-ray tube with a hybrid, photon-counting, semiconductor Medipix-detector [1]. The additional simulations were realised with our in-house developed phase-contrast simulation tool, combining both wave and particle contributions of the simulated photons. Furthermore, the propability density function (pdf) of the reconstructed differential phases were analysed. It turned out that the so called von Mises distribution is the physically correct pdf. This information advances the understanding of grating-based phase-contrast imaging and can possibly used to improve image quality.

Key words: phase-contrast, grating interferometry, X-ray imaging, photon-counting detector, Medipix, probability density function, Noise

1. Motivation

Phase-contrast imaging using a Talbot interferometer, as proposed by [3] and [2], is an approach of increasing the soft-matter contrast by exploiting the real part of the complex refractive index in addition to the imaginary part, which is used by conventional X-ray absorption imaging.

2. Theory

2.1. The Talbot Effect

This effect, stating the existence of so called "self-images" of a periodic stucture downstream the direction of wave propagation in certain distances, was first reported in 1836 by W. Talbot. For a π-shifting phase-grating with period p_1 this effect leads in particular to an intensity pattern with period $p_1/2$ at distances

$$d_n^{plane} = (2n-1)\cdot\frac{p_1^2}{8\lambda} \quad (1)$$

where n is a positive integer and λ is the wavelength of the impinging plane wave radiation.

2.2. Differential phase-contrast imaging

Putting an object into the beamline, the intesity pattern generated by the Talbot effect is locally distorted and shifted lateraly by an angle α. This shift can be detected by placing an absorption grating with period p_2 of the intensity pattern right in front of the detection plane and the differential phase can be reconstructed by

$$\frac{\partial\phi}{\partial x} = \alpha\frac{2\pi}{\lambda}. \quad (2)$$

3. Methods

3.1. Experimental setup

The experimental setup used was adapted from the proposal made by [4]. For all measurements made, we used a microfocus X-ray source with a maximum photon energy of 80 keV. For photon detection we applied a photon-counting, hybrid, semiconductor Medipix-detector [1]. The geometries were chosen according to the symmetric setup, meaning that the magnification was set to $M = 2$ and therefore the period of both the phase and the absorption grating was $p_1 = p_2 = 5\,\mu$m.

3.2. Simulation

The simulated data was produced with our in-house developed simulation framework, which combines both particle and wave contributions of the photons. The experimental setup was reproduced with the only difference that the simulated gratings were geometrically perfect compared to the real ones, what lead to a higher contrast level.

4. Results

4.1. Noise behaviour of reconstructed differential phases

In figure 1 the standard deviation of the differential phases is shown against $S_0^{-1/2} = (N_{max} + N_{min})^{-1/2}$, which is the sum

*thomas.weber@physik.uni-erlangen.de

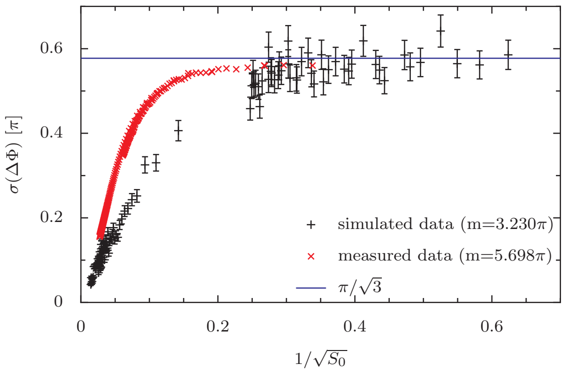

Figure 1: Measured (red) and simulated (black) standard deviations of the differential phases against S_0, that represents the measurement statistics. For high statistics (low x-values) the noise tends linearly towards zero.

of the minimum and the maximum value of counted photons in one detector pixel and represents the measuring statistics. The red graph shows the measured, the black one the simulated results, while the blue line is the maximum possible standard deviation of $\pi/\sqrt{3}$. Both the simulated, as well as the real data, show qualitatively the same dependency. While for low statistics, the uncertainty represents the value of a uniform distribution as expected, the standard deviation tends linearly to zero for an increasing number of photons detected. The slope of the values is a measure of the setup's and gratings' quality.

4.2. Probability density function of the reconstructed differential phase distribution

As a second result, the probability density function (pdf) of the differential phase distribution was analysed. It turned out, that the first approximation of the distribution, a wrapped gaussian, does not represent reality well, while significant underestimations at the borders and in the center of the distribution are made. A much better description of the measured differential phases is given by the so called von Mises distribution

$$f_{VM}\left(\Delta\Phi \,|\, \mu, \kappa\right) = \frac{1}{2\pi I_0(k)} \exp\left[\kappa \cdot \cos\left(\Delta\Phi - \mu\right)\right], \qquad (3)$$

where μ is the mean and κ is a concentration parameter of the distribution. I_0 is the modified Bessel function zeroth order of the first kind.

5. Conclusions

The measurements show the noise behaviour of the differential phases for different numbers of photons counted in each pixel. These results help to understand the physics of the experimental method and can be used to find the best configuration of image quality and radiation exposure to the sample.

References

[1] X. Llopart, M. Campbell, R. Dinapoli, D. San Segundo, and E. Pernigotti, "Medipix2: A 64-k pixel readout chip with 55-μm square elements working in single photon counting mode," *IEEE Trans. Nucl. Sci.*, vol. 49, no. 5, pp. 2279–2283, 2002.

[2] A. Momose, W. Yashiro, Y. Takeda, Y. Suzuki, T. Hattori, "Phase tomography by X-ray Talbot interferometry for biological imaging," *Jpn. J. Appl. Phys.*, 45 (6A), 5254–5262 (2006).

[3] F. Pfeiffer, T. Weitkamp, O. Bunk, C. David, "Phase retrieval and differential phase-contrast imaging with low-brilliance X-ray sources," *Nature* Phys. 2, 258–261 (2006).

[4] Weitkamp, T., et al., "X-ray phase imaging with a grating interferomter," *Optics Express* Vol. 13, No. 16, 6296–6304 (2005).

Phase-contrast imaging using hard X-ray grating interferometer

V.Altapova[1], J.Butzer[2], T. d S. Rolo[2], P.Vagovic[2], A.Cecilia[2], J.Moosman[2], E.Reznikova[3], J.Kenntner[3], J.Mohr[3], D.Pelliccia[2], and T.Baumbach [1, 2]

[1]*Laboratory for Application of Synchrotron Radiation, Faculty of Physics at Karlsruhe Institute of Technology **KIT**,76128 Karlsruhe, Germany*

[2]*ANKA - Institute for Synchrotron radiation, KIT, 76344 Eggenstein, Germany*

[3]*Institute for Microstructure Technologies, KIT, 76344 Eggenstein, Germany*

The Talbot grating interferometer was already proven to be a powerful technique of phase-contrast imaging with synchrotron radiation for biological applications and for materials research [1,2]. The integration of the method into standard laboratory x-ray set-ups offers a potential for broader usage of the system, e.g. in medical diagnostics and non-destructive testing (NDT) [3,4].

At the TOPO-TOMO beamline of the ANKA light source (Karlsruhe Institute of Technology, Germany) a Talbot grating interferometer has been implemented successfully. There the availability of both, pink and white beam allowed to investigate the suitability of white-beam interferometry, i.e., by using of a broad bandwidth. The feasibility of the grating interferometry with white beam was proven. A promising visibility of 25% has been achieved at a central energy of 25 keV and with a relative band width of 0.5%, which enabled a sufficiently good image reconstruction (in comparison to a typical value of 35-40% at monochromatic SR sources). We report about examples of application such as beetle in amber, human teeth etc., for which absorption contrast, phase contrast and dark-field images have been reconstructed from the white beam data sets. The results show good quality. 3D phase contrast, for example, provides sufficient information to segment the internal soft structures of the human tooth (pulp) and shows the microcracks and nerves connection within the tooth dentin. The experiments have demonstrated that phase-contrast grating interferometry can be carried out with the higher flux of white beams, without any additional instrumentation and with less stringent requirements to the quality of the beam. That pushes the way towards new application fields and allows the investigation of dynamic processes.

References:

[1] Pfeiffer, F., Weitkamp, T., Bunk, O. & David, C. (2006). *Nature Phys*. **2**, 258-261

[2] Weitkamp, T., Diaz, A., David, C., Pfeiffer, F., Stampanoni, M., Cloetens, P. & Ziegler, E. (2005). *Opt. Expr.* **13**, 6296-6304

[3] Momose, A., Yashiro, W., Takeda, Y., et al., (2002), *Jpn. J. Appl. Phys.*, Part 1 45, 5254-5262

[4] Pfeiffer, F., Bech, M., Bunk, O., Kraft, P., Eikenberry, E. F, et al., (2008). *Nat. Mat.* **7**, 134-137

X-RAY INTERFEROMETER WITH BENT GRATINGS: PHASE CONTRAST IMAGING WITH LARGE FIELDS OF VIEW

V. Revol[1(a,b)], C. Kottler[(a)], R. Kaufmann[(a)], I. Jerjen[(c)], T. Lüthi[(c)], F. Cardot[(d)], P. Niedermann[(d)], U. Straumann[(b)], U. Sennhauser[(c)] and C. Urban[(a)]

[(a)] *Photonics Division, CSEM SA, Zürich, Switzerland*
[(b)] *Physics Institute, University of Zürich, Zürich, Switzerland*
[(c)] *Laboratory for Electronics/Metrology/Reliability, Empa, Dübendorf, Switzerland*
[(d)] *Microsystems Technology, CSEM SA, Neuchâtel, Switzerland*

X-ray Differential Phase Contrast imaging (dPCI) achieves phase sensitive imaging in the hard x-ray domain thanks to an x-ray Talbot-Lau interferometer [1]. dPCI can be combined with standard x-ray tubes [2] and imposes strong requirements neither on the temporal coherence of the radiation nor on the mechanical stability of the components. However, the currently used x-ray energies and fields of view, in the order of some centimeters, restrain the technique to small samples made of light elements.

Here, we report on our progresses in the instrumentation in order to reach the imaging quality and the technical characteristics needed by industrial applications. A new interferometer design made of a beam-splitter grating with π/2-phase shift and an analyzer grating placed on the 12th Talbot order plane is proposed which allows the use of broad band energy spectra with large flux and shows a drastic increase in the minimal detectable phase change. Moreover, we demonstrate a new compact (60cm-long) configuration of the Talbot-Lau interferometer with gratings bent on a cylindrical form. A significant improvement of the visibility of the phase stepping curve could be achieved away from the center of the gratings in comparison to the standard geometry (see Figure 1) and induces a lower noise level as derived in [3]. The theoretical limit fixed by non-perpendicular angular incidence can thus be practically overcome and large fields of view become realistic. Additionally, our contributions to the fabrication of low-cost high aspect ratio x-ray gratings for energies up to 50keV are presented.

Examples of measurements are finally analyzed and allow us to envision the implementation of dPCI in standard compact x-raying systems in fields such as non-destructive testing and/or homeland security.

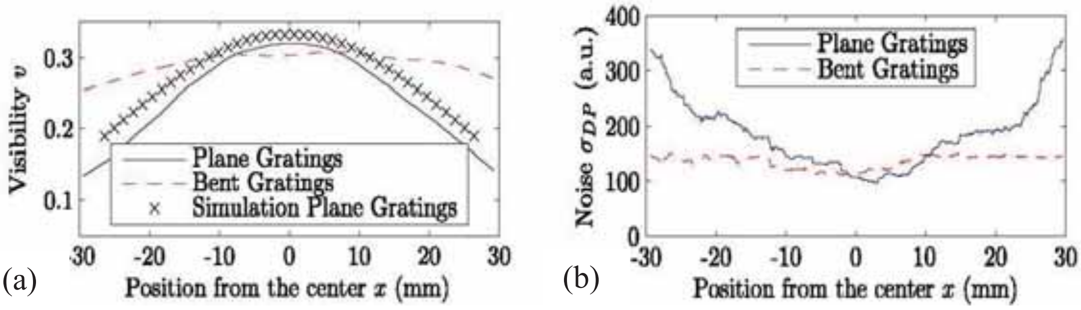

Figure 1. (a) The visibility of the phase stepping curve and (b) the level of noise in the image were measured as a function of the position from the center of the gratings for plane and for bent gratings.

[1] A. Momose, Opt. Exp. **11**, 2303 (2003)
[2] F. Pfeiffer, T. Weitkamp, O. Bunk and C. David, Nature Physics **2**, 258-261 (2006)
[3] V. Revol, C. Kottler, R. Kaufmann, U. Straumann and C. Urban, ***in prep.*** (2010)

[1] vincent.revol@csem.ch

Simulation and Measurement of Grating Based X-Ray Phase-Contrast Imaging

P. Bartl[*,a], J. Durst[a], W. Haas[a], T. Michel[a], A. Ritter[a], T. Weber[a], G. Anton[a]

[a] *University of Erlangen-Nuremberg, ECAP - Erlangen Center for Astroparticle Physics, Erwin-Rommel-Str. 1, 91058 Erlangen, Germany*

Key words: phase-contrast, grating interferometry, X-ray imaging, photon-counting detector, Medipix, simulation of X-rays

In this presentation we will present in the first part a complete simulation framework for X-ray phase-contrast imaging. Newly, the wave and the particle contributions of photons are regarded with this tool. Due to the modular concept of the framework it is possible to simulate different phase-contrast methods like propagation based [1] or grating based imaging [3]. We will present the realization of the X-ray and wave physics into a numerical based calculation. Herein, the different imaging steps of a grating interferometer will be performed as well. We will show results of different imaging parameters like focal spot size and the influence of the X-ray's energy. Figure 1 gives an example on how the X-ray energy and the duty cycle of the analyser grating yield to different visibilities of the imaging system. The visibility, thereby, is regarded as an important quality factor for the grating interferometer.

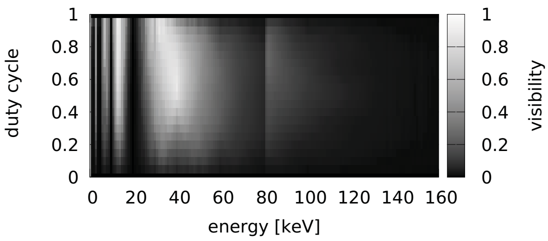

Figure 1: Visibility of a grating interferometer (in greyscale). The dependency on the duty cycle of the analyser grating and different input energies is shown. The design energy was set to 40 keV.

In our experimental setup of the grating interferometer we carried out measurements of the focal spot size and the Medipix-detector [2] in particular, so that we could adapt our simulation for a realistic laboratory setup.

In the experimental part of the presentation we will show the characterisation of the performance of the interferometer for different gratings, different Medipix-detectors, and different X-ray spectra.

Furthermore we are able to demonstrate the difference between a differential measurement like the phase gradient and a direct signal like the absorption information. The figures 2 and 3 show as an example the phase and absorption image taken with a grating interferometer. The phantom had the geometrical structure of stairs and by looking under an non-rectangular angle onto it, the difference between the phase and the absorption information is apparent.

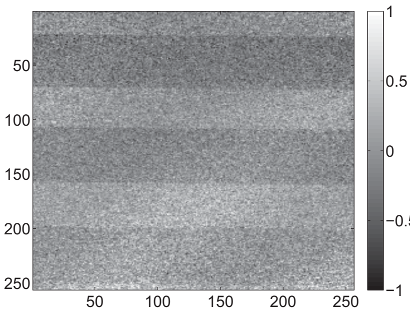

Figure 2: Differential phase image (in greyscale) of stair phantom. The inclined view onto it gives rise to the stripe pattern corresponding to the steps.

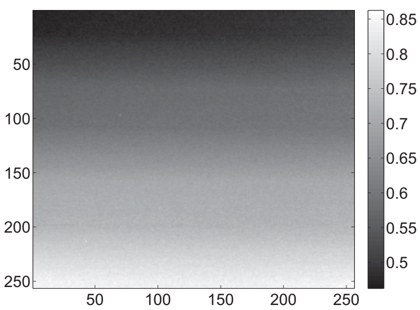

Figure 3: Absorption image (in greyscale) of stair phantom. The inclined view onto it gives rise to a stepwise darker greyscale corresponding to the steps.

References

[1] S.W. Wilkins, T.E. Gureyev, D. Gao, A. Pogany, A.W. Stevenson, "Phase-contrast imaging using polychromatic hard X-rays," *Nature* 384, 335–337, 1996.

[2] X. Llopart, M. Campbell, R. Dinapoli, D. San Segundo, and E. Pernigotti, "Medipix2: A 64-k pixel readout chip with 55-μm square elements working in single photon counting mode," *IEEE Trans. Nucl. Sci.*, vol. 49, no. 5, pp. 2279–2283, 2002.

[3] F. Pfeiffer, T. Weitkamp, O. Bunk, C. David, "Phase retrieval and differential phase-contrast imaging with low-brilliance x-ray sources," *Nature* Phys. 2, 258–261 (2006).

*peter.bartl@physik.uni-erlangen.de

Cerenkov radiation imaging of beta emitters: *in vitro* and *in vivo* results

Antonello E Spinelli[1*], Federico Boschi[2], Daniela D'Ambrosio[3], Laura Calderan[2], Mario Marengo[3], Alberto Fenzi[2], Andrea Sbarbati[2], Antonella Del Vecchio[1], Riccardo Calandrino[1]

[1]Medical Physics Department, S. Raffaele Scientific Institute, via Olgettina N. 60, Milan, Italy
[2]Department of Morphological-Biomedical Sciences, Section of Anatomy and Histology, University of Verona, Strada Le Grazie N. 8, Verona, Italy
[3]Medical Physics Department, S. Orsola – Malpighi University Hospital, via Massarenti N. 9, Bologna, Italy

[*]Corresponding author: spinelli.antonello@hsr.it

Introduction:
Cerenkov radiation (CR) is a well-known phenomenon and is generated when charged particles travel through an optical transparent material with a velocity greater than light velocity in the material. The CR emission is prevalently in the visible range and, thus, CR photons can be detected by using optical imaging techniques. We realised that CR could be used for *in vitro* or *in vivo* experiments in order to obtain optical images of samples or small animals such as mice. The main purpose of this work was to investigate both *in vitro* and *in vivo* CR emission coming from ^{18}F and ^{68}Ga. Some of the results presented here can also be found in a recently published paper by our group [1].

Materials and Methods:
CR optical images were acquired by using the IVIS 200 Vivo Vision System (Xenogen Corp., Alameda, USA) imager typically used for *in vivo* small animal imaging. In order to detect CR photons only, the IVIS 200 was used in bioluminescence mode and, thus, without using any excitation lamps. The system is composed by a back-thinned, back-illuminated CCD camera, several filters and lens. The instrument is based on a CCD detector consisting of a matrix of 2048 x 2048 with a 13.5 microns pixel. The detector has a total dimension equal to 2.7 x 2.7 cm. In order to measure the spectrum of the optical photons the instrument is equipped with several emission filters: wide and narrow band filters. Dark images were acquired before any image acquisitions. The spectral distribution of the emitted light from ^{18}F-*FDG* or ^{68}Ga solutions was measured as follow: about 30 MBq of ^{18}F-*FDG* and ^{68}Ga were placed into two separate vials, and optical images were acquired for 30 seconds in order to compare the two radiotracers spectra. In order to investigate *in vivo* the CR imaging approach we studied an experimental xenograft tumor model of mammary carcinoma (BB1 tumor cells). BB1 tumors were obtained by subcutaneous injection of BB1 cells derived from spontaneous mammary carcinomas. Mice were injected with 30 MBq of ^{18}F-*FDG* in the tail vein and right after the radiotracer injection the animal underwent a dynamic scan for 1 h. The acquisition scheme consisted of 10 frames with a 6 minutes length. Multispectral analysis of the CR was used in order to estimate the deepness of the source of Cerenkov light.

Results:
In vitro results showed that the detected light signal corresponds to CR produced by positrons emitted by ^{18}F and ^{68}Ga. The measured spectrum for both ^{18}F and ^{68}Ga matches fairly well the theoretical distribution proposed in [1]. The main difference between ^{18}F and ^{68}Ga is mainly the number of the emitted light photons, more precisely since ^{68}Ga emits high energy positrons will emits also more light photons and vice versa.
Cerenkov *in vivo* whole body images of tumour bearing mice and the measurements of the emission spectrum were obtained. Tumour tissue time activity curves reflected the well-known physiological accumulation of ^{18}F-*FDG* in malignant tissues with respect to normal tissues.

Conclusions:
The results presented here show that is possible to use conventional optical imaging devices for *in vitro* or *in vivo* study of beta emitters. We believe that such results will open new research scenarios, since it could be possible to apply the proposed approach to easily image not only β^+ but also pure β^- emitters. Future work will be focused on the *in vitro* or *in vivo* imaging of ^{32}P for different biological applications.

References:
[1] Spinelli A E, D'Ambrosio D, Calderan L, Marengo M, Sbarbati A, Boschi F. Cerenkov radiation allows in vivo optical imaging of positron emitting radiotracers. Phys. Med. Biol. 2010; 55(2): 483-95.

A High Resolution Image Guided Micro Irradiator for Translational Radiobiological Research

Jordan Birch, I-Tan Su, Haijian Chen, Alexander Silvius, and Enrique W. Izaguirre.

Washington University in Saint Louis, Department of Radiation Oncology, Saint Louis, MO, USA.

Advances in radiotherapeutic drug development, molecular reporters, and fundamental cancer research are being fostered by the development of *in vivo* imaging devices such as microCT, microMRI, microPET, microSPECT, and optical scanners. Progress of comparable magnitude in the field of radiobiology and radiation therapy is expected if small animal image guided conformal microirradiators are developed.
We present the design, development and applications of a novel small animal image guided microirradiator (microIGRT). The microIGRT was built according to specifications generated by radiobiology research requirements and specifications from clinical instrumentation scaled to preclinical cancer models. The instrument overcomes limitations of the present technology of small animal irradiation by integrating high resolution anatomical imaging, high resolution treatment planning, and conformal orthovoltage radiotherapy. A microCT provides on-board anatomical imaging for image guided treatment planning and ionizing irradiation delivery. The microCT and the microirradiator gantries are aligned using a common rotation axis in a tandem configuration (see figure 1). An axial motorized animal bed transfers the animal from the microCT field of view to the microirradiation chamber. The microCT has a resolution of 150 um and was constructed using a 80 kVp micro-focus x-ray source with a 75 x 75 um^2 focal spot and a flat panel amorphous silicon detector with 1024 x 1024 pixels. The orthovoltage microirradiator subsystem was constructed using a 320 kVp x-ray source with dual focus spots (0.4 x 0.4 mm^2 at 800 W and 1 x 1 mm^2 at 1800 W). The orthovoltage beam is collimated using orthogonal jaws and exchangeable apertures. The treatment beam can be aimed at different latitudinal and longitudinal angles in steps of 30 arc minutes and translated at 100μm steps (x, y and z). The beam cross sections can be modulated with high precision using steps of 50 um. The system is designed to conformally deliver a treatment beam with sub-millimeter penumbra. Verification of the treatment beam delivery is achieved through portal images acquired using an in-house developed orthovoltage detector.
Examples of applications that will be studied using this novel image guided microirradiator are: animal models of radiation-induced brain complications and necrosis, respiratory gated pulmonary irradiation of lung tumor models, murine models of radiation-induced thoracic injury, normal tissue complication probability (NTCP) models, radiobiology of radioresistant tumors, functional image guided radiotherapy, combined chemotherapy–radiotherapy doses, preclinical cancer models of organ targeted radiotherapy (i.e. prostate, liver ,pancreas, etc.), xenograft tumor models (i.e. breast cancer, colon cancer, neuroblastoma, etc.) and therapeutic gain of dose escalation.

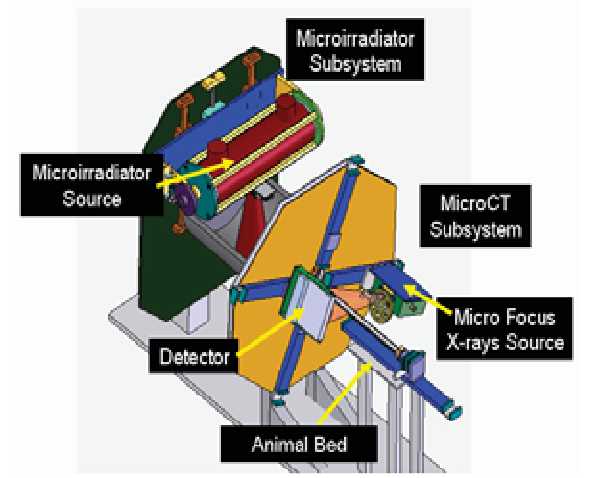

Figure 1: 3D rendering of the microIGRT instrument showing the primary components: The microCT subsystem, the microirradiation subsystem and the mouse bed and animal physiologic measurement interface. The system is designed in a tandem configuration where the animal bed is placed in the microCT field of view for anatomical imaging and is then shifted to the micro irradiator subsystem for conformal irradiation. A software interface controls the operation between these two subsystems and the treatment planning process with minimal operator intervention.

First tests in the application of silicon photomultiplier arrays to dose monitoring in hadron therapy

G. Llosá[1], J. Barrio[1], C. Lacasta[1], S. Callier[2], C. De la Taille[2], L. Raux[2].

[1]Instituto de Física Corpuscular (IFIC, CSIC-UVEG), Valencia, Spain
[2]Laboratoire de L'Accélérateur Linéaire (LAL), Orsay, France.

Hadron therapy is a technique that allows to administer the radiation dose very precisely in the location area of the tumour, but it is crucial to develop a method to monitor accurately the dose delivery. The hadron beam produces fragmentation of the nuclei in the tissue that is followed by the emission of secondary particles. Prompt gammas are emitted with energies up to about 15 MeV, which can be used for dose monitoring.

The use of a Compton telescope is an interesting option to locate the origin of these gammas and to estimate the delivered dose[1]. A Compton telescope design is under study for this application, based on several detector heads composed of $LaBr_3$ crystals coupled to silicon photomultiplier (SiPM) 2D arrays. The three-Compton technique is the most appropriate in this case, given the high energies of the photons, and the fact that the gamma energy is not known. In this approach the event is reconstructed based on three interactions, two Compton plus a third interaction of any type in three different detector heads[2].

Simulations that include the production of gammas in the tissue and the detector response are being carried out with GEANT4 to fully understand the physical processes, and to determine the optimum geometry and estimate the performance of the telescope.

Initial experimental tests have been done with a $LaBr_3$ crystal coupled to a SiPM (Multi Pixel Photon Counter - MPPC) array from Hamamatsu, in order to test the system and to assess the possibility of operating the detector with good performance. The $LaBr_3$ crystal has 16mm x 18mm x 5mm size, and it is surrounded with reflecting material in five faces. The SiPM array has 16 (4x4) elements of 3mm x 3mm size, each composed of 3600 microcells of 50µm x 50µm size. The crystal is placed directly on top of the photodetector. The SPIROC ASIC developed at LAL, that is specifically designed for Hamamatsu MPPCs for the ILC hadronic calorimeter, was employed for the detector readout[3]

Data have been taken with different sources, at energies ranging from 122 keV to 1275 keV. The detector has a linear behaviour in the whole energy range. The energy resolution obtained at 511 keV is 7% FWHM. The gain variations among the pixels have been determined by coupling a 3mm x 3mm x 10mm LYSO crystal to each of the pixels, and taking data with a Co-57 source. The variations in the peak positions are within 1%. The tests performed confirm the correct functioning of the detector and electronics, and the possibility of employing a detector of these characteristics. Further tests are being carried out to determine the timing response of the system, and the position resolution with different position determination algorithms.

[1] H-M. Richard et al. *Design study of a Compton Camera for prompt γ imaging During Ion Beam Therapy.* IEEE 2009 NSS-MIC Conf. Record. HT3-6. p4172-4175.
[2] J. D. Kurfess et al. *Considerations for the Next Compton Telescope Mission.* AIP Conference proceedings, Portsmouth, New Hampshire, 15-17 Sep 1999.
[3] M. Bouchel et al. SPIROC(SiPM integrated readout chip). *Dedicated very Front-end for an ILC prototype hadronic calorimeter with SiPM readout.* 2007 IEEE NSS MIC Conference Record. N29-5. P1857-1860, 2007.

Ongoing investigations on novel imaging techniques for ion beam therapy

I. Rinaldi[1,2], S. Brons[2], F. Cerutti[3], A. Ferrari[3], 0. Jäkel[1,2], A. Mairani[2,4], R. Panse[2], B. Voss[5], K. Parodi[2]

[1]*German Cancer Research Center, Heidelberg, Germany,* [2]*Heidelberg Ion Therapy Center, Heidelberg, Germany,* [3]*CERN, 1211 Geneva 23, Switzerland,* [4]*INFN Section of Milan, Milan, Italy,* [5]*GSI Biophysik, Darmstadt, Germany*

Contact person: Ilaria Rinaldi, i.rinaldi@dkfz.de, tel:+4962215638132

Ion beams exhibit a finite range and an "inverted" depth-dose profile, the Bragg peak. These favourable physical properties allow superior tumour-dose conformality. However, they introduce sensitivity to range uncertainties. Although these uncertainties are typically taken into account in treatment planning, delivery of the intended treatment has to be assured to prevent underdosage of the tumour or overdosage of surrounding critical structures. Thus, dedicated Quality Assurance procedures are desirable to provide in-vivo range verification before or during ion therapeutic irradiation.
Experimental investigations and Monte Carlo (MC) calculations based on the FLUKA code [1,2] are being carried out to address the feasibility and to compare the performances of particle-based radiographic or tomographic transmission and emission imaging techniques. The aim of this ongoing work is to identify alternative or complementary methods to Positron-Emission-Tomography [3] for future application at HIT (Heidelberger Ionenstrahl-Therapiezentrum). These novel imaging techniques could be performed using:

1. transmitted high energy primary particles [4, 5] for low dose 2D and 3D imaging to evaluate the correct patient positioning and verify the ion range before treatment

2. emerging secondaries [6, 7, 8], in particular gammas or protons, from the therapeutic beams to verify simultaneously and in-vivo the treatment delivery

Regarding the first technique, we initially studied the clinical feasibility of heavy ion computed tomography (HICT) at HIT, where the patient has to be irradiated before treatment with a small flux of ions of initial energy higher than the one used for therapy, such that the exit range or energy can be measured. MC results and experimental data taken with simple radiographic films and reconstructed using a simple backprojection algorithm support the applicability of HICT at HIT. Following these encouraging results, a first prototype of a dedicated detector system, a stack of ionisation chambers [9] with newly acquired electronics, has been assembled and is being characterised in collaboration with colleagues from GSI (Helmholtzzentrum für Schwerionenforschung GmbH, Darmstadt) for ongoing experimental investigations. Results will be reported. Further optimisations for an upgrade of the detector system are being evaluated and planned, also for an eventual clinical use.
Concerning the second technique, we have concentrated on the MC part and started common scientific activities with the Lyon groups (Institut de Physique Nucléaire de Lyon and CNDRI-INSA) working on the Regional Research Program for Hadrontherapy (ETOILE) [7, 8] to compare our FLUKA calculations with their Geant4 simulations to reproduce the GANIL (Le Grand Accélérateur National d'Ions Lourds, Caen) and GSI data on prompt gamma profiles using different detector setups.

[1]G. Battistoni et al, AIP Conference Proceeding 896, 31-49, 2007
[2]A. Fassò et al, CERN-2005-10 2005, INFN/TC_05/11, SLAC-R-773
[3]W. Enghardt et al, Nucl. Instrum. Meth. A 525, 284-288, 2004
[4]Y. Ohno et al, Nucl. Instrum. Meth. A 525, 279-283, 2004
[5]H. Shinoda et al, Phys. Med. Biol. 51, 4073-4081, 2006
[6]C.H. Min et al, Nucl. Instrum. Meth. A 580, 562, 2007
[7]E. Testa et al, Appl. Phys. Lett. 93, 093506, 2008
[8]E. Testa et al, Nucl. Instrum. Meth. B 267(6), 993–996, 2009
[9]B. Voss et al, GSI Scientific Report 2006

Contrast-to-noise in X-ray differential phase contrast imaging

K. J. Engel*[1], D. Geller[1], T. Koehler[2], G. Martens[2], S. Schusser[1], G. Vogtmeier[1], and E. Roessl[2]

[1] *Philips Research Europe, Aachen, Germany*
[2] *Philips Research Europe, Hamburg, Germany*

With a recently proposed method using common X-ray tubes [1], X-ray differential phase contrast imaging (DPCI) becomes interesting for medical imaging. Additionally to common X-ray absorption images, DPCI allows to map a local refraction of X-ray beams, which results in extremely high contrasts especially at interfaces to air or between different tissue types. To allow a comparison of the image quality, we developed a theory for the contrast-to-noise ratio (CNR) in DPCI, and compare it to that of images derived from classical absorption imaging. The CNR is a direct function of the geometrical system parameters, the X-ray photon wavelength, the spatial wavelength and material composition of object structures, the local visibility of fringe patterns, and the X-ray exposure. As a most important result, we find that high frequency components of object structures are best imaged with DPCI, while low frequency components are obtained with a better CNR by traditional absorption imaging. Furthermore, the optimal CNR for DPCI is usually found at higher photon energies than commonly used for absorption imaging. We demonstrate the usefulness of our CNR approach in an exemplary calculation for breast mammography, where we deduce a best CNR in absorption imaging for photon energies of 15-20 keV, and a best CNR for DPCI for photon energies of 20-40 keV.

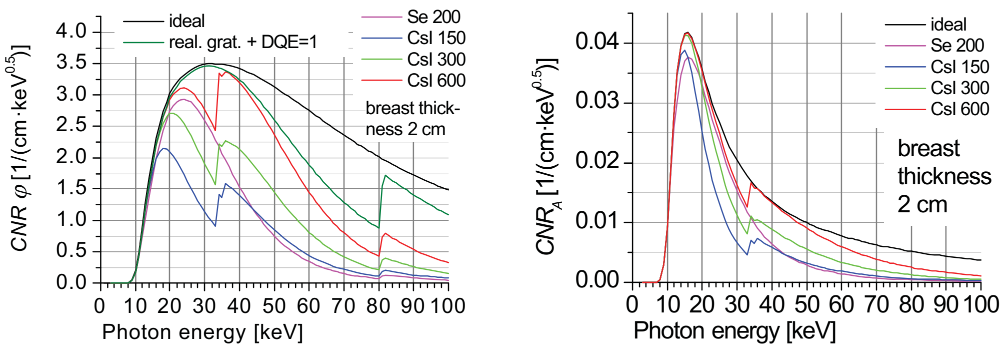

CNR dependency on photon energy E for a 2 cm thick breast phantom, under assumption of a constant-dose scenario with monochromatic radiation. The black curves represent an ideal system, while the different colors represent the use of realistic detectors (Se or CsI with various thicknesses), in case of DPCI also with realistic gratings. Left: CNR for DPCI with system geometries optimized for each E; right: corresponding CNR for absorption imaging. The plots contain only the energy dependent factors; for an absolute CNR, further energy-independent factors have to be multiplied, which are different for both modalities.

[1] F. Pfeiffer, T. Weitkamp, O. Bunk, and C. David, Nature Physics 2, 258 (2006)

* *Presenting author: Klaus.J.Engel@philips.com*

Silicon Photomultipliers

Boris Dolgoshein(boris@mail.cern.ch)
National Research Nuclear University MEPhI

The state of art of the Silicon Photomultipliers (SiPM's) – their features, possibilities and applications – is given. The significant progress of this novel technique of photo detection is described and discussed .The main trend in SiPM's developments is underlined, namely:

- the highest Photon Detection Efficiency from UV to near IR
- the highest single photon timing capability FWHM~100 ps
- the lowest optical crosstalk ~1%
- low single photoelectron dark rate

These goals being achieved shall make the SiPM's an almost ideal photo sensor for Low Level Light applications, such as astrophysics, nuclear medicine, life science etc.

AGIPD: the Adaptive Gain Integrating Pixel Detector for the European XFEL

Xintian Shi[1], Roberto Dinapoli[1], Heinz Graafsma[2], Hans Krüger[3], Beat Henrich[1], Aldo Mozzanica[1], Bernd Schmitt[1], Feng Tian[2], Ulrich Trunk[2], on behalf of the AGIPD consortium

[1]Paul Scherrer Institut, Villigen, Switzerland, [2]Desy, Hamburg, Germany, [3]University of Bonn, Germany

Abstract: The European X-Ray Free Electron Laser (XFEL) [1] is under construction in Hamburg, and will provide fully coherent, 100 fs long X-ray pulses, with up to 10^{12} photons at 12 keV. A dedicated pixel detector AGIPD [2] for the European XFEL is being developed by a consortium of DESY, PSI, University of Hamburg and University of Bonn. It is a classical hybrid pixel array detector with a readout ASIC bump-bonded to a silicon sensor. The pixel size is 200 x 200 μm^2. Each pixel contains a charge integrating amplifier (CIA) and an analogue pipe-line for storing more than 200 images at the 5 MHz XFEL repetition rate during the 600 μs bunch train. The images stored in the ASIC are read out, digitized and written to mass storage during the 99 ms inter-train spacing. The main challenges in chip design [3] are: 1) achieving a high dynamic range of $1 – 10^4$ incoming photons at 12 keV, 2) having a large storage chain (> 200) combined with the low leakage current for each storage cell, 3) being radiation tolerant to the possible high dose up to 100 MGy. A prototype ASIC with a 16 x 16 pixel array and 100 storage cells / pixel is designed and fabricated with IBM 130 nm CMOS process. The designed CIA has its gain adapted to the number of the photons to achieve the high dynamic range. The layout of the chip is shown in Figure 1. The preliminary measurements show the promising results which meet the specifications. The CIA works with proper gain switching and good linearity, therefore, the high dynamic range can be achieved. The leakage current of the memory cell is small enough. Figure 2 shows the measured output of the CIA. Further measurements will investigate the radiation tolerance of this test chip. In this talk we will present the AGIPD detector with the main focus on the chip design and test.

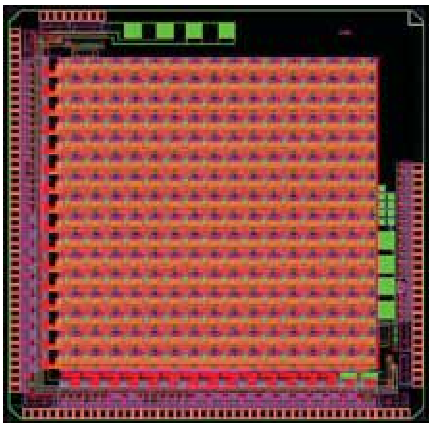

Fig 1: The layout of the test chip with 16 x 16 pixel array.

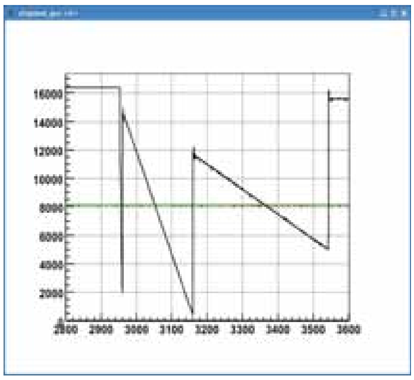

Fig 2: The measured output of the CIA. The input of the CIA is a constant current source built inside the pixel. The X axis is the charge integrating time. The Y axis is the 16-bit digitized output of the CIA.

[1] H. Graafsma, Requirements for and development of 2 dimensional X-ray detectors for the European X-ray Free Eletron Laser in Hamburg, 2009 JINST 4 P12011.

[2] B. Henrich et al., *The Adaptive Gain Integrating Pixel Detector AGIPD: A detector for the European XFEL*, Proceedings of 11th International Workshop on Radiation Imaging Detectors, June 28 – July 2, 2009, Prague, Czech Republic., to be published in Nucl. Instr. Meth. A.

[3] X. Shi et al., *Challenges in chip design for the AGIPD detector*, to be published in Nucl. Instr. Meth. A.

Liquid Phase Epitaxially grown LSO:Tb scintillator films for high resolution X-ray imaging applications at synchrotron light sources

A. Cecilia[1], A. Rack[2], P.-A. Douissard[2], T. Martin[2], P. Vagovič[1,5], T. dos Santos Rolo[1], R. Simon[1], M. Riotte[1], B. Krause[1], K. Dupré[4], V. Wesemann[4], and T. Baumbach[1]

[1]Karlsruhe Institute of Technology – ANKA, Postfach 3640, Karlsruhe, 76021, Germany
[2]European Synchrotron Radiation Facility, BP 220, Grenoble, 38043, France
[3]CEA Léti MINATEC, 17 rue des Martyrs, Grenoble, 38054, France
[4]FEE GmbH, Struthstr. 2, Idar-Oberstein, 55743, Germany
[5]Institute of Electrical Engineering, Slovak Academy of Sciences, Bratislava, Slovakia

Third generation synchrotron light sources offer new possibilities for different X-ray imaging techniques thanks to their high brilliance and the high degree of the spatial coherence. These techniques (e.g. microtomography with absorption or phase contrast and holotomography) demand highly efficient X-ray detectors with a spatial resolving power in the micrometer and even submicrometer range [1]. A successful approach for achieving X-ray imaging with submicrometer resolution is given by the combination of a transparent luminescent screen (single crystal scintillator) with diffraction limited microscope optics which magnify the luminescence image onto a CCD (Charge Coupled Detector) camera [2, 3]. In this context, a significant improvement to the spatial and time resolution performances could be provided by increasing the absorption and the luminescence efficiencies of the scintillator material. Within a project of the 6th framework program (FP6) of the European Commission (SCINTAX – STRP 033 427) we have developed a new kind of thin single crystal scintillator for high resolution X-ray imaging. Our research was based on $Lu_2SiO_5:Tb^{3+}$ (LSO:Tb) layers grown on suitable substrates. The unique combination of high density (7.4 g/cm^3) Zeff (65.2) and light yield of these scintillators significantly improved the efficiency of the X-ray imaging detectors currently used in synchrotron micro imaging applications.
In this work we present the characterization of the scintillating LSO films in terms of their optical and scintillation properties as well as spatial resolution performances. All the tests were performed at the ANKA-TopoTomo beamline, which can work either in white or in monochromatic beam-mode delivered by the recently installed double multilayer monochromator [4]. The radioluminescence measurements were performed by irradiating the scintillators with the white beam X-ray photon flux density and by using the experimental set-up described in [5]. For accomplishing the spatial resolution measurements we have integrated the LSO scintillating film in an indirect high resolution detector composed of a CCD detector (PCO4000) and a diffraction limited visible light microscope equipped with a 10x objective (NA=0.4) and a 2.5x eyepiece (total magnification of 25x). The MTF (Modulation Transfer Function) of the detection system was calculated from the ESF (Edge Spread Function) measurement in which a GaAs edge was positioned in direct contact with the scintillator.
The newly developed LSO:Tb scintillator was also used for 3D X-ray imaging application in combination with a high speed CMOS detector. The LSO:Tb high density and light yield allowed reducing the necessary time for a complete tomography scan from 2-3 hours up to 0.4 s retaining at the same time a good image quality.

References

[1] K.A. Nugent, T.E. Gureyev, D.F. Cookson, D. Paganin, Z. Barnea, Phys. Rev. Lett. vol. 77 (1996) 2961-2964.
[2] A. Koch, C. Raven, P. Spanne, A. Snigirev, J. Opt. Soc. Am. A, vol.15, no 7 (1998).
[3] A. Koch et al., Phys. Med. Imag. Conf. - Proc.of SPIE, vol. 3659, pp. 170–179 (1999).
[4] A. Rack et al., Nucl. Instrum. & Meth. in Phys. Res. B, vol. 267, no. 11, pp. 1978-1988 (2009).
[5] A. Cecilia et al., Radiation effects and defects in solids, vol 164 Issue 9, pp. 517-522 (2009).

Scintillator technology for enhanced resolution and contrast in X-ray images

Anna Sahlholm, Olof Svenonius, Per Wiklund
Scint-X AB, Kista, Sweden
E-mail: anna.sahlholm@scint-x.com

Scintillators are commonly used for converting X-rays into visible photons in X-ray imaging detectors where a silicon-based sensor is used. However, the scintillator layer often degrades the lateral resolution since secondary photons are emitted isotropically, thus blurring the image. A trade-off usually exists between image resolution and detector sensitivity: a thick scintillating layer yields high sensitivity but poor resolution; a thin layer has the opposite characteristics. Structured scintillators, on the other hand, overcome this trade-off because they function as light guides, bringing the generated secondary photons down to a single detector pixel. Deep, narrow channels are etched into silicon in order to manufacture a matrix that can be filled with CsI(Tl). When X-rays enter those channels, they are converted into green light, which is reflected by the channel sidewalls and therefore does not leave the channel.

The structured scintillator yields superior performance in terms of image resolution and contrast. Applications include dental imaging, material analysis and inspection, high resolution medical imaging, etc. The inherently high resolution and contrast capabilities of the Scint-X structured scintillator make it useful also industrial radiography. Prototypes have been manufactured with better resolution and contrast than available on the market today. These properties are particularly important in order to resolve small details when analyzing different material properties. An application for high resolution X-ray diagnostics under microgravity conditions is currently being developed in cooperation with Swedish Space Corporation and Technische Universität Dresden within the ESA GSTP study "X-ray Diagnostics for Space". The evaluations of this imaging technique show that real-time visualization of objects in the range of less than 5 microns is attainable.

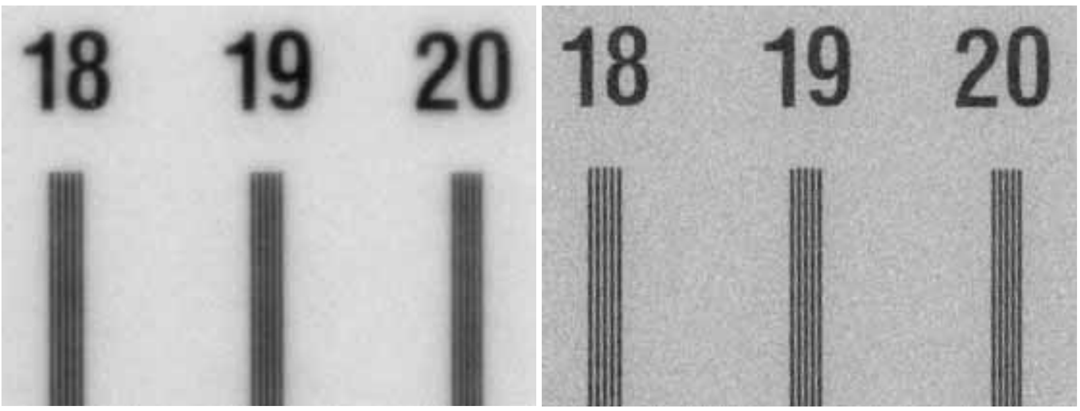

Figure 1: *The figure shows a line pair grating X-rayed using a state of the art scintillator available on the market today (left), compared to the same object X-rayed using Scint-X scintillator matrix technology(right).*

Title: Low noise thin film transistor arrays for digital x-ray imaging detectors

Author and presenter: Denny L. Lee Ph.D.

Corresponding address: Directxray Digital Imaging Technology
1009 Saber Road, West Chester, Pa 19382, USA
Email Address: dlee@directyxray.com

Abstract:

Large area Amorphous Silicon Thin Film Transistor (TFT) arrays are now widely used to capture digital x-ray images either using Direct Conversion Technology such as Selenium X-ray Detector or using Indirect Conversion Technology with phosphor screens such as Cesium Iodide coupled to photo-diode arrays. The readout line capacitance, the gate line switching potentials, and the “on/off” resistance of the FET transistors determine the major readout noise of a large area TFT array. The readout speed is also limited by the gate lines capacitance.

A new and novel detector structure is now being investigated to minimize the readout noise of large area TFT arrays. Conventional TFT panel consists of an orthogonal arrays of pixels addressed by orthogonal gate lines and data lines. The parasitic capacitance from the crossover of these gate lines and data lines inside the TFT structure resulted with a sizable data line capacitance. When charge amplifiers are used for the readout of image information, the thermal noise is greatly amplified by the ratio of the data line capacitance and the feedback capacitor of the charge amplifier. The switching of the gate voltage that is typically 12 volts or higher will also contribute to the switching noise in the readout image. By coupling linear arrays of light emission diodes (LED) or organic LED (OLED) to the bottom side of the TFT array and in the same direction as the gate lines, the crossover of gate lines and data lines in the conventional TFT can be eliminated. The data line capacitance can therefore be greatly reduced. Instead of addressing each row of transistors by the switching of gate control voltage during image readout, lines of light source with collimators are used to optically switch on and off the amorphous silicon transistors one row at a time. By minimizing the data line capacitance, the basic TFT readout noise is greatly reduced and more lower intensity x-ray can be detected. By replacing the high capacitance gate lines with linear light sources, the switching speed can also be increased.

Experimental data and measurements will be presented in this paper.

Development of a positron sensor for multi-modal endoscopy system

K. Shimazoe[1], H. Takahashi[1], K. Fujita[2], H. Mori[1], T. Momose[1], M. Fukuda[3]
[1]The University of Tokyo, [2]Japan Atomic Energy Agency, [3]HOYA Corporation

I. INTRODUCTION

Endoscopy is an important inspection device to detect cancers in human body. But there exists the case of cancer that is hard to detect with only optical device. Double inspection with optical and radio images is preferable for high accuracy diagnosis. And real time radio imaging is also promising for real time surgery with endoscope. We have simulated, designed and fabricated a Si-based positron imaging probe for more accurate cancer detection in multi-modality endoscopy system. The direct positron imaging could have an advantage over gamma imaging in its high sensitivity and resolution.

II. DETECTOR FABRICATION AND EXPERIMENT

To determine the optimal thickness, simulation was executed with EGS5 code. The energy spectra with 0.1mm, 0.2mm, 0.5mm, 1mm, 3mm, 5mm thickness detectors are simulated and the spectrum to gamma rays with less than 1mm detector thickness is almost negligible and zero for more than 340keV gamma rays. Considering this result, we have designed and fabricated Si based positron detector to be implemented inside the endoscope. The diameter should be less than 2.2mm and the thickness of 1mm is chosen from the simulation result. Fig.2 shows the fabricated detectors. We tested this detector with a radio-labeled tumor bearing mouse to count positrons. Fig. 3 shows the positron count per 5minutes for cancer, head, leg and background. We confirmed the difference between cancer and other parts, and positron direct detection is possible with this detector.

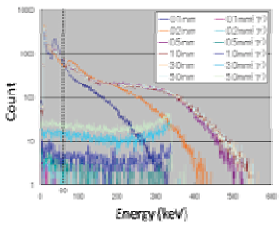

Fig.1 energy spectra simulation

Fig.2 positron sensor (ϕ 2.2mmx1mm)

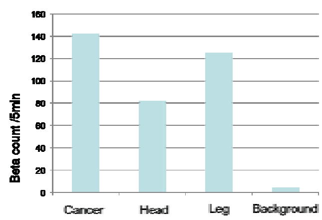

Fig.3 positron count with mouse

III. CONCLUSION AND DISCUSSION

We have simulated and fabricated Si-based positron sensor for multi-modal endoscopy system. It was successfully working with cancer bearing mouse.

REAL-TIME AND HOSPITAL-BASED NEUTRON AUTORADIOGRAPHY WITH A Si-MICROSTRIP DETECTOR

E. M. Donegani [1], A. Aiani[1], F. Basilico [6], D. Bolognini [1 2], P. Borasio [9], E. Capelli [8], P. Cappelletti [5], P. Chiari [8], M. Frigerio [5], S. Gelosa [5], G. Giannini [3 4], S. Hasan [1 2], A. Mattera [1 2], P. Mauri [6], A. F. Monti [5], A. Ostinelli [5], M. Prest [1 2], E. Vallazza [3], A. Zanini [7]

[1] University of Insubria, Como, Italy
[2] INFN sez. Milano Bicocca, Milan, Italy
[3] INFN sez. Trieste, Trieste, Italy
[4] University of Trieste, Trieste, Italy
[5] Azienda Ospedaliera S.Anna, Como, Italy
[6] CNR-ITB, Milan, Italy
[7] INFN sez. Torino, Italy
[8] University of Pavia, Pavia, Italy
[9] Azienda Universitaria Ospedaliera "S. Luigi", Orbassano (TO), Italy

Boron Neutron Capture Therapy (BNCT) is an experimental radiation therapy which requires the selective administration of the non-radioactive isotope ^{10}B to tumoral cells and subsequently the irradiation with a thermal neutron beam. The high LET particles produced in the $^{10}\mathrm{B}(n,\alpha)^{7}\mathrm{Li}$ capture reaction are exploited to induce the cellular apoptosis.

Nowadays, there are two significant limitations which prevent BNCT from becoming a routine radiotherapy technique: the thermal neutron flux which should be at least 5×10^{8} n·cm^{-2}·s^{-1} (currently available only at nuclear reactors), and the lack of specificity of the boron compounds with respect to the neoplastic cells.

Measuring and imaging ^{10}B in biological samples are compulsory to study the possibility of making BNCT a highly selective cancer therapy.

The aims of the system developed within the INFN PhoNeS project is to provide a real-time analysis of the boron content in specimens by means of neutron autoradiography. The α particles emitted in the neutron capture reaction are detected by a microstrip silicon detector.

Furthermore, the method proposed is suitable to be carried out at any radiotherapy unit: in fact, the neutrons are photoproduced by 18 MV photons from a standard radiotherapic linac (the Varian Clinac 2100 C/D in use at the Radiotherapy Department of the S. Anna Hospital in Como, Italy).

The $9.5\times9.5\times0.041$ cm^3 detector consists of 384 channels, with a readout pitch of 242 μm. Moreover, the detector is used unbiased in order to limit the sensitive volume to the first 5 μm thus minimizing the γ-background. Three self-triggering TAA1 ASICs are used to read the detector in anti-coincidence with the primary photon beam thus taking into account only the neutron-induced α-emissions. An absolute calibration was previously performed with several samples containing different known amounts of BSH (one of the main boron agents used in BNCT trials). The minimum ^{10}B detectable amount resulted to be 5 ppm.

In an attempt to investigate the applicability of BNCT in pleural mesothelioma, an explanted human lung was perfused ex-vivo with a solution of BPA (the second used ^{10}B-carrier) and several blood samples were taken at different times after the perfusion start.

A standard procedure has been defined for the preparation of the samples in order to ensure the repeatibility of the measurements. The analyte samples are placed directly on the detector surface, irradiated with thermal neutrons to obtain the ^{10}B-uptake in terms of kinetic curves (^{10}B uptake as a function of time) thus computing the time needed to have a stable boron content in the lung.

The results of the real-time neutron autoradiography were compared to the standard MS analysis on the same specimens and the relative trends are in agreement.

The Effects of Cooling and Acquisition Time Extension on a CMOS Sensor Intended for *in-vivo* Small Animal Imaging Applications

M. Breithaupt, L. Cao, J. Peter

Objective: A recently developed novel detector blueprint proposed for multi-modal *in-vivo* small animal imaging is being investigated regarding its imaging performance under low photon flux conditions. Following the construction of a tomographic detector ring assembly involving 12 large field CMOS photosensors (RadEye1, Rad-icon Imaging Corp.) and aiming to further propel this instrumentation research project from a phantom study experimental stadium towards full preclinical applicability, significant modifications with respect to sensor cooling and acquisition time extension are found essential for achieving target signal-to-noise levels and are being presented.

Material and Methods: In its initial state, a single detector unit consists of an optical alignment of a CMOS photodiode array with a plano-convex microlens array, both elements being mounted to a septum mask intended for inter-lens cross-talk suppression. Such a design yields a very thin detector form factor facilitating space-constrained tomographic instrumentation blueprints for non-contact optical imaging. First, an auxiliary cooling unit has been developed primarily to reduce the photosensor's dark noise. It consists of a sensor size mated aluminum recuperator (4 mm in thickness) that is attached to the backside of the photon detector. The meander-type pipeline inside the recuperator is flushed with a cooled liquid (up to -20°C) delivered by a circulating cooler unit (DLK 1022, FRYKA Kaeltetechnik GmbH). Also, a Peltier cooling element attachment has been studied. The latter approach, while being more cost effective and easier to implement, has been abandoned in favor of liquid cooling for compatibility reasons in multimodal use.
Secondly, software has been developed implementing new trigger pulse sequences for extending the total sensor's acquisition time capabilities (from few seconds to virtual infinity). Depending on timing clock controlling two acquisition strategies (pre-declared sequentially strobe mode, continuous executing intervention mode) are implemented and the effects of noise versus temperature are presented in detail.

Results: After successful implementation of both cooling – all 12 involved CMOS photosensors were modified – as well as acquisition time extension, a number of outcomes were found. Most importantly, cooling the sensor during operation dramatically reduces its dark current contribution and, hence, increases the signal-to-noise ratio. Whereas sensor saturation as the sole result of dark current (no light signal present) was achieved at room temperature (24°C) after 120 seconds (4000 electrons per second), at a temperature of -20°C the sensor was saturated not before 45 hours (<200 electrons per second). Dark current saturation is particularly crucial for low light imaging applications as it restrains the available acquisition time window which, for *in-vivo* small animal imaging, is commonly required to be in the order of several minutes. Even though the quantum efficiency of the CMOS sensor was not altered, the detector's performance nonetheless improved significantly and seems appropriate for small animal imaging after incorporating both alterations (first animal imaging studies are scheduled in the upcoming weeks). The two investigated acquisition strategies did not show considerable differences in data statistics or noise contributions (both not exceeding 0.5% of the dynamic range, as per temperature).

Development of a new Glass GEM with Guard-ring

Hiroyuki Takahashi, Takeshi Fujiwara, Yuki Mitsuya, Shuichi Hatakeyama, Masashi Ohno, Naoko Iyomoto

Department of Nuclear Engineering and Management, The University of Tokyo

GEMs are nowadays widely used in variety of applications. However, its flexible structure sometimes causes a careful handling and its organic component is not favorable in high vacuum environment. Therefore, we are searching for another material suitable for neutron applications. Hoya-Pentax provides a photosensitive glass process PEG3. This glass enables a fine structure made by photolithographic patterning process. We have developed a multi-hole structure of 120 um in diameter using 0.4mm thick glass. Besides this feature, we have added a guard ring close to the edge of each hole. We have tested the G-GEM with X-rays and checked the performance of the plate. When we applied a certain amount of the high voltage between the G-GEM exit and the readout plate, additional amplification occurs within this parallel electric field. The total gas gain was observed to be over 30,000 in this test structure of just one G-GEM and readout plate.

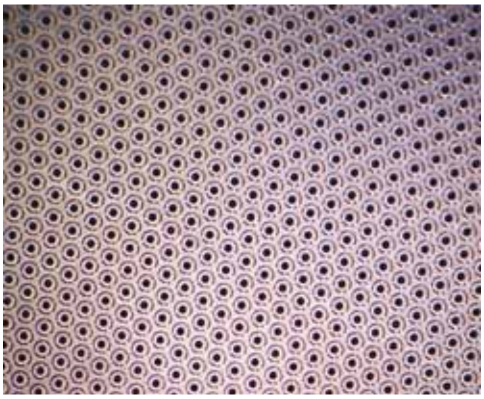

Fig.1 Photograph of the G-GEM

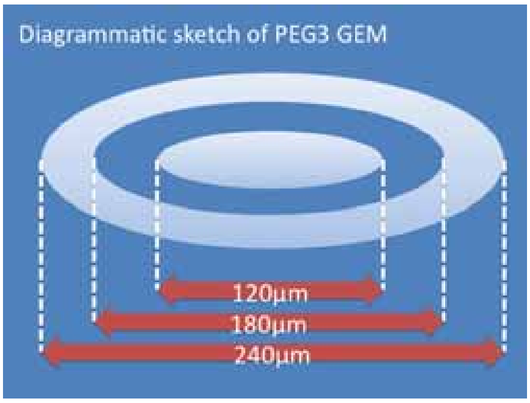

Fig.2 Hole dimension

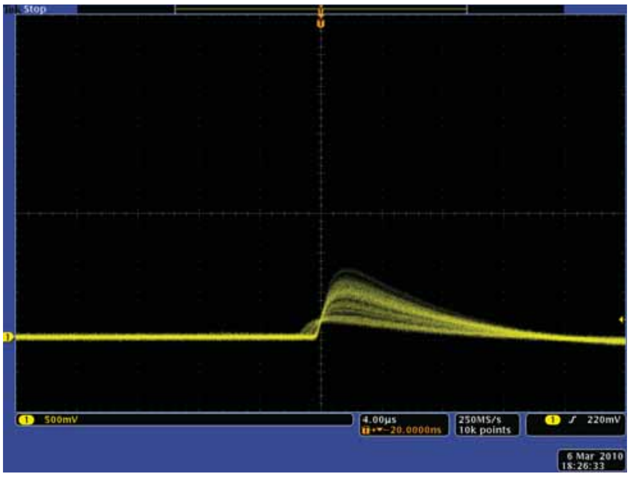

Fig.3 Observed signals for 14keV X-rays after Charge-sensitive preamp (1V/pC) Signal amplitude is over 0.5pC.

Multi-channel picosecond photon timing with microchannel plate detectors

J. S. Lapington, P. Jarron, G. W. Fraser

Microchannel plate-based detectors have the capability to photon-count at time resolutions which outperform solid-state devices such as the APD or SiPM, and have a geometry which lends itself to pixellated readouts. We describe a multi-channel, photon-counting microchannel plate detector optimised for photon timing in the picosecond regime. The detector was originally developed for application to time resolved spectroscopy in the life science area, however its performance characteristics make it suitable for applications where high time resolution, multi-channel photon-counting are required including Cherenkov light detection in nuclear physics, particle physics, and astroparticle astronomy.

We describe the prototype detector, a sealed tube device comprising an optical photocathode proximity focussed to a small pore microchannel plate stack. Event charge is collected on an multichannel readout comprising an 8 × 8 pixel array manufactured on a multilayer ceramic which provides vacuum integrity for the detector enclosure and a multi-way electrical feedthrough for the readout array. Each pixel electrode addresses one channel of a NINO ASIC, a multichannel preamplifier-discriminator device. The discriminator outputs are timed with 25 ps precision by the HPTDC time-to-digital converter ASIC, which uses a time-over-threshold technique for amplitude walk correction. Both NINO and HPTDC were originally designed and manufactured at CERN for the ALICE-TOF experiment on the LHC.

We present performance measurements using a pulsed laser of the 64 channel prototype system comprising a 25 mm detector, NINO front-end and a CAEN V1290A VME module utilizing the HPTDC. We discuss the next phase in the project; design and manufacture of a 40 mm detector with a 16 × 16 pixel^2 readout coupled to custom NINO/HPTDC electronics constructed as an series of 64 channel modules, expandable to even larger channel densities.

Characterisation of a Broad Energy Germanium (BEGe) detector

B o [1,*] Bo o [2] H Bo o [2] B [1]
o [1] U o [2] oo [2] [2]

[1] *Laboratorio de Radiaciones Ionizantes, Universidad de Salamanca, Spain*
[2] *Nuclear Physics Group, University of Liverpool, United Kingdom*

Abstract

Characterisation of Germanium detectors used for gamma-ray tracking or medical imaging is one of the current goals in the Nuclear physics community. Pulse Shape Analysis (PSA) techniques (see [1]) have been developed for different detector geometries or setups. In this work, we present the results of the application of PSA for a Canberra Broad Energy Germanium (BEGe) detector. This detector was scanned across its front and bottom face using a fully digital data acquisition system in the University of Liverpool; allowing to record detector charge pulse shapes from well defined positions with different collimated (to a 2mm diameter) sources such as ^{241}Am, ^{22}Na and ^{137}Cs.

With the study of the data acquired, the position of the contact and passivation layer can be defined, as well as the crystal axis for the Germanium. The best scan for characterising contact properties was done with the ^{137}Cs source from the back face, and its results are presented in figure 1. Therefore, the characterisation of this detector can be enlightening for future uses of BEGe detectors, such as double β decay experiments like in GERDA (see [2]) or MAJORANA collaborations.

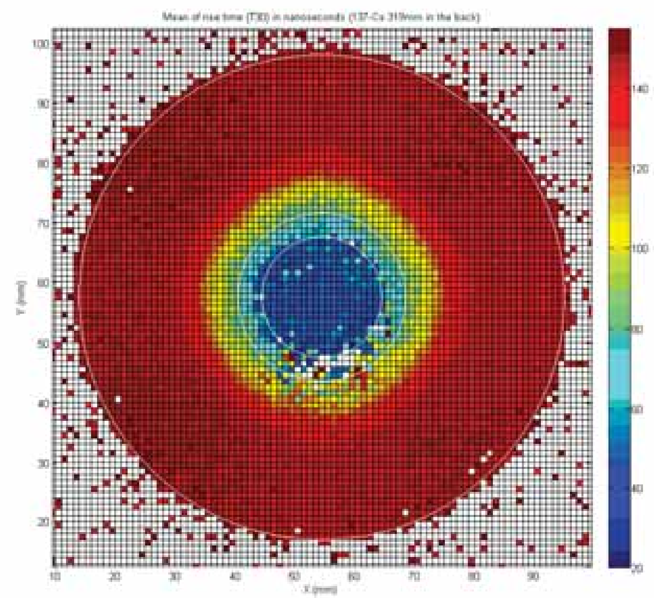

FIG. 1: Risetime plot with the mean value for the T30 (in nanoseconds) for each scan position. T30 is the time taken to rise from 10% of the pulse height to 30% of the pulse height. For this detector, the T30 gives information on the electrons mobility inside the Ge. The white circles correspond (from the center) to the contact, passivation layer and detector limits.

[1] B. Bruyneel, P. Reiter, G. Pascovici, *Characterization of large volume HPGe detectors. Part II: Experimental results*, Nuclear Instruments and Methods A 569 (2006) 764-773.

[2] D. Budjas, M.B. Heider, O. Chkvorets, N. Khanbekov and S. Schonert, *Pulse shape discrimation studies with a Broad-Energy Germanium detector for signal identification and background suppression in the GERDA double β decay experiment*, J. Instrum. 4 (2009) p10007.

*Corresponding author: `diego_barrientos@usal.es`

CHARACTRERIZATION OF MEDIPIX2 EDGELESS PIXEL DETECTORS

J. Kalliopuska[1], L. Tlustos[2], S. Eränen[1], T. Virolainen[1]
[1] VTT Micro and Nanoelectronics, Tietotie 3, Espoo, PO. Box 1000, FI-02044 VTT, Finland
[2] CERN, CERN/PH, CH-1211 Geneva 23, Switzerland
email: juha.kalliopuska@vtt.fi

VTT has developed a straightforward and fast process to fabricate edgeless (active edge) microstrip and pixel detectors on 6" (150 mm) wafers. The process relies on advanced ion implantation to activate the edges of the detector instead of using polysilicon [1]. The presentation summarizes the fabrication process of 150 µm thick p-on-n and n-on-n prototypes having dead layer at the edge below a micron.

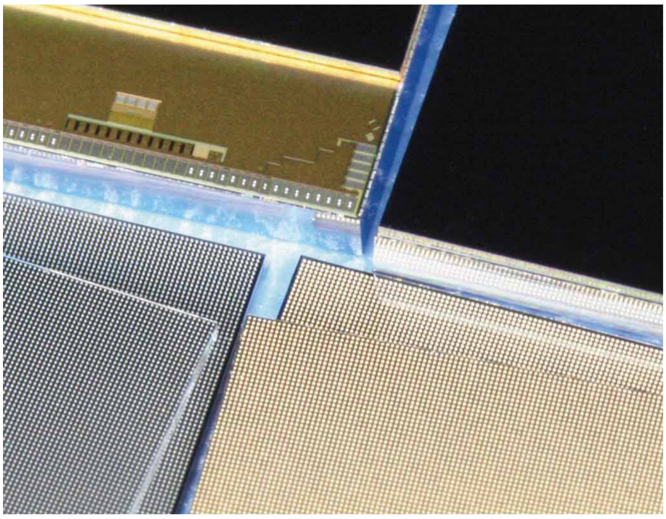

Fig. 1. ***Top:*** **packaged (flip-chip bonded) imaging detector modules, where the detector is on top (face down) and the Medipix2 readout chip on bottom.** ***Bottom left:*** **active edge pixel detectors.** ***Bottom right:*** **active edge pixel detectors with under bump metallization to allow bonding to the readout chips.**

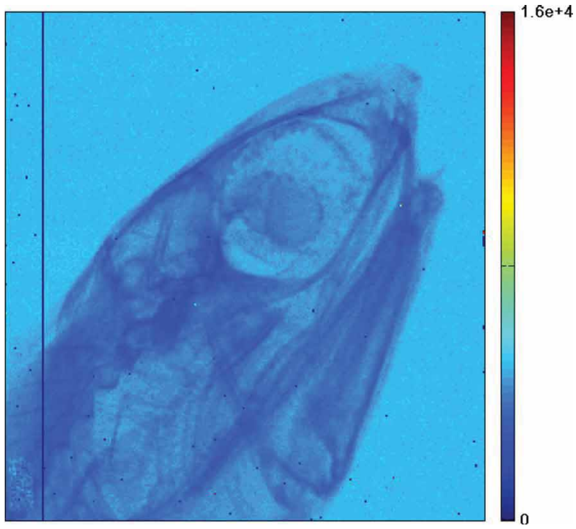

Fig. 2. X-ray image of a small fish with active edge imaging module. Image was taken with a 20 keV X-ray tube with acquisition time of 36 s. Seamless large area images can be obtained by tiling the detectors in to matrices.

Electrical and radiation response characterization of 1.4x1.4 cm^2 n-on-n edgeless detectors has been done by coupling them to the Medipix2 readout chips. Fig. 1 shows a photograph of 150 µm thick edgeless detectors with and without UBM and two flip-chip bonded assemblies. The leakage currents were measured to be ~90 nA/cm^2. Radiation response characterization includes X-ray tube and source responses. Fig. 2 shows a flat-field corrected X-ray image taken with the assembly shown in Fig 1. X-ray tube characterization results show that the edge response depends dramatically on the active edge distance from the nearest pixels.

[1] J. Kalliopuska, et al., *3D processing on 6 in. high resistive SOI-wafers: Fabrication of edgeless strip and pixel detectors*, Nucl. Instr. Meth. in Phys. Res. A, In Press, doi:10.1016/j.nima.2009.03.243.

CZT Performance for Different Anode Pixel Geometries and Data Corrections

Kristen Wangerin, Yanfeng Du, and Floris Jansen
GE Global Research, Niskayuna, NY

The high cost of CZT material makes its use cost prohibitive in many applications. In this work we investigate the performance difference of various anode pixel geometries and the performance improvement obtained after two data correction steps. We found a strong negative relationship between road size (gap between anode pixels) and absolute detection efficiency, and the use of corrections was able to compensate for some of this reduced sensitivity. We developed a Monte Carlo model that accounts for detector geometries and charge diffusion physics and compared the simulations to our measurements.

We acquired Co-57 energy spectra using a NOVA R&D RENA3 ASIC. For three anode geometries, we measured the energy resolution of the 122 keV peak, absolute photopeak efficiency in a 109-129 keV energy window, and charge-sharing fraction for 5 mm thick CZT detectors (Redlen, Vancouver, Canada). We calibrated the incident counts on the CZT detector using a large NaI(Tl) crystal. The energy resolution is found by fitting a Gaussian to the photopeak. The charge-sharing fraction is defined as the ratio of two-pixel events to one + two-pixel events.

A summary of results is shown in Table 1. For the 2.46/0.6 mm form factor, the energy resolution is 6.5 keV, and the absolute detection efficiency is only 26%. We found there is as much as 50% charge loss for two-pixel events occurring over the road. The charge loss is most likely due to the surface state of the CZT and changes in the electric field, such that some of the charge never makes it to the anode pad [1]. For 1.8 and 1.3 mm pitch, we expect the charge collection properties to improve as a result of the small pixel effect and at the expense of increased charge sharing due to charge diffusion [2]. Our measurements confirm this and demonstrate further gains from narrower roads, similar to Kuvvetli et al. [3] who found that charge loss is linearly dependent on road width. With 0.1 mm roads, the absolute photopeak efficiency improves to > 50% with little charge loss.

After measuring detector performance with different pixel geometries, we implemented charge sharing (CS) and depth of interaction (DOI) corrections to further improve performance. The energy resolution improves up to 1 keV, and efficiencies for the three designs improve by 145%, 115%, and 125%, respectively. The most significant improvement was for the 2.46/0.6 mm form factor, shown in Figure 1. The efficiency is still very low, however, and we suspect that some events are not being detected at all. A weak electric field near the anode and field lines terminating in the road are contributing to charge loss effects, and signals fall below the 30 keV lower energy threshold and are not read out by the ASIC. For 0.1 mm roads, our measurements and simulations are in relatively good agreement. Charge loss effects, which are very difficult to model, can explain the difference between measurements and simulations for wider roads.

By optimizing CZT detector geometry, we can trade-off detector performance and read-out electronics requirements. With continued understanding of detector physics, including surface passivation and charge loss, we can further improve detector performance to realize the use of CZT in a broader application space.

Table 1. Energy resolution and absolute efficiency calculations without and with corrections and twopixel event fraction

Pitch / Road (mm)	Without Corrections	+ CS Correction	+ DOI Correction	Two-Pixel Events
2.46 / 0.6	6.5 keV 26%	7.4 keV 35%	6.0 keV 38%	12%
1.8 / 0.1	6.3 keV 56%	5.9 keV 62%	5.4 keV 64%	8%
1.3 / 0.1	4.8 keV 51%	5.5 keV 63%	5.1 keV 64%	13%

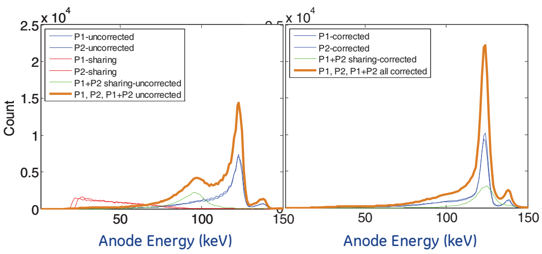

Figure 1. Anode spectra of 2.46/0.6 mm form factor before (left) and after (right) corrections.

[1] Iniewski, Kris, et al. Modeling Charge-Sharing Effects in Pixelated CZT Detectors. IEEE NSS (2007) 4608-4611.
[2] Gros D'Aillon, Eric, et al. Charge sharing on monolithic CdZnTe gamma-ray detectors: A simulation study. NIMA 563 (2006) 124-127.
[3] Kuvvetli, Irfan and Budtz-Jorgensen, Carl. Measurements of Charge Sharing Effects in Pixilated CZT/CdTe Detectors. IEEE NSS (2007) 2252-2257.

Abstract for IMAGING 2010

Large-Format Gamma-Ray Imaging Systems Using CdZnTe Coplanar-Grid Detectors

Paul N. Luke, Mark Amman, Julie S. Lee, Lucian Mihailescu, Kai Vetter
Lawrence Berkeley National Laboratory, Berkeley, CA, USA

Andreas Zoglauer, Michelle Galloway, Steven E. Boggs
Space Sciences Laboratory, University of California, Berkeley, CA, USA

Henry Chen, Glenn Bindley
Redlen Technologies, British Columbia, Canada

Gianluigi De Geronimo
Brookhaven National Laboratory, Upton, NY, USA

A highly modular CdZnTe detector design has been developed to enable the assembly of a large gamma-ray imaging system for standoff detection – the High Efficiency Multi-mode Imager (HEMI). The basic building block in this design is a single-channel detector element consisting of a 1-cm^3 CdZnTe coplanar-grid detector, analog readout electronics and detector biasing network, all of which is packaged in a compact polycarbonate housing. The detector elements can be plugged into a motherboard to form an array and can be easily unplugged for replacement or re-arrangement. Each element is individually optimized using an automated test system and thereafter deployed without further adjustments or electronic corrections. The detector elements are optimized at the same detector bias voltage and grid bias voltage so that all elements in an array can operate with one common detector bias supply and one common grid bias supply. This modular detector element design provides a high degree of flexibility, allowing the assembly of imaging systems of different sizes and configurations, such as Compton, active or passive coded-aperture, and hybrid (multi-mode) imaging systems. By using large single-channel detectors as detection elements, large-format imagers can be produced with reduced electronics and signal processing complexity as well as lower power consumption.

At the present time, the detector element design has been successfully developed and ~30 detector elements have been produced. The detector elements exhibit a median energy resolution of 2.0% FWHM at 662 keV. A test array that can accommodate 2 planes of 8X8 detector elements has been built to evaluate the performance capability of this instrument concept. Imaging tests have been performed with the array partially populated with 24 detector elements. The figures below show a photograph of the test array and measurement results demonstrating spectroscopic imaging of multiple gamma sources.

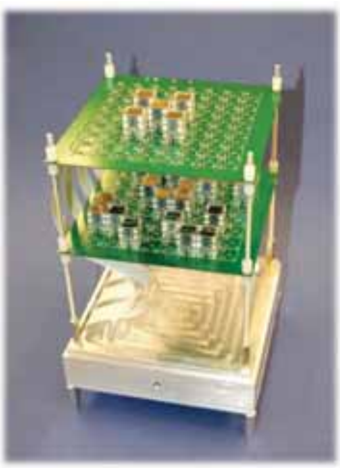

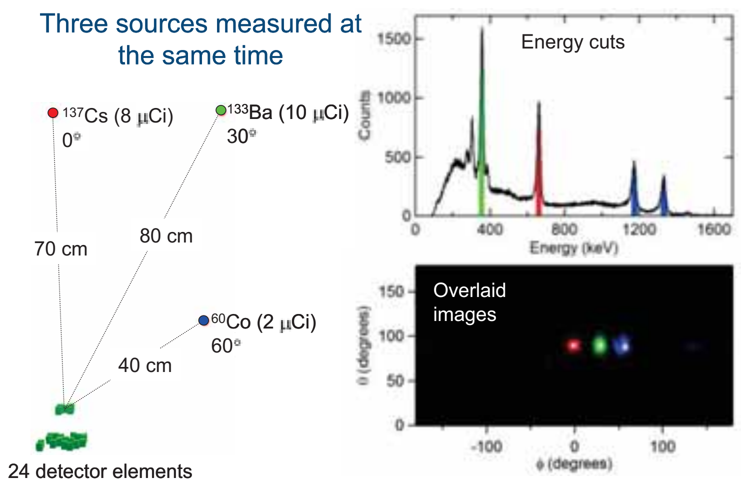

Spectral Resolution of a CdTe Medipix Hexa Detector with a 165 µm Pixel Pitch

Thomas Koenig[1], Andreas Zwerger[2], Marcus Zuber[1], Patrick Schuenke[1], Simeon Nill[1], Alex Fauler[2], Michael Fiederle[2] and Uwe Oelfke[1]

[1] German Cancer Research Center (DKFZ), Im Neuenheimer Feld 280, 69120 Heidelberg, Germany
[2] Freiburg Materials Research Center (FMF), Stefan-Meier-Strasse 21, 79104 Freiburg, Germany

Purpose

X-ray imaging based on photon counting pixel detectors has received increased interest during the past years. Attached to a semiconductor of choice, some of these devices enable to resolve the spectral components of an image. We aim at characterizing a Medipix[a] 2 MXR Hexa detector, where six individual Medipix detectors were combined to form a 3×2 array of 4.2×2.8 cm^2 size. In this work, we present initial results from measuring the line widths of characteristic x-rays obtainable with such a device.

Materials & Methods

In order to achieve a pixel pitch of 165 µm rather than the 55 µm that are provided by the Medipix architecture, only every ninth pixel was connected to the sensor, which was made up by a 1 mm thick Cadmium Telluride (CdTe) single-crystal.
The detector was calibrated according to standard procedures[b]. In particular, a Siemens Powerphos X-ray tube was operated at 100 kVp to induce the emission of characteristic x-rays in both Silver and Molybdenum foils. The detector was then placed outside of the primary x-ray beam. A drift voltage of 200 V was applied. X-ray spectra were recorded using the Medipix USB[c] interface and the Pixelman[d] software by scanning in single-threshold mode and subsequent derivation of the data. The full width half maximum (FWHM) of the silver peak in single-threshold mode was determined for each pixel.

[a] Llopart, X.; Campbell, M.; Dinapoli, R.; San Segundo, D.; Pernigotti, E., "Medipix2: A 64-k pixel readout chip with 55-µm square elements working in single photon counting mode", Nuclear Science, IEEE Transactions on, vol.49, no.5, pp. 2279-2283, Oct 2002

[b] Tlustos, L.; Ballabriga, R.; Campbell, M.; Heijne, E.; Kincade, K.; Llopart, X.; Stejskal, P., "Imaging properties of the Medipix2 system exploiting single and dual energy thresholds", Nuclear Science, IEEE Transactions on, vol.53, no.1, pp. 367-372, Feb. 2006

[c] Vykydal, Z.; Jakubek, J.; Pospisil, S., "USB interface for Medipix2 pixel device enabling energy and position-sensitive detection of heavy charged particles", Nucl. Instr. and Meth. A, vol.563, no.1, pp. 112-115, February 2006

[d] Holy, T.; Jakubek, J.; Pospisil, S.; Uher, J.; Vavrik, D.; Vykydal, Z., "Data acquisition and processing software package for Medipix2", Nucl. Instr. and Meth. A, vol.563, no.1, pp. 254-258, February 2006

Results & Conclusion

The FWHM was found to be $3.2\,\mathrm{keV} \pm 0.4\,\mathrm{keV}$. Fig. 1 shows a single pixel spectrum, which was filtered with a binomial kernel of size 21 in order to reduce standard deviation. It clearly demonstrates that the silver and molybdenum peaks can be well separated.

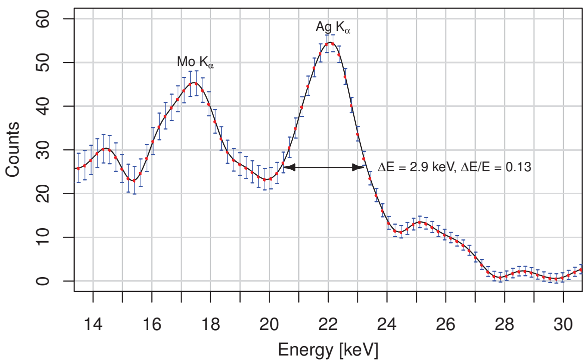

Figure 1

Fig. 2 indicates the image quality achievable with the Medipix platform. It shows a picture of a metal watch acquired in single threshold mode above an x-ray energy of 85 keV. Apart from some defective bump bonds at the bottom and on the right, it exhibits low noise and sharp structures. Detailed measurements of the modulation transfer function, detective quantum efficiency and line widths in dual threshold mode will be carried out in future experiments.

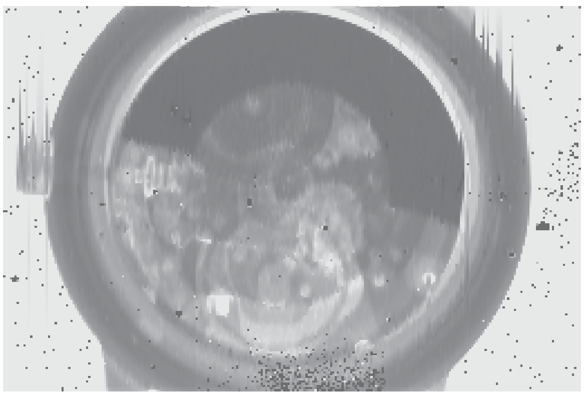

Figure 2

3-D Position Sensitive Room-Temperature Semiconductor Imaging Spectrometers

Zhong He

Nuclear Engineering and Radiological Sciences Department

The University of Michigan, Ann Arbor, Michigan, USA

Abstract

The performance of three-dimensional position sensitive room-temperature semiconductor gamma-ray detectors, in particular CdZnTe and HgI_2, has been improved significantly since 1998. The detector volume has increased from 1×1×1 cm^3 to 2×2×1.5 cm^3, a factor of six larger, while the energy resolution has been improved from 1.7% FWHM to 0.48% FWHM at 662 keV for single-pixel events. These detectors provide the energy deposition and position in 3-dimensions for each individual radiation interaction. The combined capability of 3-D position sensing and gamma-ray spectroscopy enables real-time gamma-ray imaging based on Compton scattering kinematics. Recent development on these room-temperature semiconductor gamma-ray imaging spectrometers will be reviewed.

Ultra High-Speed X-Ray Imaging of Hypervelocity Projectiles

[1]Stuart Miller, [1]Bipin Singh, [1]Gerald Entine, [1]Vivek V. Nagarkar*,
[2]Larry Campbell, [3]Ron Bishel, and [3]Rick Rushing

[1]Radiation Monitoring Devices, Inc., 44 Hunt St., Watertown, Massachusetts 02472 USA

[2]ATA Range Operations Lead, Arnold AFB, Tennessee 37389 USA

[3]USAF, AEDC/DOT, 1099 Avenue C, Arnold AFB, Tennessee 37389 USA

** Corresponding author:* vnagarkar@rmdinc.com, *Tel.: 617-668-6937*

High-speed X-ray imaging is extremely important for healthcare, industrial, military and research applications such as medical computed tomography, non-destructive testing, imaging exploding ordnance, and analyzing ballistic impacts. We report on the development of a modular, ultra high-speed, high-resolution digital X-ray imaging system with large active imaging area and microsecond time resolution, capable of acquiring at a rate of up to 150,000 frames per second. The system is based on a high-resolution, high-efficiency, fast-decay scintillator screen optically coupled to an ultra-fast image-intensified CCD camera designed for ballistic impact studies and hypervelocity projectile imaging. A specially designed multi-anode, high-fluence X-ray source with 50 ns pulse duration provides a sequence of blur-free images of hypervelocity projectiles traveling at speeds exceeding 8 km/second (18,000 miles/hour). This paper will discuss the design, performance, and high frame rate imaging capability of the system.

Large Area MEMS Based Ultrasound Device for Cancer Detection

Robert Wodnicki, Charles Woychik, Kai Thomenius, Fong Ming Hooi[1], Paul L. Carson[1], Elvis Der-Song Lin[2], Pierre Khuri-Yakub[2]

GE Global Research,
1 Research Circle, KW C1804
Niskayuna, NY12309, USA

1. Radiology and Biomedical Engineering
3218 Med. Sci. I
Ann Arbor, MI 48109-56677

2. Department of Electrical Engineering
Stanford University, Stanford, CA 94309

The project described was supported by Grant Number 1R01CA1152677 from the National Cancer Institute. Its contents are solely the responsibility of the authors and do not necessarily represent the official views of the National Cancer Institute or NIH.

ABSTRACT

Ultrasound is an important imaging modality for diagnosis and, in some countries, detection of breast cancer, particularly in women with dense breasts. As compared to the standard of care (digital x-ray mammography) full field 3D imaging of the breast with ultrasound could add sensitivity and specificity to screening in most clinical practices. We have previously described the main design goals in the development of what we call reconfigurable arrays. It is anticipated that such large area arrays offer superior imaging capability and greater flexibility than conventional approaches. One of the main challenges with a full field array is the large number of ultrasound transducer array elements that would be required to be interconnected to form the array. We have been developing a new array architecture based on Capacitive Micromachined Ultrasound Transducers (cMUTs) and reconfigurable arrays in order to address this challenge. The full field array will be composed of a series of tileable modules comprising the cMUT transducer devices as well as co-integrated High Voltage capable interface electronics. The modules will be built up using an advanced organic semiconductor interposer having 11-layers with a total cross-sectional thickness of only 0.5mm. State of the art flip-chip assembly methods are used for mounting both the topside MEMS transducers and the integrated interface electronics ASICs on the backside of the interposer. Reconfigurable array elements will allow imaging with modest numbers of signal acquisition channels. We will present initial imaging results using a preliminary array that integrates the transducers and the substrate. We will compare these results to a state-of-the art existing production ultrasound probe and provide simulated and experimental results on a new Speed of Sound through-transmission method for detection of breast cancer that would become imminently practical with full field arrays on both sides of the compressed breast.

Boron-coated straw detectors: Novel approach for Helium-3 neutron detector replacement

Lacy, Jeffrey L. (1)
Proportional Technologies, Inc.
8022 El Rio, St. Houston, TX 77054
Phone: 713.747.7324 x. 11
jlacy@proportionaltech.com

US efforts to equip major seaports and other critical points of entry with large area neutron detectors to intercept smuggled nuclear materials have been undermined by a critical shortage of 3He gas. Annual demand for 3He in US security applications alone is roughly 22 kiloliters and exceeds current worldwide supply. Significant limitations have been placed on neutron science, safeguards, defense, and other applications that depend exclusively on 3He-based detectors. Alternative neutron detection technologies capable of supporting large sensitive areas while maintaining low gamma sensitivity and low costs must be investigated to ensure the long term viability of the United States' critical detection and interdiction capabilities. We propose a technology based on closely-packed arrays of long, 4mm diameter, aluminum or copper tubes (straws) internally coated with a thin layer of 10B-enriched boron carbide ($^{10}B_4C$) as a ready replacement for 3He in the world's nuclear nonproliferation infrastructure.

In this paper, we review three distinct BCS detector prototype configurations and applications, including a large-area neutron-imaging panel, a stand-off detector, and a portal monitor for fissile materials. The unique, close-packed straw array in each reviewed detector configuration offers a neutron stopping power equivalent to 2.68 atm of 3He gas. Boron's naturally high abundance on Earth and the low cost of 10B enrichment give boron-coated straw (BCS) technology distinct advantages over conventional 3He-based detectors. Faster signals, short recovery time (ion drift), low weight, portability (no pressurization), and low production costs are additional advantages.

The large area imaging panel incorporates 1100 aluminum BCS detectors, each 4 mm in diameter, 1 meter long, and lined with non-enriched B_4C. The imager features a sensitive area of 1 m^2, 3D spatial resolution of 7x4x4 mm^3, and can sustain count rates up to 200,000 cps per readout channel (22 channels total) without significant loss in resolution. Testing with a pulsed neutron beam at ORNL's HFIR is also reported.

The stand-off detector incorporates 1100 copper BCS detectors: each 4 mm in diameter, 1 meter long, and lined with a nominal 1 μm thick coating of enriched $^{10}B_4C$. The monitor has undergone temperature cycling and mechanical vibration testing at ORNL, and has been operated successfully in real-time, maritime field conditions.

Finally, a BCS design is presented for portal monitoring of fissile materials. The design adopts the outer dimensions of currently deployed 3He-based designs, but takes advantage of the small BCS diameter to achieve a more uniform distribution of neutron converter throughout the moderating material. We estimate that approximately 100 BCS detectors can exceed or match the detection efficiency of typical monitors fitted with a 5-cm diameter 3He tube pressurized to 3 atm.

In silico imaging: possibilities and challenges

Aldo Badano, CDRH/FDA

The capability to simulate the imaging performance of new detector concepts is crucial to develop the next generation of medical imaging systems. Proper modeling tools allow for optimal designs that maximize image quality while minimizing patient and occupational radiation doses. This talk reviews current progress and challenges in the simulation of imaging systems with a focus on Monte Carlo approaches to indirect and direct detection, acceleration approaches for realistic anatomical modeling, and validation strategies.

The Silicon Photomultipliers (SiPM) as novel Photodetectors for PET (**)

Alberto Del Guerra (*)
Department of Physics, University of Pisa and INFN, Sezione di Pisa
Largo Bruno Pontecorvo 3, Pisa, I-56127 Italy

Silicon Photomultipliers (SiPM) are a novel type of photodetectors that show great promise for Nuclear Medicine applications and especially for the next generation of PET scanners. The INFN collaboration DASIPM2 is investigating in depth the properties of the SiPM and SIPM matrices developed at FBK-irst (Trento, Italy), whose performance [1] compete successfully with those of similar devices produced by commercial companies, but have in addition novel and attractive properties, such as monolithic matrix arrangement and in the future feed-through contact for backplane read-out.

In this presentation I will illustrate the major advantages of the SiPM for PET applications. In addition to their compatibility in magnetic field and magnetic field gradient, thus giving the possibility of constructing a "state of the art" PET insert within a MRI scanner [2], very attractive features are:
- an intrinsic time resolution well below 70 ps (sigma), that coupled to a high PDE could allow Time Of Flight PET coincidence time resolution well below ~ 500 ps (sigma) [3,4];
- a very high photodetector granularity that allows 2-D/3-D position determination with monolithic crystals, possibly including Depth Of Interaction [5,6], thus paving the way for the construction for the next generation of PET cameras.

We report on the most recent experimental results we have obtained at our institution for SiPM and SIPM matrices performances for PET and on the design of a novel block detector with 4-D capability.

[1] C. Piemonte, et al., IEEE Trans Nucl Sci, 2007, 54(1), 236-244,
[2] R.C.Hawkes, et al., Conf. Records of the 2007 IEEE Nuclear Science Symposium and Medical Imaging Conference, 2007, Vol.5, 3400-3403.
[3] G.Collazuol et al., Nucl Instr and Methods A 2007, A581, 461-464
[4] G. Llosa, et al., IEEE Trans. Nucl. Sci., 2008, 55(3), 877 – 881.
[5] S.Moehrs, et al., Phys Med Biol, 2006, 51,1113-1127.
[6] G.Llosa, et al, IEEE Trans Nucl Sci 2009, 56(5), 2586-2593.
****

(*) - Spokesman of the DaSiPM2 collaboration (INFN-Group V):
[University and INFN Bari, Bologna, Perugia, Pisa, Trento and FBK-irst Trento (Italy)]
- Spokesman of the PRIN 2007: "A very high spatial resolution small animal PET scanner based on high granularity silicon photomultipliers [University of Pisa, Bari, Bologna, Perugia (Italy)]

(**) - This work is supported in part by the ENVISION Project funded by FP7 (2010).

Title:
The Forward Silicon Vertex Tracker and Custom Electronics Readout for the PHENIX Experiment at RHIC

Author:
Jon S Kapustinsky, Los Alamos National Laboratory, for the PHENIX Collaboration

Abstract:

We are designing a Forward Silicon Vertex Tracker (FVTX) upgrade for the PHENIX detector at the Relativistic Heavy Ion Collider (RHIC) at Brookhaven National Laboratory to extend the vertex capability of the central PHENIX Silicon Vertex Tracker (VTX) to forward and backward rapidities, (η), and also to extend the reach in the low momentum-fraction region, (x). The FVTX is designed with adequate spatial resolution to separate decay muons coming from the relatively long-lived heavy quark mesons (Charm and Beauty), from particles that originate at the primary collision vertex. These heavy quarks can be used to probe the high density medium, the quark-gluon plasma, that is formed in Au+Au collisions at RHIC. The FVTX is designed as two endcaps. Each endcap is comprised of four silicon disks covering opening angles from 10 to 35 degrees to match the existing muon arm acceptance. Each plane consists of p-on-n, silicon wedges, with ac-coupled mini-strips spaced on 75μm pitch in the radial direction and varying projective length in the phi direction increasing from 3.35 mm at the inner radius to 11.65 mm at the outer radius. The performance criteria of a custom front-end chip, the FPHX, was specified by the FVTX collaboration and designed and laid out by the ASIC Design Group at Fermilab. The chip combines fast trigger capability with data push architecture in a low power design. The production rounds of the sensor and chips are complete. The sensors and readout chip are described in technical detail and test results are presented.

First Results from the LHCb Vertex Locator

Submitted by the project leader on behalf of the LHCb VELO group

LHCb is a dedicated experiment to study new physics in the decays of beauty and charm hadrons at the Large Hadron Collider (LHC) at CERN. The beauty and charm hadrons are identified through their flight distance in the Vertex Locator (VELO), and hence the detector is critical for both the trigger and offline physics analyses.

The VELO is the silicon detector surrounding the interaction point, and is the closest LHC vertex detector to the interaction point, located only 7 mm from the LHC beam during normal operation. The detector will operate in an extreme and highly non-uniform radiation environment. The VELO consists of two retractable detector halves with 21 silicon micro-strip tracking modules each. A module is composed of two n^+-on-n 300 micron thick half disc sensors with R-measuring and Phi-measuring micro-strip geometry, mounted on a carbon fibre support paddle. The minum pitch is approximately 40 µm. The detector is also equipped with one n-on-p module. The detectors are operated in vacuum and a bi-phase C02 cooling system used. The detectors are readout with an analogue front-end chip and the signals processed by a set of algorithms in FPGA processing boards. The performance of the algorithms is tuned for each individual strip using a bit-perfect emulation of the FPGA code run in the full software framework of the experiment.

The VELO has been commissioned and successfully operated during the initial running period of the LHC. The detector has been time aligned to the LHC beam to within 2 ns, and spatially aligned to 4 µm. The halves are inserted for each fill of the LHC once stable beams are obtained. The detector is centred around the LHC beam during the insertion through the online reconstruction on the primary vertex position. Preliminary operational results show a signal to noise ratio of 20:1 and a cluster finding efficiency of 99.6 %. The small pitch and analogue readout, result in a best single hit precision of 4 µm having been achieved at the optimal track angle.

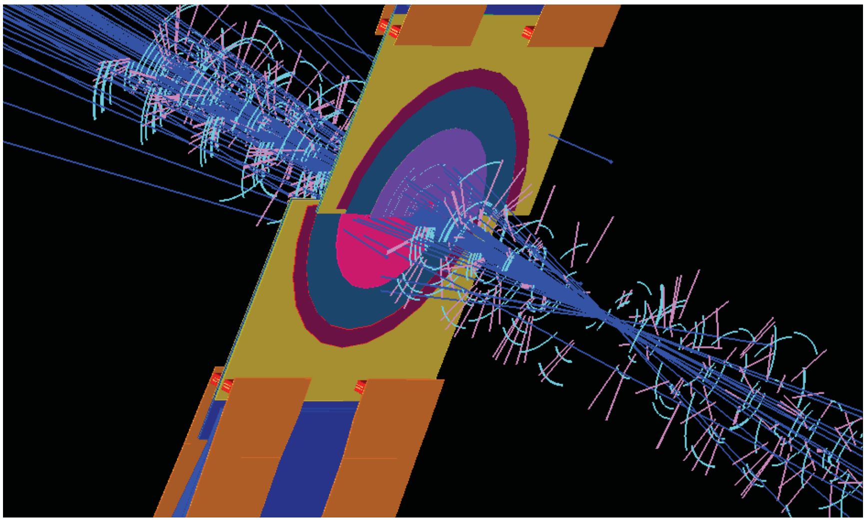

Figure 1: Reconstructed hits and tracks in the LHCb VELO detector from a 7 TeV centre-of-mass energy collision in the LHC. Two modules are shown.

Construction and initial studies of a two block small animal PET scanner

C. Pafilis[1], A. Gaitanis[2], C. Gatis[1], G. Kontaxakis[5], E. Logaras[1], S. Pavlopoulos[3], G. Panayiotakis[4], G. Spyrou[2], G. Tzanakos[1], D. Vamvakas[1]

[1] University of Athens
[2] Biomedical Research Foundation, Academy of Athens (BRFAA),
[3] National Technical University of Athens
[4] University of Patras
[5] Universidad Politécnica de Madrid

Abstract

Detectors used in the majority of the small animal PET tomographs, consist of detector blocks constructed from small inorganic scintillator crystals (BGO, LSO, GSO, etc), coupled to position sensitive and multi-anode photomultiplier tubes (PMT). We are developing a small animal PET prototype, in order to study specific design characteristics and measure its performance. We have constructed two detector blocks, each made of 216 BGO crystals, cylindrically arranged and coupled to a position-sensitive photomultiplier tube (Hamamatsu R2486 PSPMT).

In order to measure the distortion characteristics of each PMT we used a home made computer controlled x–y stage system, to shine light pulses from a blue LED via an optical fibre, on the cathode surface of each of the two PMTs. For every physical position (x, y) of the fiber we measured and digitized the analogue signals from the PMTs and computed the "position" variables (X_r, Y_r). In this way we constructed a map connecting the real (physical) positions (x,y) of the fiber to the computed "position" variables (X_r, Y_r). This map allows to convert measured variables to real position on the cathode surface of the PMTs, and therefore remove spatial distortions.

In order to remove these distortions two multilayer perceptron (MLP) feed-forward neural networks were used, one for each axis. The training of the networks was performed, using half of the data from the two arrays of the PMTs and checked with the whole maps. Correct training of the MLPs was verified using several images as input while the error of the reconstructed output from the neural networks and the real positions of the LED was calculated. Using the collected data we also estimated the intrinsic resolution of each PMT as well as the response uniformity as a function of position. In order to measure the spatial resolution of each block we used a Na-22 point source with the two block detectors in time coincidence mode. The annihilation photons were detected and the image of the source was reconstructed. Using data in this configuration we were able to develop a method for the correction of misalignment of the two blocks. Finally, a rotating gantry is being constructed for the positioning of the two detectors and the production of 3-D tomographic images.

Extraction of Input Function from Cardiac Dynamic PET Images in Rodents using Wavelet Packets Based Sub-band Decomposition Independent Component Analysis.

Jhih-Shian Lee[1], Kuan-Hao Su[1], Wai-Peng, Shirmy Tam[1], Ren-Shyan Liu [2,3], and Jyh-Cheng Chen[1,4*]

[1] Department of Biomedical Imaging & Radiological Sciences, National Yang-Ming University, , No. 155, Sec. 2, Li-Nong Road, Baitou, Taipei city 112, Taiwan, ROC.

[2] National PET/Cyclotron Center, Taipei Veterans General Hospital, No. 201, Sec. 2, Shih-Pai Road, Taipei 112, Taiwan

[3]National Yang-Ming University Medical School, , No. 155, Sec. 2, Li-Nong Road, Baitou, Taipei city 112, Taiwan, ROC.

[4]Department of Education and Research, Taipei City Hospital, 145 Zheng Zhou Road, Taipei City, Taiwan R.O.C.

Purpose: The term input function usually refers to the tracer plasma time activity curve (pTAC), which is necessary for quantitative positron emission tomography (PET) studies. The purpose of this study was to acquire an input function or whole-blood time-activity-curve (wTAC) by wavelet packets based sub-band decomposition independent component analysis (WP-based SBICA).

Methods: In four real Sprague-Dawley rats, arterial blood samples were obtained at 0, 8, 15, 30, 60, 120, 180, 300, 450, 600, 900, 1500, 2400 s following the injection of 18F-FDG and microPET scan. The wTACs were determined in a well counter and they were treated as the reference values. Each wTAC was estimated by WP-based SBICA from cardiac dynamic PET images. We also used FastICA and EPICA (extraction of the pTAC using independent component analysis) estimated wTACs to compare with the results of our method using the normalized root mean square error (NRMSE) and error of area under curve (EAUC).

Results: The averaged NRMSEs for the three methods were 0.3384, 0.6546, and 0.2063 for FastICA, EPICA, and WP-based SBICA, respectively. The averaged EAUCs were 0.2304, 0.6278 and 0.1145 for FastICA, EPICA, and WP-based SBICA, respectively.

Conclusion: The method, WP-based SBICA extends applicability of standard independent component analysis through the relaxation of the independence assumption. Our results show that the accuracy of estimation of the input function using WP-based SBICA outperforms that obtained by FastICA and EPICA.

PAMELA - a satellite-based observatory for precision studies of cosmic rays

Mark Pearce
KTH, Department of Physics and
The Oskar Klein Centre for Cosmoparticle Physics, AlbaNova University Centre, Stockholm, Sweden.

The PAMELA satellite experiment is making precision measurements of the charged cosmic radiation while executing a low earth orbit. The combination of a permanent magnet silicon strip spectrometer and a silicon-tungsten imaging calorimeter permits measurements over an unprecedented energy range (~100 MeV - ~200 GeV) with excellent statistics. A prominent scientific goal of PAMELA is to study the energy spectra of cosmic ray antiparticles in order to search for exotic contributions from (e.g.) dark matter particle annihilations. Results from these studies will be presented, as well as other recent PAMELA measurements.

Spatial resolution and efficiency-fundamental limits and state-of-the art of SPECT

Freek J. Beekman Ph.D.

Pivotal questions in pharmacology and biology concern how function of localized cells relates to disease. For example in experimental neuroscience we have dreamt about a magnifying glass that would allow us to see neurotransmitters in action, in cardiovascular research about a system that would provide us simultaneously with myocardial anatomy, mechanical function and cell function, and in cancer research to see detailed dynamic distributions of pharmaceuticals and markers, in small animals serving as models for human disease. Such studies have been limited by the availability of methods to study such molecular dynamics. Recently multi-pinhole Single Photon Emission Computed Tomography systems (e.g. U-SPECT) have been built that can quantify tracer dynamics in <0.35mm structures e.g. in a mouse brain, heart and tumors. These devices use sophisticated focusing pinhole geometries together with unique 3D focusing technology and list mode data acquisition. Novel iterative reconstruction methods that enable to enhance resolution are applied, accelerated by novel block-iterative methods

Examples of biological applications that will be shown include imaging the density and occupancy of dopamine transporters in sub-compartments of the brain, sub-half-mm resolution dynamic myocardial perfusion imaging or imaging of anti-cancer agents (e.g. antibodies) in tumors, all during a range of points in time. Applied to different models of disease this will aid our understanding of dynamic processes that underlie tissue functions and human pathology.

An overview of the U-SPECT technologies will be given as well as current research on novel collimation methods, image reconstruction and detector technologies for next generations SPECT and combined SPECT/PET with advanced 511keV pinhole technologies in my group. Furthermore, limitations of pinhole SPECT performance will be discussed.

References:
1. F. van der Have et al. U-SPECT-II: An Ultra-High-Resolution Device for Molecular Small-Animal Imaging, J. Nucl.Med. 2009
2. F.J. Beekman and F van der Have. “The Pinhole: gateway to ultra-high resolution three-dimensional radionuclide imaging”, Eur. J. Nucl. Med. Mol. Im, 4(2):151-61, 2007
3. B Vastenhouw et al. Movies of dopamine transporter occupancy with ultra-high resolution focusing pinhole SPECT. Mol. Psych., 2007
4. M. Rentmeester, F. van der Have and F.J. Beekman, “Optimizing SPECT multi-pinhole geometries using an analytical model”. Phys. Med. Biol., 2007
5. W. Branderhorst, B. Vastenhouw & F.J. Beekman. Pixel-based subsets for rapid multi-pinhole SPECT reconstruction. Phys. Med. Biol., 2010
6. M.C. Goorden, M. Rentmeester and F.J Beekman, Theoretical analysis of multi-pinhole brain SPECT, Phys. Med. Biol., 2009
7. M.C. Goorden and F.J. Beekman, High-resolution tomography of positron emitters with clustered pinholes. Phys. Med. Biol., 2010

Fundamental Limits of Spatial Resolution in PET

William W. Moses

Lawrence Berkeley National Laboratory

The physical processes affecting reconstructed spatial resolution in conventional PET have long been quantitatively understood. The dominant factor is usually the width of the detector crystal, and the position of interaction within the crystal is not determined. However, reducing the crystal width to zero will not produce infinitely good spatial resolution because of three other factors. First, the positron is ejected from the nucleus with on the order of an MeV of kinetic energy, so it travels some distance in the patient before it thermalizes and it captures an electron, forming positronium which subsequently decays into a pair of annihilation photons. Because the position where the annihilation photons are created is different than the position of the parent nucleus, there is some blurring whose magnitude depends of the parent radioisotope species. In addition, the positronium has non-zero kinetic energy, so although the annihilation photons are back-to-back in the positronium rest frame, they are slightly acollinear in the lab frame. This angular uncertainty causes a spatial blurring that is proportional to the diameter of the tomograph ring. Most PET cameras employ some form of optical multiplexing, where there are more scintillation crystals than photodetector elements. This decoding is often imperfect, which degrades the spatial resolution slightly. Finally, having discrete scintillator crystals results in something similar to quantization error in the reconstruction algorithm, Mathematically, the reconstructed spatial resolution Γ is:

$$\Gamma = 1.25\sqrt{(d/2)^2 + (0.0022D)^2 + s^2 + b^2} \quad \text{(mm fwhm)} .$$

where d is the crystal width, D is the detector ring diameter, s is the effective source size, b is crystal decoding error factor, and the factor of 1.25 is due to the reconstruction algorithm.

How small can we reasonably make each factor, and hence the spatial resolution of a human or animal PET camera? The decoding error factor b is typically 2 mm in block detectors but is 0 mm for detectors that do not use light sharing to decode crystals, thus optical decoding schemes cannot be used. The effective source size s is limited by the positron range, which is isotope dependent but the minimum among the common positron emitting isotopes is 0.5 mm for ^{18}F. The acollinearity factor $0.0022D$ can be made arbitrarily small by reducing D, but the ring must be large enough to accommodate the subject being imaged and minimize the penetration artifacts that degrade resolution. This is roughly 80 cm diameter for humans and 20 cm diameter for small animals. Thus, an animal PET camera can achieve 1.0 mm reconstructed resolution by employing 0.8 mm cross section scintillator crystals, which is challenging but not impossible. Similarly, 2.5 mm spatial resolution can be achieved in a clinical PET camera if it uses 1.6 mm cross section scintillator crystals.

Finally, it must be remembered that the camera spatial resolution is usually measured with an effectively infinite number of events, and that the effective spatial resolution that is achieved in a typical imaging situation is usually worse.

Exploring the Strengths (and Weaknesses) of a Planar Germanium Small Animal PET Imager

D.C. Oxley[a)]*, A.J. Boston[a)], H.C. Boston[a)], S.J. Colosimo[a)] , F. Filmer[a)], L.J. Harkness[a)], M. Jones[a)], D.S. Judson[a)], J. McGrath[a)], S. Moon[a)], C. Unsworth[a)], M. Slee[a)], A. Sweeney[a)]

a) Oliver Lodge Laboratory, Department of Physics, University of Liverpool, L69 7ZE, UK

The quality of a reconstructed image of a radioisotope can be limited by many experimental and physical parameters. When evaluating an imaging system, it is important to understand these parameters both for the comprehension of the results and for valuable input into future design.

In this paper, a detailed and quantitative assessment of the various stages which add uncertainty to a positron emission tomography (PET) reconstruction has been carried out. The study focusses on a dual-head, high-purity, planar germanium small animal PET camera, while many of the results can be applied to PET systems in general.
Using a thoroughly validated Monte-Carlo model of the system (SmartPET [1]), individual sources of error were systematically incorporated into the simulated data, both in isolation and combination, to evaluate their impact on a reconstructed PET image. These parameters included the positron range, the size of the detector elements, the depth of interaction and the effects of ordering multiple interactions.
An experimental study was then conducted to address the parameters which were determined to have the highest impact on the resolution of a PET image. Namely, a thorough detector characterisation [2] was performed in order to allow pulse shape database matching [3] of experimental data. The development of these techniques [2, 3] has reduced the position resolution achievable in the detector down to $1mm^3$, helping to produce high-quality PET images.
The ability to identify and reconstruct the gamma-ray path within a single detector element shall also be introduced.
These results shall be presented with an outlook toward the future of radioisotope imaging and the areas where the discussed abilities will be most beneficial. An overview on which imaging modalities are best suited to such techniques will be provided.

[1] H.C.Boston et al. Nucl. Instr. and Meth. A **579** (2007) 104
[2] M. Descovich et al. Nucl. Instr. and Meth. A **553** (2005) 535
[3] K. Vetter et al. Nucl. Instr. and Meth. A **452** (2000) 223

COMPET Monte Carlo Simulations - a novel preclinical PET scanner with sub-millimeter resolution

Erlend Bolle*, Jo Inge Buskenes*, Ole Dorholt*, Michael Rissi*‡, Ole Røhne*, Steinar Stapnes*†
*Universitetet i Oslo, NO-0317 Oslo, Norway
† CERN, PH Department, CH-1211 Geneva, Switzerland
‡ presenter, michael.rissi@fys.uio.no

***Abstract*—We present the Monte Carlo simulations of COMPET - a preclinical PET scanner implementing a novel block detector geometry. One detector block is built up from layers of long LYSO crystals. Perpendicular and interleaved between the crystals, Wave Length Shifting (WLS) fibers are used. The scintillation light created by a gamma ray interacting with a crystal is measured with Geiger mode Avalanche Photo Diodes (GAPDs) at one end of the crystals. A small part of the scintillation light escapes the crystals and enters the WLS, where it has a certain probability to scintillate. The re-emitted light is measured at one end of the WLS by a GAPD. With this setup, the depth of interaction of the gamma ray is deduced, making it possible to achieve 3D event reconstruction, which was first proposed in the AxPET project [1]. Using 4 modules, the total detector comprises a total amount of 1000 readout channels, where 600 are used for the crystals and 400 for the WLS. We performed Monte Carlo simulations of this novel approach. For the γ-ray simulations, the GATE [3] software package was used, see figure 2. Gamma-rays were produced back-to-back with both an energy of 511 keV. The oblique sinograms were rebinned to the transaxial planes, using the FORE-J algorithm [2]. The 2D source reconstruction in the transaxial planes was performed with filtered back projection.**

The resolution for a central point source was found to be below 1 mm FWHM in the transaxial plane and below 1 mm in axial direction, see figure 3. The point source resolution degrades slightly when placing the source off-center. For a source at 15mm distance from the center, the resolution is at 1.8mm in the transaxial plane. The sensitivity to detect coincident gamma rays emitted at the centre of the field of view is 16%. In figure 1, the sensitivity to detect two coincident γ-rays in two modules is plotted for a point source moved along the z-axis.

With its compact geometry, high point source resolution, high sensitivity and its low amount of readout channels, the COMPET detector geometry provides a promising detector layout for future preclinical PET scanners.

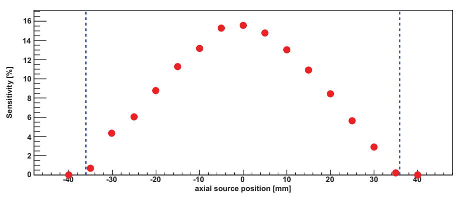

Fig. 1. The sensitivity for coincident γ-rays measured in two modules for a point source moved along the z-axis. In the transaxial plane, the source is placed in the center. To fire a trigger, the deposed energy in each of two modules is required to be above 450 keV.

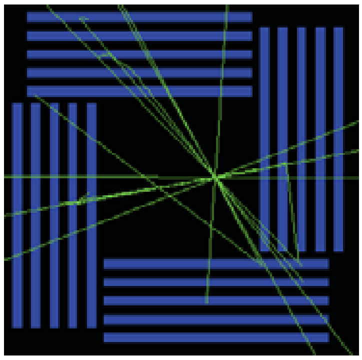

Fig. 2. Gate simulation of a point source at $x = z = 0$ mm and $y = 12$ mm. The green lines denote the γ-ray trajectories.

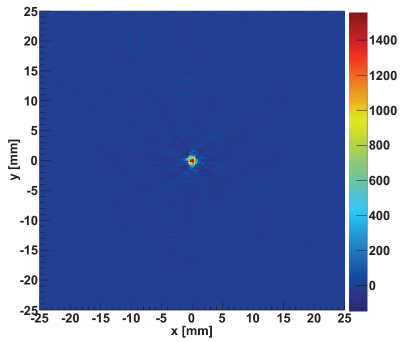

Fig. 3. The reconstructed point source for the transaxial slice at 0.9 mm $< z <$ 1.5 mm. The point source is located at $x = y = 0$ mm and $z = 1$ mm. The FWHM resolution in x, y and z direction is below 1 mm.

References

[1] A. Braem et al, *Wavelength shifter strips and G-APD arrays for the read-out of the z-coordinate in axial PET modules*, Nucl. Instr. and Meth., 586, 2, 300-308, 2008
[2] M. Defrise and X. Liu, *A fast rebinning algorithm for 3D positron emission tomography using Johns equation*, Inverse Problems 15 1047, 1999
[3] S. Jan et al., *GATE: a simulation toolkit for PET and SPECT*, Phys. Med. Biol. 49 (2004) 4543-4561

COMPET – High Resolution and High Sensitivity PET Scanner with Novel Readout Concept

Erlend Bolle*‡, Jo Inge Buskenes*, Ole Dorholt*, Michael Rissi*, Ole Røhne*, Steinar Stapnes*†
*Universitetet i Oslo, NO-0317 Oslo, Norway
† CERN, PH Department, CH-1211 Geneva, Switzerland
‡ Presenter, erlend.bolle@fys.uio.no

Abstract—**COMPET is an innovative system implementation for a small animal imaging scanner, allowing for high resolution and sensitivity with a novel readout scheme. This is realized through 3D(x,y,z) event reconstruction of all events, design of a compact scanner geometry and the latest FPGA technology for fast digitization and timestamping of events.**

The scanner is built up of four block detectors arranged in a circular pattern, rotated 90 degrees with respect to each other (see Figure 1). Each detector module is built up by 150 long LYSO crystals interleaved with 100 Wave Length Shifters (WLS) stacked in 5 layers (see Figure 2). Both the LYSO and WLS is read out by MPPCs from Hamamatsu [2]. The detector geometry covers a FOV of $5\ \mathrm{cm}$ in the transaxial plane and $7.2\ \mathrm{cm}$ in the axial plane without any inter crystal or inter module gaps.

Simulation of the full system show that a FWHM point source resolution below $1\ \mathrm{mm}^3$ and a sensitivity of $16\ \%$ can be achieved. Due to the 3D reconstruction of the interaction point, Compton scattered events can be reconstructed or rejected and the detector blocks can be located close to the object, without being dominated by the parallax error. This results in a high sensitivity.

A novel high throughput readout scheme is implemented as a part of the COMPET design. It makes use of advances within the field of FPGAs. The detector response is converted to a digital pulse were the length is proportional to the energy of the signal. Using low cost general purpose FPGA IO-pins sampled at high frequency, the length of the pulse is measured with a nanosecond resolution. This provides an accurate energy and time stamping of the events and the possibility for a high throughput system. Events are selected by the trigger logic and an eventbuilder in the FPGA allocate hits to the correct event if they satisfy the triggering criteria. Ethernet communication is then used for readout to the computer were the global event number determines which computer the event is sent to. This approach ensures equal event numbers from different readout boards end up on the same computer and gives a equal load on all links.

COMPET with its innovative compact geometry, high resolution, high senstivity, low amount of readout channels and novel readout concept, makes it a promising candidate for future preclinical PET scanner.

REFERENCES

[1] A. Braem et al, *Wavelength shifter strips and G-APD arrays for the read-out of the z-coordinate in axial PET modules*, Nucl. Instr. and Meth., 586, 2, 300-308, 2008
[2] MPPC data sheet of Hamamatsu Photonics: http://sales.hamamatsu.com/assets/pdf/catsandguides/mppc_kapd0002e07.pdf

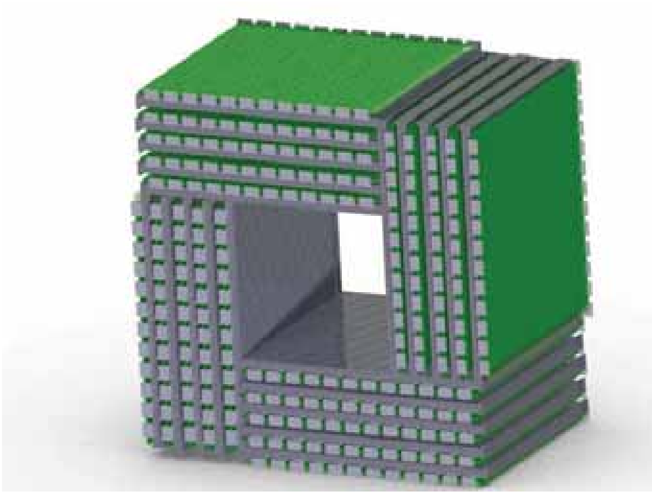

Fig. 1. Drawing illustrating how the four detector modules are arranged to ensure no inter crystal or inter module gaps.

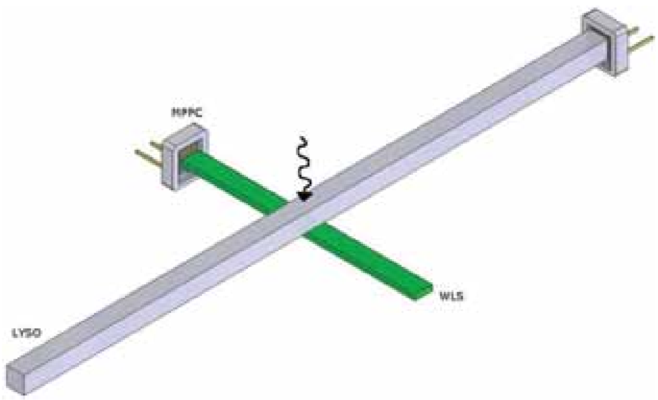

Fig. 2. Illustration of how the 3D reconstruction is done by using the signal from the WLS to determine the location of the hit in the crystal. The idea was first proposed in the AX-PET collaboration [1].

Progress in time-of-flight PET scintillation detectors based on silicon photomultipliers

D.R. Schaart[1], S. Seifert[1], H.T. van Dam[1], R. Vinke[2], P. Dendooven[2], H. Löhner[2], F.J. Beekman[1,3]

[1] *Delft University of Technology, Mekelweg 15, NL-2629 JB Delft, The Netherlands*
[2] *KVI - University of Groningen, Zernikelaan 25, NL-9747 AA Groningen, The Netherlands*
[3] *University Medical Centre Utrecht, Heidelberglaan 100, 3584 CX, Utrecht*

Email: d.r.schaart@tudelft.nl

The use of time-of-flight (TOF) information in positron emission tomography (PET) enables significant improvement in image noise properties and, therefore, lesion detection. Silicon photomultipliers (SiPMs) are solid-state photosensors that have several advantages over photomultiplier tubes (PMTs). SiPMs are small, essentially transparent to 511 keV gamma rays, and insensitive to magnetic fields. This enables novel detector designs aimed at e.g. compactness, high resolution, depth-of-interaction (DOI) correction, and MRI-compatibility. We are studying the timing performance of SiPMs in combination with LYSO:Ce and $LaBr_3$:Ce scintillators. Measurements were performed using pairs of 3 mm × 3 mm × 5 mm scintillation crystals, each coupled to a 3 mm × 3 mm Hamamatsu MPPC-S10362-33-050C SiPM. Using a ^{22}Na point source placed at various positions in between the two detectors, a coincidence resolving time (CRT) of ~100 ps FWHM was demonstrated for $LaBr_3$:Ce(5%), corresponding to a TOF positioning resolution of ~15 mm FWHM, while LYSO:Ce yielded a CRT of ~170 ps FWHM, see figure 1. At the same time, pulse height spectra with well-resolved full-energy peaks were obtained. These results indicate that SiPM-based PET detectors may perform at least as good as detectors based on conventional PMTs. In larger crystals, variations in scintillation photon transit times affect the timing resolution. A correction for this effect can be applied making use of the independently measured position of interaction. Preliminary measurements on detectors consisting of larger, monolithic $LaBr_3$:Ce(5%) crystals (e.g. 18 mm × 16 mm × 10 mm), coupled to an array of 4 × 4 SiPMs (Hamamatsu S11064-050P(X)) yielded a detector timing resolution of ~225 ps FWHM. Further improvement of this value is expected from ongoing research. At the conference, the prospects for SiPMs in TOF-PET will be discussed in more detail.

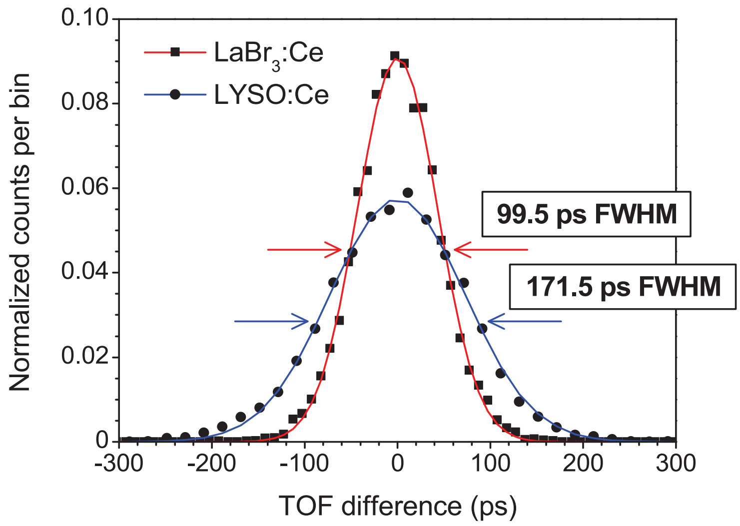

Figure 1. Timing spectra obtained with Hamamatsu MPPC-S10362-33-050C SiPMs optically coupled to 3 mm × 3 mm × 5 mm crystals of $LaBr_3$:Ce(5%) (squares) and LYSO:Ce (circles). The solid curves indicate Gaussian fits to the measured data.

State of the Art and Prospectives of Time-Of-Flight PET

Maurizio Conti

Siemens Healthcare Molecular Imaging, Knoxville, Tennessee, USA

Abstract — After a brief review of the history of time-of-flight (TOF) positron emission tomography (PET) instrumentation from the 1980's to present, the principles of TOF PET are introduced, the concept of time resolution and its effect on TOF gain in signal-to-noise ratio (SNR) are discussed. The factors influencing the time resolution of a TOF PET scanner are presented, with focus on the intrinsic properties of scintillators of particular interest for TOF PET. On the clinical side, we report on recent experimental assessment of TOF image quality, where the advantages of TOF reconstruction have been demonstrated, namely the SNR improvement and the new evidence of robustness of the reconstruction method in presence of inconsistency in the data. Finally, some open issues, challenges and prospectives of TOF PET are discussed both in the field of instrumentation and reconstruction algorithms.

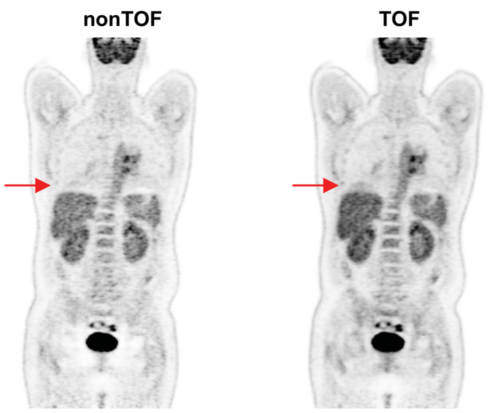

Fig. 1: TOF PET shows better handling of respiratory artifacts

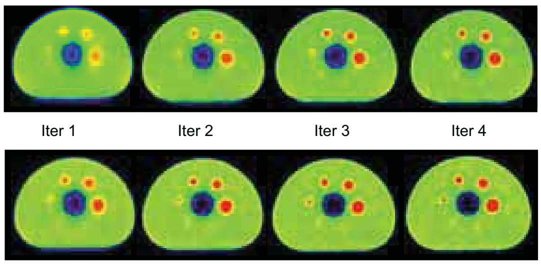

Fig. 2: improved SNR in TOF PET (bottom) allows for detection of small lesions not visible with non-TOF reconstruction (top).

Selected references

[1] M. Conti, "State of the art and challenges of Time-of-Flight PET", *Physica Medica*, vol. 25, no.1, pp. 1-11, 2009.

[2] M.Conti et al., "Comparing fast scintillators with TOF PET potentiality", *IEEE Trans. Nucl. Sci.* 56, No.3, pp. 926-933, 2009.

[3] W.W. Moses, "Time of flight in PET revisited", *IEEE Trans. Nucl. Sci.*, vol.50, no.5, pp. 1325-1330, 2003.

[4] J. S. Karp et al. , "Benefit of Time-of-Flight in PET: Experimental and Clinical Results", *J. Nucl. Medicine*, vol. 49, no.3, pp. 462-470, 2008.

[5] S. Vandenberghe et al., "Optimization of time-of-flight reconstruction on Philips Gemini TF", *Eur. J. Nucl. Med. Mol. Imaging*, vol. 36, pp.1994-2001, 2009.

[6] C. Lois et al., "An assessment of the impact of incorporating Time-of-Flight (TOF) information into clinical PET/CT imaging", *J. Nucl. Medicine*, vol. 51, pp. 237-245, 2010.

[7] M E Daube-Witherspoon et al.,"The imaging performance of a LaBr3-based PET Scanner", Phys. Med. Biol. 55, pp. 45–64, 2010.

Applications of the ATLAS Detector Technology

M. Nessi

The LHC project at CERN has started operation in Winter 2009, with proton beams colliding at an unprecedented center of mass energy of 7 TeV. The ATLAS detector, which will exploit the physics potential of this new research facility, is fully commissioned and operational. The ATLAS project represents the effort of a large fraction of the high-energy physics community worldwide, to integrate modern detection technology into a very complex environment. ATLAS is a 7000 tons magnetic device counting more than 80 million active channels, operating at a 40 MHz readout frequency. The detector is performing according to its design parameters and is showing excellent performance. The variety of technologies used represents an important test bench for many future applications in several domains of hardware and software technology.

John M. Boone, Ph.D.

Title of Talk:
Dedicated Breast CT (with PET) for Screening, Diagnosis, and Breast Cancer Treatment.

Learning Objectives:
(1) Introduce the use of cone beam breast CT for breast imaging
(2) Show the design and imaging performance of breast CT
(3) Describe theoretical approaches for comparing breast CT with mammography

Abstract
Mammography has been successful in reducing the mortality from breast cancer, however the breast imaging community recognizes that mammography is still not perfect, especially for women with dense breasts. In response to these concerns, we have designed, fabricated, and tested a dedicated breast computed tomography (CT) system for breast imaging in the pendent position. The breast CT system made use of commercially available flat-panel detector, x-ray system, and motor components, and all other components were designed at UC Davis, fabricated by a local machine shop, and assembled in our laboratory. The breast CT scanner acquires 500 cone beam projection images (1024 x 768) around 360° in 17 seconds, and these projection images are preprocessed and then used to reconstruct a breast CT volume data set of 512 x 512 x 512 voxels. Voxel dimensions are approximately 0.25 to 0.35 mm, depending on the size of the breast. Very importantly, the system was designed to make use of the same radiation dose to the breast as two view mammography. Breast Imaging on the UC Davis breast CT scanners has been performed on almost 300 patients to date (100 at University of Pittsburgh), and >50 of these patients were imaged both pre-and post-contrast injection. We have also integrated a high-resolution positron emission tomography (PET) system, and having imaged four patients with combined PET and CT. Qualitative assessment of the breast CT images by an experienced mammographer has demonstrated superior depiction of mass lesions compared to mammography, while currently mammography still has superior depiction of microcalcifications. Quantitative assessment of anatomical noise properties as well as ideal observer performance image assessment also suggest that breast CT images are superior for the detection of mass lesions when compared to mammography. The use of iodinated contrast with breast CT demonstrates diagnostic performance which is likely to be equal or superior to contrast enhanced breast MRI. A third breast CT scanner is currently being designed, which will have robotic biopsy and treatment (e.g. radiofrequency ablation) capabilities. We hypothesize that the breast CT platform represents an ideal opportunity for image guided robotic biopsy and interventional therapies. The breast CT platform with appropriate modifications may also be useful for the application of external beam radiation therapy in a prone position.

Biographic Information
John M. Boone received his undergraduate degree in Biophysics from the University of California at Berkeley, and he went on to get M.S. and Ph.D. degrees in Radiological Sciences at the University of California Irvine. After faculty positions at University of Missouri and Thomas Jefferson University, he joined the faculty at University of California Davis in 1992. He is currently Professor and Vice Chair for Research in the Department of Radiology, and he also holds an appointment in the Department of Biomedical Engineering. Dr. Boone is a fellow of the American Association of Physicists in Medicine (AAPM), Society of Breast Imaging, and American College of Radiology. Dr. Boone is board certified in diagnostic imaging by the American Board of Radiology, and currently chairs a committee on CT dose and image quality for the International Commission on Radiological Units and Measurements (ICRU). He also chairs the Science Council for the AAPM. Dr. Boone is Associate Editor for *Radiology*, and was formerly Associate and Deputy Editor for *Medical Physics*. He currently sits on the NIH study section which reviews many medical imaging applications. Dr. Boone's research interests include image analysis and image quality optimization, breast imaging, whole body CT, breast CT, small animal imaging systems, radiation dosimetry, Monte Carlo computation, and computer simulation of medical imaging systems.

Preclinical Spectral Computed Tomography

Ewald Roessl[a,*], Bernhard Brendel[a], Gerhard Martens[a], Axel Thran[a], Roland Proksa[a]

[a] *Philips Research Europe - Hamburg, Germany*

May 1, 2010

Abstract

Today's state-of the art clinical computed tomography (CT) scanners exclusively use current-integration, scintillator detector technology, despite the fact that a part of the information carried by the transmitted x-ray photons is lost during the detection process. Room-temperature semiconductors, like CdTe or CZT, however, operated in energy-discriminating, photon-counting-mode provide information about the energy of every single x-ray detection event. Most importantly, this possibility stimulates novel promising approaches to overcome probably the most crucial shortcoming of modern CT: the inherently weak contrast between various types of soft tissue and, more specifically, between healthy and diseased tissue types like, e.g., cancerous tissue, atherosclerotic plaque, etc. In addition to multi-dimensional material decomposition and labeling techniques, like the high specificity K-edge imaging of high-Z contrast agents (CA), the suppression of beam-hardening artifacts as well as the potential reduction of radiation dose will be natural consequences of this development towards spectral computed tomography (spectral CT).

Two aspects of spectral CT will be treated in more detail: firstly, we will discuss technological hurdles to be overcome when attempting to realize a human spectral CT scanner. Here, the "count-rate problem" arising from the ultra-high x-ray fluxes used in clinical CT today stands out as the most challenging one. Other effects like in-homogenous sensor material, incomplete charge collection, charge sharing, pulse pile-up, scattered radiation and dark-currents in the sensor complicate the pre-processing, calibration and image reconstruction of the date from such a detector, not to mention the increased data transfer rates off the CT-gantry due to the spectroscopic readout of several energy channels the pixel and smaller pixel sizes. Secondly, we report on the most recent imaging results in the domain of pre-clinical, energy-sensitive photon counting CT and illustrate the potential of the novel approach focusing on single and dual K-edge imaging. In this technique, the tuning of threshold levels in the detector electronics to the K-edge in the attenuation of a contrast agent offers highly specific quantitative imaging of the distribution of the CA on top of the conventional anatomic image information. The combination of the high specificity of the K-edge imaging technique together with the powerful tool of targeting specific diseases in the human body by dedicated contrast materials enrich the CT modality with capabilities of functional imaging hitherto known only from modalities like positron-emission-tomography but with the additional prime advantages of CT of high spatial and temporal resolution of the anatomical image.

Numerous examples of this technique in the preclinical imaging domain will be given, the most recent of which will demonstrate the feasibility of separating the anatomy of a mouse from an iodinated blood-pool agent and a targeted agent based on gold nano-particles taken up by macrophages all from a single spectral CT scan.

[*] ewald.roessl@philips.com

Poster presentations

NEW TYPE OF ELECTROSTATIC ENERGY ANALYZERS FOR IMAGING DETECTION

A.M.Ilyin

Physical Department, Kazakh Nat. University, Tole-bi Str., 96a, Almaty, Kazakhstan

A new family of high-resolving electrostatic energy analyzers, with a wide abilities for applications in electron spectroscope and, in particular, for imaging detection is presented. The focusing field used is a solution of a Laplace equation $\nabla^2 U(r,z) = 0$ with boundary conditions $U(r_1, z) = 0$, $U(r,0) = 0$, $U(r,L) = V_{tun}$, $U(r_2, z) = V_{foc}$, and restricted by concentric cylindrical surfaces and two flat surfaces perpendicular to the axis of symmetry. Here V_{foc} is a focusing potential on the outer cylindrical electrode and V_{tun} is a tuning potential applied to one of the flat electrodes, which allows to perform fine tuning of resolution ability. That's why these instruments are the next step in relation to that previously described in [1]. The picture presents the cross-section view of a cylindrical analyzer for measuring electron energies and imaging the extended electron-emitting objects.

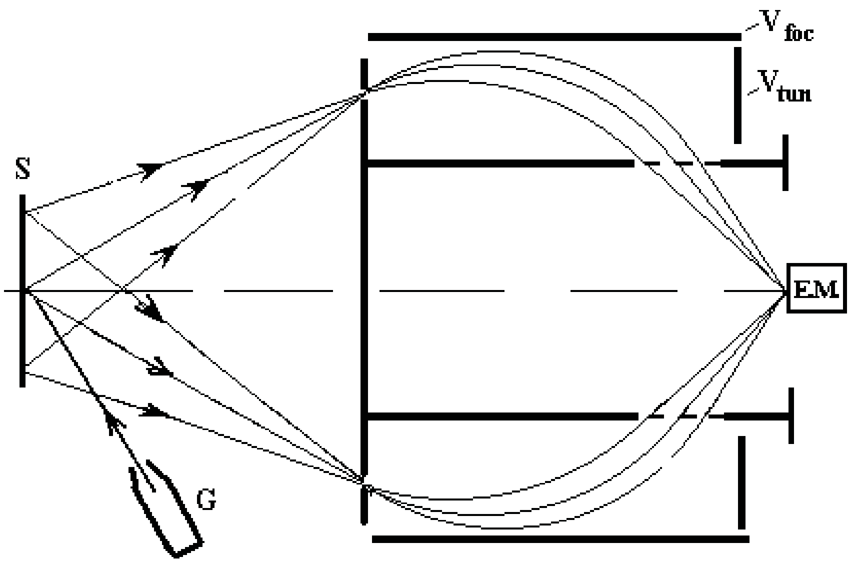

Fig. Here G is an electron gun, scanning a surface or a volume S, EM – an electron multiplier.

References

1. A.M.Ilyin. New class of electrostatic energy analyzers with a cylindrical face-field. Nucl. Instrum.Meth. Phys.Res.A, 500 (2003) 62-67.

Title

Performance evaluation of the General Electric eXplore CT 120 micro-CT using the vmCT phantom

Authors

M.A. Bahri[1], A. Plenevaux[1], P. Choquet[2], G. Warnock[1], A. Constantinesco[2], A. Seret[3]

[1]Cyclotron Research Centre (CRC), Université de Liège, Liège, Belgique
[2]Biophysique et Médecine Nucléaire, Hopitaux universitaires de Strasbourg, Strasbourg, France
[3]Experimental Medical Imaging, Université de Liège, Liège, Belgique

Abstract

Aim. The eXplore CT 120 is the latest generation micro-CT from General Electric. It is equipped with a high power tube and a flat panel detector. It allows high resolution and high contrast fast CT scanning of small animals.
The aim of this study was to compare the performance of the eXplore CT120 and of the eXplore Ultra, the one on which the methodology using the vmCT phantom was described using the same phantom and methodology [1].

Methods. The vmCT phantom was imaged using two sets of typical in-vivo scan parameters: 70 kVp, 32 mA, 220 projections over 192° (fast scan or F) or 100 kV, 50 mA, 360 projections over 360° (high resolution scan or H). Slices with an isotropic voxel of 0.1 mm were reconstructed using the built-in filtered backprojection algorithm and analyzed using the methodology described in [1].

Results. With the slanted edge method, a 10% MTF was observed at 3.8 (F) 4.2 (H) mm^{-1}. A larger MTF was obtained with the coils and the MTF for the thinner coil was 0.26 (F) 0.34 (H) at 3.3 mm^{-1}. The geometric accuracy was better than 0.3%. There was a highly linear ($r > 0.999$) relationship between measured and expected CT number for both the CT number accuracy and linearity plates of the phantom. A cupping effect was clearly seen on the uniform slices but the uniformity-to-noise ratio ranged from 0.52 (F) to 0.89 (H). The air CT number also depended on the amount of polycarbonate surrounding the area where it was measured: a difference as high as approx. 200 HU was observed. This hindered the calibration in HU of this scanner. This is likely due to the absence of corrections for beam hardening and scatter in the reconstruction software. However in view of the high linearity of the system, the implementation of these corrections would allow a good quality calibration of the scanner in HU.

Conclusion. The eXplore CT120 achieved a better spatial resolution than the eXplore Ultra but still needs software development for beam hardening and scatter correction.

[1] Du, L Y et al., Phys Med Biol 2007 ; 52 :7087-7108.

Use of Fractional Packet Counting for High Dynamic Range Imaging Applications

A. Nascetti[1] and P. Valerio[2]
[1] Dept. Aerospace and Astronautics Engineering, [2] Dept. of Electronic Engineering
University of Rome "La Sapienza"

Having a very wide dynamic range is an important specification in many imaging applications, such as computed tomography (CT). The readout electronics is often the main limit to the dynamic range of a system, so many novel solutions are currently being investigated.

In this work, an asynchronous self-reset with residue readout scheme, further referred to as Fractional Packet Counting is proposed. The Fractional Packet Counting circuit consists in a switched integrator followed by a comparator whose output is used to reset the integrator itself and to increment a counter. At the end of the sampling time, the total signal charge is given by the number stored in the counter multiplied by the charge packet size defined by the integration capacitance and the threshold voltage of the comparator. The basic concept of the Fractional Packet Counting is to increase the resolution of the conversion by quantifying the last incomplete charge packet that occurs at the end of the signal integration time. The binary fractional representation of the input current is given by the combination of the integer counts and the fraction of the last incomplete charge packet. Advantages of this solution include constant integration time without the need for gain switching, thus reducing the possibility of image artifacts and allowing for an easy pixelwise calibration.

A circuit implementing this principle for CT applications is proposed and simulated. In particular, the proposed circuit uses a constant relative resolution, which means to use floating point representation with a constant number of significant bits: with N bits, the least significant bit (LSB) is $(1/2)^N$ times the most significant bit (MSB). Operation with a single output register can be achieved provided that the resolution of the A/D conversion of the fractional part changes according to the input signal level and that a binary point register is used to store the transition point from integer digit locations to fractional digit locations, for the correct decoding of the output string. Using an N bits output register, $\log_2 N$ bits are necessary to store the binary point information and thus $N+\log_2 N$ bits per pixel have to be readout for each frame. However, the dynamic range of the signal is equivalent to 2N bits operation with a relative resolution of N bits.

The different blocks of the circuit (integrator, 10-bit cyclic residue ADC and control logic) have been simulated with Cadence IC using AMS 0.35 μm technology and performance figures, such as linearity, resolution and noise figure have been obtained. These data have been used to develop a mathematical model for the SNR, proposed in this work, accounting the different noise sources. A comparison with another similar readout architecture is shown as well, describing how the SNR and dynamic range vary according to the performances of the various blocks. The resulting analysis shows that with this approach a very high dynamic range can be achieved without the need of gain switching. In particular, a dynamic range of 132 dB can be achieved using a 16 bits output string composed by the 12-bit output register and 4-bit binary point register. An additional increase of the upper end of the dynamic range can be obtained by using an additional "flag" bit (for a total dynamic range up to 156 dB with a 17 bits output register).

Detailed quantitative analysis shows that the use of the constant relative resolution approach does not affect the Signal-to-Noise Ratio of the measurement being it limited by other factors as switching noise and photon shot noise. The proposed solution thus enables the design of a pixelated readout chip with a significant number of channels without affecting the imaging properties

Quasi-pixel structured nanocrystalline Gd_2O_3(Eu) scintillation screens and imaging performance for indirect X-ray imaging sensors

Bo Kyung Cha[1], Jong Yul Kim[2], Gyuseong Cho[2], Sungchae Jeon[1], Young Huh[1]

[1]*Advanced Medical Device Research Center, KERI, Gyeonggi-do 426-170, South Korea*

[2]*Dept. of Nuclear and Quantum Engineering, KAIST, Daejeon 305-701, South Korea*

Abstract

Indirect detection type for digital X-ray imaging is essentially consisting a converter (scintillator) and 2D imaging sensor such as a-Si:H flat panel, CCD and CMOS imaging devices. The spatial resolution of indirect X-ray imaging detector unlike direct X-ray conversion method is limited by light spreading effect in the used scintillator film. An alternative method is the usage of pixelated scintillation screen with polymer or silicon based-pixel array structures for high resolution X-ray imaging applications such as mammography, dental imaging and micro-CT (computed tomography). Novel quasi-pixelated (Gd_2O_3:Eu) screens with micro-pixel array structure template were developed for high sensitive and better spatial resolution X-ray imaging detectors. In this work, nanocrystalline Gd_2O_3(Eu) scintillator powder with 100nm particle sizes was synthesized by a hydrothermal process. The as-synthesized sample was subsequently calcinated at 1100℃ temperature and 5 hour time for nanocrystalline powder with high light output. And pixel-structured nanocrystalline Gd_2O_3(Eu) scintillation screens were fabricated by filling the slurry type with nano-sized powder into silicon pixel structured array with 100μm and 50μm pixel pitch through a vacuum process. Additionally, thin Gd_2O_2S:Tb (Gadox) scintillation layers were deposited on pixel-structured nanocrystalline Gd_2O_3(Eu) screens in order to improve the light intensity as well as spatial resolution. The microstructures of nanocrystalline Gd_2O_3(Eu) scintillator screen with pixel structured arrays were investigated by SEM as shown in Fig. 1. The X-ray imaging performance such as the light response to X-ray exposure dose, signal-to-noise-ratio (SNR) and modulation transfer function (MTF), etc were measured and compared by coupling the fabricated films with CCD or CMOS imaging devices under practical radiographic systems as shown in Fig. 2.

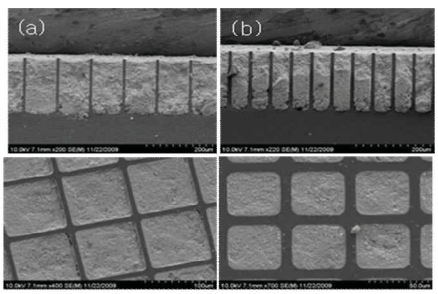

Fig. 1. SEM images of nanocrystalline Gd_2O_3(Eu) scintillator screen with 100μm (a) and 50μm pixel(b).

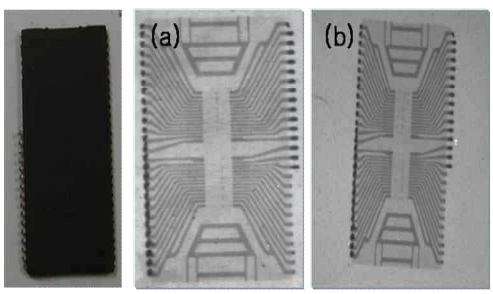

Fig. 2. X-ray images of nanocrystalline Gd_2O_3(Eu) scintillator screen with 100μm (a) and 50μm pixel(b).

A new electron track model in silicon detectors

Cheng Xu, Hans Bornefalk and Mats Danielsson

Department of Physics, Royal Institute of Technology, AlbaNova University Center, SE-106 91 Stockholm, Sweden

Spherical approximations have been used extensively in low-energy X-ray imaging to represent the initial charge cloud produced by the photon interaction in the detector, mainly because of its simplicity. However, for high energy X-rays, where the ejected photoelectron travels far and the initial charge distribution is as important as the diffusion process, the spherical approximations will not result in a realistic detector response.

In this paper, we present a new model that simulates the initial charge distribution in the silicon detector for the photons in the energy range of medical imaging. We extracted three parameters from the Monte Carlo-simulated electron tracks; the barycenter, the polar angle with respect to the barycenter and the size of the tracks. The histograms of these three parameters were fit perfectly with normal and Weibull distributions, respectively. A photoelectron track can be rebuilt by sampling barycenter, polar angle and the size of the track from these three probability distributions and by distributing a certain proportion of photon energy into the bubble and line parts; 68% of the photon energy is distributed uniformly in the bubble part in this model.

We evaluated the new model with a dedicated program that can simulate the charge transport and pulse induction processes and compared the results of the new model with those of spherical approximations and Monte Carlo simulation. We found that this new model can simulate the detector response accurately and accords well with the results of Monte Carlo simulation.

Poster presentation

Large-Angle Pinhole Gamma Camera with Depth-Of-Interaction Detector for Contamination Monitoring

Cheol-Ha Baek[1,2], Ji Yeon Hwang[1,2], Su Jeong An[1,2], Hyun-Il Kim[1,2], Kwang Hyun Kim[3], Yong Hyun Chung[1,2*]

[1]*Department of Radiological Science, College of Health Science, Yonsei University, Wonju, 220-710, Korea*
[2]*Institute of Health Science, Yonsei University, Wonju, 220-710, Korea*
[3]*Department of Biomedical Engineering, Jungwon University, Goesan, 367-805, Korea*

Abstract

The gamma camera system was designed for monitoring the medical fields such as a radiopharmaceutical preparation lab or a patient waiting room (after source injection) in the division of nuclear medicine. However, gamma cameras equipped with a large-angle pinhole collimator and a thick monolithic crystal suffer from the degradation of the spatial resolution at the periphery region due to parallax error by obliquely incident photons. To improve the uniformity of the spatial resolution across the field of view (FOV), we proposed a three-layer crystal detector with a maximum-likelihood position-estimation (MLPE) method which can measure depth of interaction (DOI) information. The aim of this study was to develop and evaluate the performance of new detector experimentally. The proposed detector employed three layers of monolithic CsI(Tl) crystals, each of which is $50.0\times50.0\times2.0$ mm^3, and a large-angle pinhole collimator with an acceptance angle of 120°. The bottom surface of the third layer was directly coupled to an 8×8 channel position-sensitive photomultiplier tube (PSPMT, Hamamatsu H8500C). The PSPMT was read out using a resistive charge divider, which multiplexes 64 anodes into 8(X)+8(Y) channels. Gaussian-based MLPE method has been implemented by using experimentally measured detector response functions (DRFs). Tc-99m point source was imaged at different positions with and without DOI measurements. Experimental results showed that the spatial resolution was degraded gradually as the source moved from the center to the periphery of the FOV without DOI information but the DOI detector showed the marked improvement in the spatial resolution, especially at off-center by correcting the parallax error. In this paper, our new detector with DOI capability proved to characterize reliably the gamma event position with the high and uniform spatial resolution, so that the large-angle pinhole gamma camera could be a useful tool in contamination monitoring.

* *corresponding author e-mail: ychung@yonsei.ac.kr*

Gamma-luminescence of yttrium-aluminum garnet crystals doped with Ce^{3+} and Pr^{3+}

A.Kh. Islamov, E.M. Ibragimova, I. Nuritdinov
Institute of Nuclear Physics, pos. Ulugbek, Tashkent, 100214, Uzbekistan

Lately wide gap complex oxides attract a particular interest because of development of scintillator materials for high sensitive detectors with a high resolution, applied in positron emission and computer tomography [1]. Selection of scintillator materials is based on understanding radiation stimulated processes at evolution of various electron excitations (electrons, holes and excitons), including scintillation acts. Silicates, garnets and other oxide matrices doped with ions of praseodymium (Pr) and cerium (Ce) may turn out prospective.

Therefore the objects of study were yttrium-aluminum garnet crystals $Y_3Al_5O_{12}$ (YAG) both undoped and doped with Pr^{3+} (0.1 at.%) and Ce^{3+} (0.2 at.%), grown by the Czochralski techniques. Gamma-luminescence spectra (GL) were studied at 77-300 K upon preliminary ^{60}Co-gamma-irradiation at 77 K and the dose rate of 3.5 Gy/s up to the dose of $0.2{\cdot}10^4$ Gy, when the radiation induced color gained saturation and did not change during GL measurements. Intensive wide band emission with maximum at 315 nm occurs in the GL spectrum at 77 K of the undoped crystals, the band is asymmetric and contains 2-3 short wave components in the range of 240-300 nm. When increasing temperature to 110 K, the band becomes much narrower and symmetrical with the same maximum at 315 nm of unchanged intensity. This band is attributed to the self-trapped exciton emission and anneals at 150 K [2]. Unlike the undoped YAG, the presence of Pr^{3+} and Ce^{3+} dopants causes a few bands in the GL spectra at 77 K: in the both cases there appear very weak bands at 250 and 280 nm and known very intensive ones at 336 and 370 nm corresponding to d→f transitions, and lines at 500-510 nm of f→f transitions of Pr^{3+}, and also emission bands at 410, 540 and 566 nm related to d→f transitions of Ce^{3+}. As in the undoped samples, the intensities of 250 and 280 nm bands of YAG doped with Pr^{3+} and Ce^{3+} descend quickly when heating to 110 K. Bands at 250 and 280 nm appear due to exciton localization near vacant sites of Al^{3+} and Y^{3+} cations, which are hole traps and generated near Pr^{3+} and Ce^{3+} dopants. The common feature in behavior of the doped YAG is that at 77 K in ~10 minutes after beginning GL run the intensities of d→f transitions decreased 1.6 times and later remained unchanged. The time corresponded to the absorbed dose of $0.2{\cdot}10^4$ Gy and saturation of the density of low temperature color in the range of 300-1000 nm. In the temperature interval from 77 to 140 K the intensities of emission of d→f transitions of Pr^{3+} and Ce^{3+} are stable, while at temperatures above 140 K to 200 K the intensity grows ~5-6 times. It was shown, that the dominating peak of low-temperature glow was observed near 200 K in the doped YAG preliminary irradiated to the dose of $0.2{\cdot}10^4$ Gy at 77 K with the spectrum corresponding to d→f transitions of Pr^{3+} and Ce^{3+}.

The obtained results evidence about two mechanisms of energy transfer to the dopant centers: 1) low effective at T<140 K and 2) high effective at T> 140 K. Excitation of weak emission of the dopants at T<140 K is caused by the excitons formed from mobile electrons and the holes localized near the dopants. While the following relaxation at heating up to T>140 K the holes become mobile (delocalized) that results in decay of these excitons. By means of exchange interaction the excitons transfer their energy for excitation of the dopant emission. The YAG:Ce crystals possessing intensive emission at 540 and 580 nm bands stable at T> 200 K can be recommended for scintillation detectors.

1. J. Touš, M. Horváth, L. Pína, K. Blažek, B. Sopko, Nucl. Instrum. and Meth. A, 591, 264, 2008.
2. Sh.A.Vakhidov, E.M. Ibragimova, I. Nuritdinov, A.F. Rakov, G.I. Ikramov. Phys. Stat Sol. (b), 106, 31, 1981.

FUZZY SCATTER CORRECTION FOR SPECT IMAGES

Farshid Babapour Mofrad, Narmin Panahimehr, Farzaneh Ghafari

Faculty of Engineering, Science and Research Branch, Islamic Azad University, Tehran, Iran

Triple energy window (TEW) [1] method has been proposed in order to scatter correction in SPECT images. The method calculates the count of primary photons at each pixel by estimating scatter from additional scatter energy windows [1, 2]. We propose a fuzzy triple energy window (FTEW) technique including three steps. First, image pixels divided into three areas: high, middle and low counts. Then the appropriate coefficients were selected for each area. Next we apply TEW to each area. A Monte Carlo modeling method was employed for fuzzy scatter correction simulation. The results showed that FTEW is more accurate to scatter correction with maintain the contrast and increasing the SNR.

1. K. Ogawa, H. Harata, T. Ichihara, A. Kubo, and S. A. Hashimoto, "Practical method for position dependent compton-scatter correction in single photon emission CT," IEEE. Trans. Med. Imag., vol. 10, pp. 408–412, 1991.
2. J. K. Bong, H. K. Son, J. D. Lee, and H. J. Kim, "Improved scatter correction for SPECT images: a Monte Carlo study," IEEE Trans. Nucl. Sci., vol. 52, pp. 1263-1270, 2005.

Signal Fluctuations in Crystal-APD systems

F. Kocak and I. Tapan
Department of Physics, Uludag University, 16059, Bursa - Turkey

$PbWO_4$ and CsI(Tl) crystals are used widely in high energy physics experiments. The photons generated from incident particles in the crystal material are detected from the Avalanche photodiodes (APD) placed at the end of the crystals. In this work, the light generated by 0.1-5 GeV electrons in the crystals has been obtained using with the GEANT4 simulation code. The Single Particle Monte Carlo technique has been used to calculate APD output signals and their fluctuations at a constant avalanche gain value of 50 for both the CsI(Tl) and $PbWO_4$ crystals emission spectrum. The simulated results are agreed well with the experimental results. CsI(Tl) crystal- APD system has provided a good material-device combination. The high signal values and the low signal fluctuations make this combination an excellent choice for scintillating light detection.

Preference for presentation: Poster

Address for correspondence: Fatma Kocak
Uludag Universitesi, Fen-Edebiyat Fakultesi, Fizik Bolumu, 16059, Bursa-Turkey
e-mail: fkocak@uludag.edu.tr

Analog Acquisition Channels for a Diamond Matrix Dosimeter ASIC

F. Petullà†, F. de Notaristefani†, V. Orsolini Cencelli†, E. D'Abramo†, A. Fabbri†, M. Marinelli†† and G. Verona-Rinati††

Abstract– **Radiotherapy treatments planning is an important issue in cancer defeat. Strong is the need to verify and characterize the beam and also the dose transferred to the patient.**

Monocrystalline CVD grown diamond is a very good base material for clinical dosimetry sensors and sensor matrixes. The calibration and on-line dose verification are performed with bulky and expansive electrometer so an ASIC is the right solution to measure a diamond sensor matrix dosimeter.

We present a short description of our ASIC main functional blocks. The ASIC has been realized and now is under tests.

I. Introduction

IN modern Radiotherapy[2] and Hadron Therapy[1] a very important issue is to achieve good dose uniformity to be delivered to the patient in order to defeat cancer affected tissues and preserve the healthy ones. One of the main objectives of the oncologist and also the medical physicist is to develop a treatment plan strictly customized to the patient needs. To achieve these objectives it is necessary to study the propagation of the beam, and also to calibrate the source and furthermore is necessary to characterize the beam section to obtain an image and to verify that the ideal treatment beam distribution is very close to the delivered one. Nowadays the use of ions had increased thanks to their deeper depth of interaction with matter[3] and especially for on-line dose estimation, so it is growing the interest for diamond dosimeter matrixes. The wide used dosimeters for beam calibration and treatment planning are ionizing chambers (IC) and silicon diodes (SD). For these two types of detectors there are some drawbacks concerning resolution and acquisition speed for the formers and temperature dependence for the latter. Diamond is the optimal candidate [1][2][4][5] for radio and hadro – therapies due to its tissue equivalence, wide band gap leading to very low dark currents, high thermal conductibility, and also thanks to the possibility to realize sensor matrixes capable to work without biasing [6][7]. Diamond sensor matrixes are characterized with electrometers, by the use of shielded triaxial cables that make their use in on-line dose verification impossible, so it has been necessary to develop an ASIC to realize a diamond integrated dosimeter.

II. ASIC DEVELOPMENT

Starting from the requirements of the mono crystalline diamond CVD grown detector produced by the University of Rome "Tor Vergata" laboratories, we developed and simulated an ASIC whose aim is to integrate the signal currents from the diamond matrix; we also added into the ASIC another only – analog channel to integrate the dark currents from the sensors. The ASIC is designed in 0.18um technology with 3.3V supply, used for the analog circuitry, and 1.8V supply for the logic circuitry. The integration capacitor is made with "metal - metal capacitor" technology, where the capacitor structure is made by a dedicated oxide layer for the capacitor dielectric between METAL5 and METAL6 layers.

A. Dual Slope Interleaved ADC

The architecture we choose for this acquisition channel is the dual slope one. For the timing requirements of this application (10 to 100 ms), this is a good compromise of accuracy and speed of integration (see Figure 1).

The analog frontend with the aid of a dedicated non clocked comparator, to limit the charge feed-trough phenomena, drives a 10 bit counter, that with a dynamic range of about 2V leads to a resolution of about 2mV, corresponding to an integrated charge of 2 fC. In the presented design the channel integration process, for the available full scale dynamic of 2V, takes 20ms for the maximum signal current, and 2s for the minimum signal current. On the other side for the fixed integration time of 33ms (to achieve the goal of 30 frame per seconds) the voltage signal across the integration capacitor saturates the dynamic range for the maximum signal current, while reaches 33mV for the minimum signal current. This system with a single Dual Slope channel is blind to radiation during the discharging phase, so we added a second dual slope stage operating in quadrature in respect to the first stage. The two stages work sequentially, so when the former is integrating, the latter is idle (see figure 1B).

B. BGMI Channel

To integrate the dark currents from the sensor, spanning from tents to hundreds of fA, we have designed a single Buffered Gate Modulation Input (BGMI) channel. This readout configuration shows very good characteristics due to the forthcoming current signal amplification [8]. The amplification of this stage depends on two parameters: the operational amplifier amplification and the injection efficiency. Our aim is to maximize the injection efficiency from the sensor to the input stage so we worked on feedback MOS MP in Figure 2 to increase its width, now the current amplification is controlled by the input mirror g_m ratio and MOSFET mismatch. To increase output resistance we modified the mirror structure into a regulated cascode one. This mirror structure feeds an integration capacitor of 1 pF and when it reaches the full dynamic of 2.3 V is auto reset by the combination of two comparators and an RC network.

III. Conclusions

We developed and simulated the analog acquisition channels required to produce an ASIC to realize a diamond matrix dosimeter. The ASIC has been submitted to foundry and is now ready for tests, so now we're involved into the development of the test environment.

†Dep. of Electronic Engineering University of Rome "Roma Tre" and INFN Sezione Roma III.

††Dep. of Mechanical Engineering University of Rome "Tor Vergata and INFN Sezione Roma II

Energy sensitive X-ray imaging for mobile non-destructive testing applications

AUTHORS:

Frank Nachtrab[1,2*], Stefan Hebele[1], Markus Firsching[1], Norman Uhlman[1]

INSTITUTES AND ADRESSES:

[1] Fraunhofer Development Center X-ray Technology EZRT, Dr.-Mack-Straße 81, 90762 Fürth, Germany

[2] Cluster „Engineering of Advanced Materials" EAM, University Erlangen-Nürnberg, Dr.-Mack-Straße 81, 90762 Fürth, Germany

ABSTRACT:

The photon counting X-ray detector Medipix2 [1] is used in a portable computed tomography (CT) system designed for non destructive testing and biomedical imaging. The quad version of the Medipix2 consists of 512 x 512 pixels with a pixel size of 55 µm x 55 µm. The sensor layer is 300 µm thick and is made of silicon. The Medipix2 has a 13-bit counter and two adjustable thresholds per pixel, thus allowing energy sensitive ("spectral") X-ray imaging.

We designed a compact and light weight (350 mm × 300 mm × 230 mm, 19 kg) CT-system ("CTportable") especially adapted for the Medipix2 quad detector. The system can be carried by a single person allowing mobile operation for research in the field. With a maximum acceleration voltage of 50 kV, the applications are for example non destructive testing, medical research and biology. Samples up to a diameter of 45 mm and a height of 41 mm can be scanned completely using the extended field of view technique and helical CT geometry. The helical CT acquisition and reconstruction eliminates artefacts due to direct cone beam reconstruction ("Feldkamp artefacts") and ensures homogenous image quality throughout the complete volume. The maximum resolution of the system is 27.5 µm voxel size. The system is connected to a computer via USB. Besides that (e.g. a standard high end notebook) no additional hardware is required.

With the CTportable simple radioscopy is possible as well as 3D-CT. Thanks to the photon counting and energy sensitive detector, the unit is suitable for low energy applications and dual energy techniques. We present examples of material characterisation by CT using the aforementioned system. Further improvements like multi-energy methods for material analysis are currently being developed.

[1] X. Llopart, M. Campbell, R. Dinapoli, D. San Segundo and E. Pernigotti, IEEE Trans. Nucl. Sci. NS49 (2001), p. 2279.

---

* Corresponding author. Tel. +49 911 58061 7564, E-mail address: frank.nachtrab@iis.fraunhofer.de

Low-resource synchronous coincidence processor for positron emission tomography

Giancarlo Sportelli[1,2], Nicola Belcari[3], Pedro Guerra[2], Andrés Santos[1,2]

[1]BIT - Universidad Politécnica de Madrid, Madrid, Spain
[2]CIBER - Research Center in Bioengineering, Biomaterials and Nanomedicine, 50018 Zaragoza, Spain
[3]Department of Physics "E. Fermi", University of Pisa, Pisa, Italy

I. Introduction

Coincidence detection is the most challenging stage in a Positron Emission Tomography (PET) acquisition system, and the one to which most expensive and cutting edge hardware is dedicated. This is because of the tight timing constraints and the high complexity required to monitor in real-time each possible detector combination. Part of PET technology literature is committed to the research of new coincidence detection techniques, with the two main aims of reducing complexity and improving timing resolution.

Current coincidence processors are mainly based on two different approaches: AND-gating and Time-to-Digital conversion (TDC). In AND-gating, for each received photon a digital pulse is generated, with a well-timed rising edge and fixed width W. Pulses from all detectors are fed to a combinatorial circuit that generates a coincidence trigger when two of them overlap. With this technique, two photons can be resolved if they are separated in time by $2W$. This value is what we refer to as coincidence resolution. The main advantage of AND-gating is its relatively simple architecture, and the prompt coincidence. Its main disadvantage is that it scales badly, being its complexity of the order of $O(n^2)$, where n is the number of detectors.

TDC based processors are more recent and much more sophisticated. They consist in labeling each single event with a timestamp, either by sampling a digital timing signal or interpolating the analog energy pulse. Coincidence detection is then made by calculating time differences, and the obtained coincidence resolution is due to the same of the Time-to-Digital converter. Time conversion can be performed in parallel for each detector, and coincidence processing can be also performed on-line. This greatly improves scalability. Moreover, digital data processing can be used to improve timing resolution beyond the intrinsic hardware limits. However TDC techniques require very low skew clocking networks, a synchronization protocol, and most of all they need to acquire all events, including single ones, which dramatically increases storage and bandwidth demands.

We propose a new, FPGA-based method for coincidence resolution that requires low device resources and no specific peripherals in order to resolve digital pulses within a time window of a few nanoseconds. The method has been developed specifically to be applied in high-resolution positron emission tomography.

The method consists in synchronizing input triggers into pulses of width $W = 2\tau$, where τ is the clock period. The goodness of the method comes from a local clock boosting that allows reducing τ to the intrinsic limits of the target FPGA, thus reducing the timing feature on which depends the coincidence resolution. The outputs of the boosted clock domain are then resynchronized with the slower global synchronous domain in order to be processed. A simplified schematic of the synchronous coincidence processor is showed in Figure 1.

Having narrow synchronous pulses, timely related with the incoming triggers, allows for a more effective combinatorial gating in terms of both device power dissipation and design cost. The delayed window technique for random counts estimation can be implemented by means of shift registers, and the FPGA-compatible implementation allows the architecture to be automatically synthesized from VHDL source code.

In this case, resolving coincidences by selecting those pulses that overlap at least in one clock cycle results in a coincidence resolution of 3τ.

Experiments have been conducted with a low-end Spartan-3E FPGA that demonstrate that 9 ns can be easily achieved (Figure 2). The achieved resolution depends directly on the maximum available clock frequency and signal propagation delay on the specific device, therefore it is expected to be sensibly improved in higher-end FPGAs.

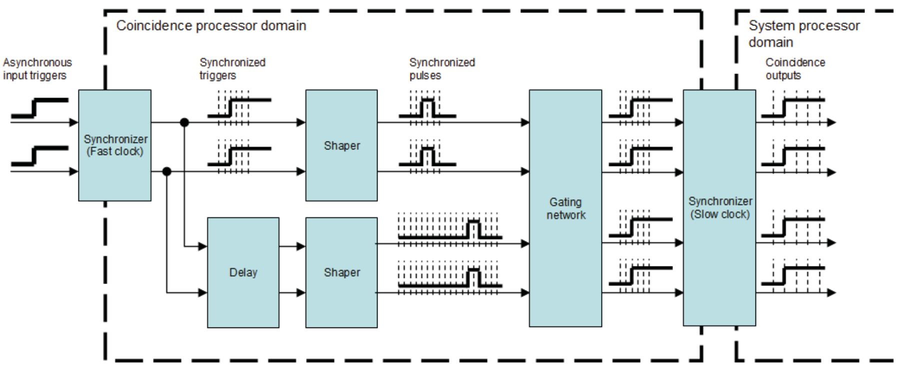

Figure 1: Architecture of the synchronous coincidence processor

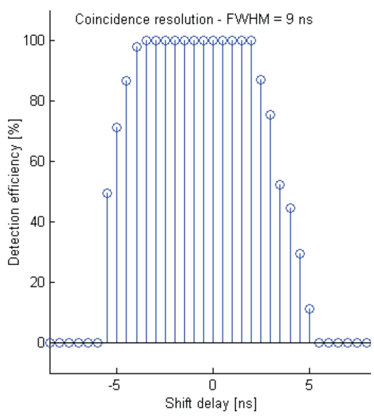

Figure 2: Coincidence detection efficiency

A CAD system for cerebral glioma based on texture features in DT-MR images

Giorgio De Nunzio,[1*] Gabriella Pastore,[2] Marina Donativi,[3] Antonella Castellano,[4] Andrea Falini[4]

[1] Dept of Materials Science, University of Salento, and INFN (Istituto Nazionale di Fisica Nucleare) (Lecce, Italy)
[2] PO 'Vito Fazzi' - UOC Fisica Sanitaria, and Dept of Materials Science, University of Salento (Lecce, Italy)
[3] Dept of Materials Science, University of Salento (Lecce, Italy)
[4] Neuroradiology Unit and CERMAC, San Raffaele Scientific Institute (Milano, Italy)

* speaker

The diffuse infiltration of white matter tracts by cerebral glioma is a major cause of their appalling prognosis: tumour cells invade and displace white matter, and can destroy it.

Non-invasive detection of the microscopic infiltrations is of outstanding importance for surgical and radiation therapy planning, or to assess response to chemotherapy. While glioma cells usually spread well beyond the abnormal area seen on conventional MRI, Diffusion Tensor Imaging (DTI) can identify peritumoral white-matter abnormalities and infiltrations, as confirmed by image-guided biopsies.

The aim of this study was to characterize pathological and healthy cerebral tissue in DTI datasets by 3D statistical texture analysis, with the purpose of developing and validating a semi-automated detection technique (CAD, Computer Assisted Detection) of cerebral tumors.

MR-DT images of twenty patients with glioma were acquired (3T, single-shot EPI sequence, $b = 1000$ s/mm^2, 32 gradient directions). Isotropic and anisotropic maps (FA, MD, p and q) were calculated, and pathological ROIs were manually drawn.

Texture features (from the intensity and the gradient histogram, and from the cooccurrence and the run length matrix) were calculated in the segmented ROIs and in the contralateral healthy tissue, with a sliding-window approach. The most discriminating features were selected by the Fisher filter score, and the feature-space dimensionality was reduced by Principal Component Analysis. A back-propagation, feed-forward artificial neural network (ANN) was trained on about half of the patients, and tested on the others.

The classification performance was assessed by receiver operating characteristic (ROC) curves. Preliminary results were obtained for the p map (AUC = 0.96, sensitivity and specificity equal to 90.0%, classification error 10.0%) and the FA map (AUC = 0.98, sensitivity and specificity equal to 92.6%, classification error equal to 7.3%). Test images were automatically segmented by tissue classification, and manual and automatic segmentations were in good agreement.

This approach looks promising for preoperative assessment of structural heterogeneity and extension of cerebral glioma. It could allow objective identification and quantitative measurement of glioma, especially in view of a patient follow-up during chemotherapy.

A new pulse width signal processing with delay-line and non-linear circuit (for ToT)

Tadashi Orita, Kenji Shimazoe, Takeshi Fujiwara, Hiroyuki Takahashi

The University of Tokyo, Nuclear engineering and management

Each channel of the energy resolving multichannel system has to spend low power consumption and be composed of simple circuits. The Time over Threshold (ToT) method provides an inexpensive way in that system. However, the ToT method obtains a poor linearity. We improve the poor linearity with the dynamic Time over Threshold method that obtains a dynamic threshold voltage and the trapezoidal shaping.

The ToT method is a pulse processing method that compares input pulse with a threshold voltage and measures the time while input pulses is higher than a threshold voltage. As a result, the ToT method changes pulse heights into time widths. The ToT method is composed of simple circuits and utilized for front-end circuits in a multichannel system. However, The ToT method suffers from poor linearity. Our research group provides the dynamic Time over Threshold (dToT) method with Trapezoidal Shaping for improving the ToT method's poor linearity. Unlike the ToT method that obtains a constant threshold voltage, the dToT method obtains dynamic threshold voltage.

Beam hardening corrections for a microCT scanner prototype

J. Kikushima, A. Martínez-Dávalos, M. Rodríguez-Villafuerte

Instituto de Física, Universidad Nacional Autónoma de México, A.P. 20-364, 01000 D.F., México

The radiographic projections acquired with a microCT scanner prototype developed in our laboratory were corrected for beam hardening effects using the linearized signal to equivalent thickness (LSET) method. This method requires a calibration curve for each pixel obtained from a set of images with filters of increasing thickness. The radiographic projections are corrected on a pixel-by-pixel basis by converting the projection signal to an equivalent thickness using interpolation over the calibration images.

The method was first validated using simulated projections of three different phantoms using two calibration sets based on aluminum and water filters of thicknesses ranging from 0.5 to 5.0 mm and from 0.5 to 50 mm, respectively. Simulations of the same phantoms using a monoenergetic beam were also made to establish the reference intensity on the tomographic images when no beam hardening related artifacts are present. Experimental measurements were performed using a *Defrise* phantom containing a set of Lucite and Teflon disks. The experimental calibration signals were obtained using ultra-pure aluminum slabs with thicknesses ranging from 0.5 to 4 mm and solid water slabs with thicknesses ranging from 1 to 50 mm. The corrected and uncorrected tomographic images were compared by obtaining profiles along the central axis for both the simulated and experimental data.

For the simulated data, the results show that both the cupping and streaking artifacts produced by beam hardening can be effectively corrected by the LSET method, and that this result is independent of the calibration material in the ideal case (no scatter, ideal detector). The experimental results show that the cupping artifact that arises from beam hardening can be reduced considerably through the LSET method and the results show no significant difference between different calibration materials.

Fully-3D GPU PET Reconstruction

J. L. Herraiz[1], S. España[2], J. Cal-González[1], M. Desco[3], J. J. Vaquero[3], and J. M. Udias[1]

[1] Grupo de Física Nuclear, Dpto. Física Atómica, Molecular Nuclear, UCM, Madrid, Spain
[2] Department of Radiation Oncology, Massachusetts General Hospital and Harvard Medical School, Boston, MA, USA.
[3] Unidad de Medicina y Cirugía Experimental, Hospital GU "Gregorio Marañón", Madrid, Spain

Tomographic image reconstruction is computationally very demanding, especially when iterative methods based on realistic models for the emission and detection of radiation are used [1]. Graphics Processing Unit (GPU) have been proposed for many years as potentially accelerators in complex scientific problems like image reconstruction, with large amount of data and high arithmetic intensity. But it has not been until the recent advances in the programmability of GPUs [2] that the best available reconstruction codes have started to be implemented to be run on GPUs.

This work presents a GPU-based fully-3D PET iterative reconstruction software. This new code reconstructs sinogram data from several commercially available PET scanners like VrPET [3] and Biograph TruePoint [4]. This code has been designed to be easily adapted to reconstruct sinograms from any other PET scanner, so it may also be used for fast and accurate reconstruction of acquisitions from scanner prototypes.

The main characteristics of the scanners have been modeled using the Monte Carlo simulation code PeneloPET [5] and the resulting models have been validated against real data. The reconstruction code makes use of these models to create an accurate representation of the forward and backward projection operations, the more important and time-consuming parts of the code. These operations have been massively parallelized on the GPU and a very significant speed-up of the reconstruction has been obtained. For the PET scanners considered, the GPU-based code is 50 to 100 times faster than a similar code running on a single core of a fast CPU, obtaining in both cases the same images.

Supporting data:

Coronal and transverse views of the reconstructed image of a 200 g rat injected with FDG acquired with the VrPET small animal PET scanner. The differences between both images are visually negligible, but a speed-up factor of 72 was obtained with the new GPU-based code.

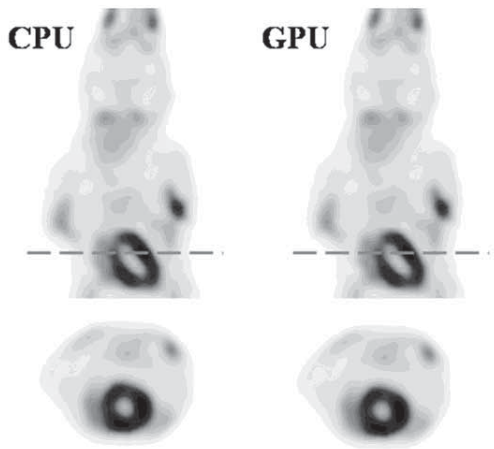

CPU Intel® Core™ i7 [2.93GHz, 6GB DDR3-800 MHZ RAM] (one core)	GPU TESLA C1060 [4GB – 27 SM]
3460s	50s

References:

[1] J. L. Herraiz et al., "FIRST: Fast Iterative Reconstruction Software for (PET) Tomography," Phys. Med. Biol., vol. 51, pp. 4547-4565, 2007.
[2] "NVIDIA CUDA Programming Guide v.2.3," http://www.nvidia.com/object/cuda_home.html
[3] E. Lage et al., "Design and performance evaluation of a coplanar multimodality scanner for rodents imaging," Phys. Med. Biol, vol. 54, pp. 5427-5441, 2009.
[4] B.W. Jakoby et al., Performance Characteristics of a New LSO PET/CT Scanner With Extended Axial Field-of-View and PSF Reconstruction," IEEE Trans. Nucl. Sci., vol. 56, no. 3, pp. 633-639, 2009.
[5] E. España et al., "PeneloPET, a Monte Carlo PET simulation toolkit based on PENELOPE," Phys. Med. Biol. vol. 54, pp. 1723–1742, 2009.

Poster presentation

Nuclear Material Monitoring System (NMMS) for Security Screen

Kwang Hyun Kim[1*], Jea Yong Jeon[2] , Yong Hyun Chung[3]

[1]*Department of Biomedical Engineering, Jungwon University, Goesan, 367-805, Korea*

[2]*Research Center for RadTek Co., Ltd, Dukjin-Dong,Yusung-Gu, Daejeon, South Korea*

[3]*Department of Radiological Science, College of Health Science, Yonsei University, Wonju, 220-710, Korea*

Abstract

As a Nuclear Material Monitoring System (NMMS), two large volume plastic detectors and a NaI detector for the gamma-ray sources and two He-3 tubes for the neutron sources have been integrated in a mobile box which can be mounted on a vehicle. Our own designed preamplifiers, shapers, and MCA (Multi-Channel Analyzer) for each detector are invented and built in a compact circuit board to collect and integrate different data from each detector. The collected data, counts rates and spectra of the detected radiations, are continually monitored and plotted on several user-friendly display windows in a laptop computer. The system performance in a vehicle-mounted condition has been tested for Co-60, Cs-137, and Cf-252 sources at various distances and speeds.

** corresponding author e-mail: radkim@jwu.ac.kr*

Poster presentation

Development of Portable X-ray Scan System (PXSS)

Kwang Hyun Kim[1*], Jun Man Park[2], Yong Hyun Chung[3]

[1]*Department of Biomedical Engineering, Jungwon University, Goesan, 367-805, Korea*

[2]*Research Center for RadTek Co., Ltd, Dukjin-Dong,Yusung-Gu, Daejeon, South Korea*

[3]*Department of Radiological Science, College of Health Science, Yonsei University, Wonju, 220-710, Korea*

Abstract

We have developed a portable X-ray scan system, 830 (L) x 550 (W) x 55 (H) mm, with an X-ray generator. The system is a battery powered portable X-ray scan system that offers maximum scan speed of 40 cm per second with 0.8 mm and 576 pixels resolution. The scanner module consisted of phosphor screen coupled linear array photodiodes of 1.0 kΩ·cm and front-end electronics based on discrete charge sensitive preamplifiers. Dual X-ray energies of 100 kVp and 60 kVp can be generated for each exposure time of 5 seconds, and dual X-ray imaging can be acquired in a short scan interval for security screen and non-destructive evaluation. This system also contains a counting mode nuclear material detection system as a small module to inspect nuclear materials in a baggage or briefcase. The results of performance test and technical information of the system will be announced in more detail.

** corresponding author e-mail: radkim@jwu.ac.kr*

Poster presentation

Trapezoidal-Shaped Detector to Reduce Edge Effects in Small Gamma Camera

Ji Yeon Hwang[1,2], Cheol-Ha Baek[1,2], Su-Jung Ahn[1,2], Hyun-Il Kim[1,2], Kwang Hyun Kim[3], Yong Hyun Chung[1,2*],

[1]*Department of Radiological Science, College of Health Science, Yonsei University, Wonju, 220-710, Korea*

[2]*Institute of Health Science, Yonsei University, Wonju, 220-710, Korea*

[3]*Department of Biomedical Engineering, Jungwon University, Goesan, 367-805, Korea*

In recent years, there has been a growing interest in compact and high resolution small gamma cameras for the early detection of breast cancer and thyroid diseases. We proposed a new detector consisting of a trapezoidal-shaped crystal and a position-sensitive photomultiplier tube (PSPMT) to reduce the edge effect. In this study, design parameters of the proposed detector were optimized by DETECT2000 simulation and the experimental validation of the simulation was performed. NaI(Tl) and CsI(Tl) crystals with a back face of 50.0×50.0 mm^2 and a thickness of 6.0 mm were modeled and the trapezoidal angle varied from 45° to 90° in steps of 15° with 90° being a rectangular block. Crystals in all cases were coupled to a PSPMT and the 2-dimensional event positions are calculated using the Anger-logic. Tc-99m (140 keV) and I-131 (364 keV) gamma rays were generated on evenly spaced points with 3.0 mm spacing in the X-Y plane starting 1.0 mm away from the corner surface in the center of crystal thickness for 1/4 of the detector area because of the symmetrical configuration. 10,000 gamma events were simulated at each location. The simulated results demonstrated that all the Tc-99m and I-131 point sources were clearly identified only in the NaI(Tl) crystal with a trapezoidal angle of 45°. CsI(Tl) crystal with a trapezoidal angle of 45° could image I-131 sources without edge effect but did not distinguish Tc-99m points at the periphery region due to low light yield. To validate the simulation results, CsI(Tl) detector with a trapezoidal angle of 45° coupled to H9500 PSPMT was implemented and the simulation and the related experimental results agreed well each other. In conclusion, our new detector with an enlarged FOV without increasing crystal size could be a useful tool in breast imaging as well as thyroid imaging.

* *corresponding author e-mail: ychung@yonsei.ac.kr*

Impact of early PET response in predicting the outcome of liver malignancies after Yttrium-90 radioembolization

Ko-Han Lin[1,2], Rheun-Chuan Lee[3], Chi-Wei Chang[1,2], Ching-Sheng Liu[1,2], Bang-Hung Yang[1,2], Bo-Kai Huang[1,2], Ren-Shyan Liu[1,2], Shyh-Jen Wang[1,2]

[1]National PET/Cyclotron Center and [2]Department of Nuclear Medicine, Taipei Veteran General Hospital

[3]Department of Radiology, Taipei Veteran General Hospital

Purpose:

The PERCIST (PET Response Criteria in Solid Tumors) is to assess the metabolic response to anti-cancer therapies and provides further information than the anatomic criteria, RECIST. The aim of this study is to evaluate the response of liver malignancies to Yttrium-90 radioembolization and compare the result measured by PERCIST and RECIST.

Materials and method:

20 patients of FDG-avid liver malignancies were included and underwent baseline CT and PET/CT scans before the radioembolization. Follow-up scans were obtained at 6-8 weeks after the therapy. Response was determined using PERCIST for PET and RECIST for CT. The result was classified as complete response (CR), partial response (PR), and stable disease (SD). Correlation between response using different criteria and survival was analyzed (Kaplan-Meier method).

Result:

There were 2 CR, 10 PR, and 8 SD by PERCIST; while 6 PR and 14 SD by RECIST. Mean Survival was 311 days in PERCIST CR/PR group versus 152 days in PERCIST SD group ($p=0.007$). Excluding extrahepatic disease, mean survival is 433 days in PERCIST CR/PR group versus 195 days in SD group ($n=12$, $p<0.001$). There is no statistical significance by RECIST classification.

Conclusion:

The PERCIST, which represents reduction of tumor metabolic activity, could assess the response earlier and is more predictive of outcome than the RECIST.

New 1π sr Acceptance Angle Display-type Ellipsoidal Mesh Analyzer for Electron Energy and Two-Dimensional Angular Distribution as well as Imaging Analysis

László Tóth[1,2], Kentaro Goto[1], Hiroyuki Matsuda[1], Fumihiko Matsui[1] and Hiroshi Daimon[1]

[1]*Nara Institute of Science and Technology, 8916-5 Takayama, Ikoma, Nara 630-0192, Japan,*

[2]*University of Debrecen, Faculty of Informatics, 4032 Debrecen, Egyetem Tér 1, Hungary*

We propose a Display-type Ellipsoidal Mesh Analyzer (DELMA) (Fig. 1) using a newly developed 1π sr wide acceptance angle electrostatic lens (WAAEL), energy aperture and some other electrostatic lenses [1-5]. It can display two-dimensional angular distributions of charged particles within the acceptance angle of ±60°, which is much larger than the largest acceptance angle range so far and comparable to the display-type spherical mirror analyzer developed by Daimon [6]. It also has a focusing capability with 5-times magnification and ~30 μm lateral-resolution. The relative energy resolution is typically from 2 to 5×10^{-3} depending on the emission area on the sample, as well as on the diameter of energy aperture.

Because this new analyzer has a function of low magnification photoemission electron microscope, this instrument will be extended and applied as a new type Stereo-PEEM [7] in near future.

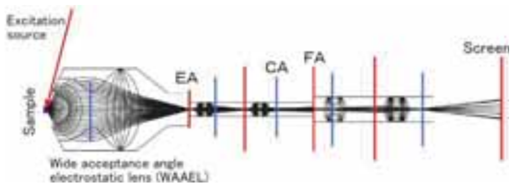

Fig. 1

References

[1] H. Matsuda, H. Daimon, M. Kato and M. Kudo, Phys. Rev. E, 71, 066503 (2005)

[2] H. Matsuda, H. Daimon, Phys. Rev. E, 74, 036501 (2006)

[3] H. Matsuda, H. Daimon, L. Toth, F. Matsui, Phys. Rev. E, 75, 046402 (2007)

[4] L. Tóth, H. Matsuda, T. Shimizu, F. Matsui and H. Daimon, J. Vac. Soc. Jpn. 51, 135 (2008).

[5] L. Tóth, H. Matsuda, H. Daimon, J. Electron Spectroscopy and Related Phenomena, 171, 64 (2009)

[6] H. Daimon, Rev. Sci. Instrum. 59, 545 (1988)

[7] H. Daimon, H. Matsuda, L. Toth, F. Matsui, Surface Science, 601(20) 4748, (2007).

Phoswich solutions for the PET DOI problem

L. Eriksson, C.L. Melcher, M. Zhuravleva, M. Eriksson, M. Conti

Positron Emission Tomography (PET) has two main missions, spatial resolution and sensitivity. The present work concerns spatial resolution. The spatial resolution is related to the pixel size, but since long pixels are needed for sensitivity, many detection element combinations will have a substantial radial elongation. The elongation problem can be solved by registering the depth-of-interaction (DOI) in the detection elements. A relatively easy way to achieve this is to use the phoswich concept, that is, to subdivide the pixel into two or more sections with different scintillators and then identify the different scintillators sections based on pulse shape discrimination techniques. This has been done for the Siemens HRRT systems having a phoswich combination based on LSO and LYSO. Separation is based on scintillation decay time with LSO having a decay time around 40 ns and LYSO (30%Lu) having a decay time of 55 ns. This is an example of a classical phoswich with non-interaction scintillators. Recently other combinations have been successfully tried such as LuYAP and LSO (ref Crystal Clear and animal PET). A potential problem is that LuYAP emission occurs in the excitation band of LSO changing the emission characteristics making it important in what order, relative to the PMT, the scintillators are arranged. By placing the LSO in the front with LuYAP behind, close to the PMT, the interactions can be minimized and good phoswich functionality can be obtained.

The interaction between the scintillators generates scintillations via photo-luminescence giving decay times sometimes quite different from the decay time from gamma excitations. Photo-luminescence of GSO excited at 371 nm gives a decay time of around 25 ns, while excitations based on gamma rays may give a decay time of around 70 ns [1]. Furthermore, the interaction and the scintillation emission can be described as a convolution of the two decay times of the two scintillators.

An elegant way to solve the DOI problem may be to place a thin scintillator layer on top of a scintillator pixel where the scintillator pixel light interacts with the scintillating top layer adding a mixture of different scintillation times that can be used for DOI determination [2].

By understanding the physics behind the interacting scintillators the phoswich concept can be extended and may provide much more elegant solutions to the DOI problem.

[1] M. Zhuravleva, C. L. Melcher, L. Eriksson, Photoluminescence Characterization of Scintillators for Phoswich Detectors, Presented at the 2009 IEEE Nuclear Science Symposium in Orlando, Florida, In Conference Records, J04-6

[2] H. Du, Y. Yang, J. Glodo, Y. Wu, K. Shah, S.R Cherry, Continuous depth-of-interaction encoding using phosphor-coated scintillators, Phys. Med. Biol. 54 (2009) 1757–1771

Computation of Mean Glandular Dose in Digital Breast Tomosynthesis using a Novel Anthropomorphic Breast Phantom

Marios E Myronakis[1] and Dimitra G Darambara[1],

[1] Joint Department of Physics, Institute of Cancer Research and Royal Marsden NHS Foundation Trust, Fulham Road, London, SW3 6JJ, UK.
e-mails: Marios.Myronakis@icr.ac.uk, Dimitra.Darambara@icr.ac.uk

The advent of flat-panel solid-state detectors and full-field digital mammography (FFDM) allowed the realization of three-dimensional (3D) techniques that ameliorate the problem of tissue overlay in breast imaging. Digital breast tomosynthesis (DBT) is one of them, offering 3D images through reconstruction of image slices obtained from a limited number of x-ray projections. The technique is based on the different projection positions of tissues located at different heights from the detector surface when the tissues are irradiated from different angles.

There is on-going research in the field of breast tomosynthesis to assess and optimize image acquisition and reconstruction, as well as the mean glandular dose (MGD). Studies on conventional breast mammography and the aforementioned 3D techniques have been greatly assisted by the Monte Carlo method through several software applications. Computerised simulations allowed for extensive investigation of the impact of acquisition techniques and geometrical parameters on the imaging and dosimetric performance of the breast imaging system.

In the present study, the GATE toolkit using Geant4 Monte Carlo libraries was utilised to assess the MGD from DBT in a novel, 3D, anthropomorphic, voxelised breast phantom [1]. GATE is extensively used in nuclear medicine studies and has recently implemented the modelling of x-ray systems. It provides a flexible and intuitive framework to model complex geometries, physics, system movement and x-ray sources, under the robustness of the Geant4 libraries. However, GATE does not explicitly allow MGD calculation, and therefore, its code was properly modified to accommodate the requirements for MGD calculation. The DeBRa phantom was recently developed by our team. It is a realistic and detailed, voxelised phantom, completely configurable by the user. The phantom is also capable to model micro-calcifications and lesions of different sizes and types to imitate clinical-like conditions. It has versatile design and can be incorporated in several Monte Carlo applications. The DBT system model is equipped with 0.2 cm thick amorphous Selenium detector (a-Se) and 85 um pixel size. The x-ray tube is positioned 65 cm above the detector and rotate around a pivot point in 6° steps (-40° to 40°) .

The phantom suitability for dosimetric studies is assessed through comparison with published results from other studies that use simple dosimetry phantoms. Tungsten source with aluminum (W/Al) and aluminum plus silver (W/Al+Ag) filters are used to assess the MGD for the DeBRa phantom at different tube potentials (20-40 kV) and for several compressed breast thicknesses (3, 5, 8 cm).

References

1. Ma, A.K.W., Spencer, G., Darambara, G.: Introducing DeBRa: a Detailed Breast Model for Radiological Studies, Phys. Med. Biol., 54, 4533--4545 (2009)

VARIABLE HEIGHT MULTI-SLIT COLLIMATOR AND OPTIMIZED IMAGE RECONSTRUCTION IN A PHOTON COUNTING SYSTEM FOR DIGITAL MAMMOGRAPHY

Authors	E-mail:	Phone:	Fax:
Björn Cederström[a]	bjorn@mi.physics.kth.se	+46 8 5537 8190	
Magnus Åslund[b]	magnus.aslund@sectra.se	+46 8 623 5252	
Mats Lundqvist[b]	mats.lundqvist@sectra.se	+46 8 623 5255	
Björn Svensson[b]	bjorn.svensson@sectra.se	+46 8 623 5200	

[a] Dept. of Physics, Royal Institute of Technology (KTH), AlbaNova University Center, 10691 Stockholm, Sweden
[b] Sectra Mamea AB, Smidesvägen 5, 17141 Solna, Sweden

Keywords: Observer performance, Mammography, Optimization, Photon counting, Collimator, Image reconstruction

Abstract

A photon-counting scanned multi-slit mammography system with an array of silicon-strip detectors[1, 2] was introduced in the European market in 2003. The multi-slit geometry with a pre-breast collimator and a matching post-breast collimator provide intrinsic and efficient scatter rejection.[3] Compared to energy-integration, photon-counting provides improved energy weighting,[4] and it is possible to eliminate virtually all electronic noise. The detector and pre-collimator are scanned across the object with the center of rotation collinear with the focal spot. The detector consists of several edge-on silicon-strip detector lines. Each line is coupled to a collimator slit in the pre-breast collimator.

With Vinnova-funding[5], further optimization of this system is explored. We present results from using an observer model for optimizing a new and improved pre-breast collimator able to operate in at least two positions depending on breast thickness. The current system uses a pre-collimator that has a single fixed position that was determined to allow for imaging of all women. A variable height pre-collimator reduces the focal blurring which can either be used to improve the detective quantum efficiency (DQE) and dose efficiency for imaging small objects such as micro calcifications, or it can be used to decrease the imaging time. In the optimization of the pre-breast collimator the slit width and collimator position (height above breast support) are varied. In addition to altering the modulation transfer function (MTF) and imaging time, the collimator position affects the breast thickness that the system can accept. The MTF used in the model observer optimization of the pre-breast collimator is therefore performed using a theoretical model of the imaging chain with respect to resolution that includes: width of focal spot, width of the pre-collimator slits, the continuous scan motion and non-aligned detector lines. The scan time and the dose efficiency for imaging a 100 µm diameter object were chosen as figures of merit in the optimization. Four different observer models were used to calculate the dose-efficiency and compared. In addition, a prototype of the new pre-collimator was build and used to acquire images of a CDMAM phantom (version 3.4)[6]. The images were evaluated using the CDCOM[7] for automatic reading of the 100 µm discs.

Furthermore, an improved image reconstruction is investigated in which the images generated by the different detector lines are added with linear interpolation instead of adding pixel values of nearest neighbors. This reduces the modulation (MTF), and noise power spectrum (NPS) in a way that the DQE is increased for high and intermediate spatial frequencies. The new software for image reconstruction was evaluated by comparing the threshold thickness of the 100 µm disc in the CDMAM

[1] M. Danielsson et al, Proc. SPIE, Physics of Medical Imaging, vol. 3977, pp. 239-249 San Diego, 2000
[2] M. Lundqvist et al, IEEE Transactions on Nuclear Science, Vol 48 (4), pp. 1524-1529, 2001
[3] M. Åslund et al, Med Phys, vol. 33, pp. 933-940, 2006
[4] R.N. Cahn et al, Med. Phys., vol. 26 (12), pp. 2680-2683, 1999
[5] "www.vinnova.se"
[6] Artinis, St Walburg 4, 6671 AS Zetten, The Netherlands
[7] "www.euref.org"

phantom for images acquired with this and with the current software. The threshold thickness was extracted using CDCOM for automatic reading.

It was found that optimizing the pre-collimator parameters can improve the dose efficiency by 12% using a height 6 cm above the patient support with maintained scan time. For a 6 cm object, the collimator would be in its lower position and the dose efficiency can be further improved to a total of 22% by also extending the scan time by 10%. The new software for image reconstruction improved the threshold thickness of the 100 µm disc with 17±5%, i.e. dose efficiency increased by 35±10%.

Laboratory soft x-ray nano-imaging

M. Bertilson, O. v Hofsten, A. Holmberg, J. Reinspach, U. Vogt, and H. M. Hertz,

Biomedical and X-Ray Physics, Department of Applied Physics,
Royal Inst. of Technol./Albanova, SE-106 91 Stockholm, Sweden,
E-mail: michael.bertilson@biox.kth.se

We developed the first sub-visible-resolution laboratory water-window (approx. 0.5 keV) x-ray microscope.[1] In its present configuration the λ=2.48 microscope[2] is based on a liquid-nitrogen-jet laser-plasma source[3] in combination with in-house fabricated 25-nm zone-plate optics and a multilayer condenser. With this microscope we have demonstrated imaging of test objects with <30 nm resolution[2], imaging of wet soil-science samples with synchrotron quality[4] (Fig. 1), and the first high-resolution tomography in laboratory x-ray microscopy[5].

Our present work aims at higher resolution, decreased exposure times, and three-dimensional biological imaging. This requires improved x-ray optics, improved sources, and cryogenic sample handling, respectively. With an improved nano-process we recently succeeded in fabricating single-write nickel zone plates with down to 13 nm outer zone width[6] and few-percent efficiency. Further improvement in efficiency is expected from the use of the germanium-enhanced nickel zone-plate concept[7]. In addition, we recently fabricated a compound zone plate and demonstrated sub-25 nm resolution imaging with this diffractive element in the laboratory microscope.[8] For improved source performance we are presently installing a 280 W/0.8 ns/2 kHz slab laser. Calculations show that this laser will reduce the exposure time more than an order of magnitude, to <10 s per image, thereby reaching the exposure range of synchrotron-based microscopes. This is especially important for the three-dimensional nano imaging of biological cells, where the tomographic data acquisition benefits from the shorter exposure times. In addition, a cryo sample chamber was recently installed for appropriate sample preparation. Figure 2 shows an example, imaging of cryo fixed yeast cells. We are now producing the first 3D images of cryo-fixed materials in laboratory x-ray microscopy.

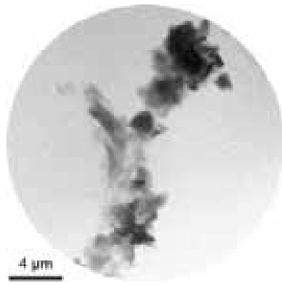

Figure 1. Example of a soil science sample imaged with the laboratory XRM.

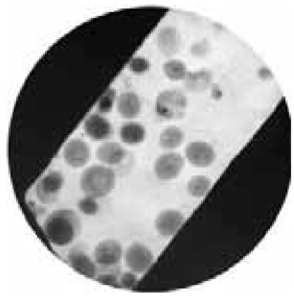

Figure 2. Cryo fixed yeast cells. Full field of view 38 µm

References

[1] M. Berglund et al, J. Microsc. **197**, 268 (2000)
[2] P. Takman et al, J. Microsc. **226**, 175 (2007)
[3] P. Jansson et al, Rev. Sci. Instrum. **76**, 043503 (2005)
[4] J. Thieme et al, J. Physics:Conf. **186**, 0120107 (2009)
[5] M. Bertilson et al, submitted to Opt. Express
[6] J. Reinspach et al, J. Vac. Sci. Technol. B. J. Vac. Sci. Technol. **B 27**, 2593 (2009).
[7] M. Lindblom et al, J. Vac. Sci. Technol. B **27** L5 (2009)
[8] O. von Hofsten et al, Opt. Lett. Opt. Lett. **34**, 2631 (2009).

The portable X-ray apparatus with GaAs linear array.

E.N. Ardashev, S.A. Gorokhov, M.K. Polkovnikov, A.P. Vorobiev, Yu.P. Tsyupa
Institute for High Energy Physics, 142281 Protvino, Moscow reg.

Abstract

The widely growing interest to the digital (non-film) diagnostic and analysis systems, which have a lot of advantages in comparison with the traditional (film) systems, in data taking, data storing, and data transmitting, require the new detection technology. One of the most promising systems for medical roentgenography today is the scanning type apparatus with gallium arsenide linear array detectors. The present paper describes the results of the construction and testing the portable X-ray unit for traumatic examination and orthopedic manipulation in stationer clinics and first aid in medicine of catastrophe. Apparatus is the digital device with the digital detectors to form image while scanning object. The scanner has semiconductor GaAs detectors as the sensitive elements. GaAs detectors are detectors of direct transformation X-ray radiation into electrical signal with efficiency near to 100%. The moving collimator is being used to reduce the dose obtained by the patient during examination. Detector line consists of 16 assembles. Each assemble is a combination of analog chip and 128 sensitive GaAs elements (micro strips). Chip transforms each detector element current in a voltage signal then all 128 signals multiplex to one signal. After amplifying all 16 signals again multiplex to one result signal and digitize by a twelve-digit ADC. X-ray flow, which has passed through the object, detected by a detector array. The detector is moving mechanically through the frame during exposition. Acquired information stored in the scanner's random access memory. The apparatus uses USB bus for connection with PC. During the test runs the parameters of the apparatus have been measured: the space resolution, contrast threshold and dynamic range. The scanning region is 400x400 mm^2. The scanning time is ~3 seconds. The roentgen pictures at very low dose load have been obtained and presented in this paper. To get these pictures the special mathematical approach has been adopted.

Development of a head module for multi-head Si/CdTe Compton camera

[1, 3] Mitsutaka Yamaguchi, [1] Tomihiro Kamiya, [2] Naoki Kawachi, [2] Nobuo Suzui, [2] Shu Fujimaki, [3, 4] Hirokazu Odaka, [3, 4] Shin-nosuke Ishikawa, [3,] Motohide Kokubun, [3, 4] Shin Watanabe, [3, 4] Tadayuki Takahashi, [5] Hirofumi Shimada, [1, 5] Kazuo Arakawa, [6] Yoshiyuki Suzuki, [5] Kota Torikai, [5] Yukari Yoshida, [5, 6] Takashi Nakano

[1] Takasaki Advanced Radiation Research Institute, Japan Atomic Energy Agency (JAEA), [2] Quantum Beam Science Directorate, JAEA, [3] Institute of Space and Astronautical Science, Japan Aerospace Exploration Agency, [4] Department of Physics, University of Tokyo, [5] Gunma University Heavy Ion Medical Center, Gunma University, [6] Graduate School of Medicine, Gunma University

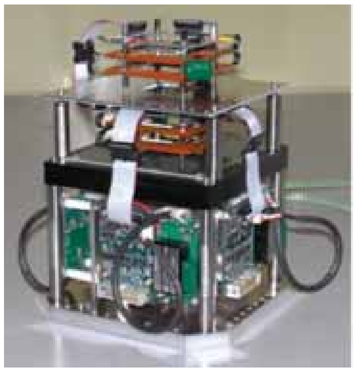

Fig. 1. Inner circuit of camera head.

For the mainstream imaging techniques in the field of life science research like PET or SPECT, simultaneous imaging of multiple nuclei is difficult because the energy of the measurable gamma ray is a specific energy or in a restricted energy range. Therefore we are constructing a three-dimensional imaging system for medical and biological applications as a device that can provide simultaneous imaging, having high spatial and energy resolutions and wide energy range from several tens keV to a few MeV, by diverting the most advanced space-observation technology, Si/CdTe semiconductor Compton camera, developed in ISAS/JAXA. The Si/CdTe Compton camera was developed under the assumption that the use of moderate temperature and the Analog ASIC for signal processing. Moreover, because the solid and thin scattering layer allows close placement of the measured object, good angular resolution corresponds to good spatial resolution directly. These aspects allow construction of compact medical system.

In contrast to space-observation use, three-dimensional imaging ability becomes important for life science research. In order to achieve a good three-dimensional spatial resolution, modularizing the Compton camera into a small camera head and allowing multi-angle imaging with multi-head structure is required. In this work, a head module has been developed as a prototype module of the multi-head system. Fig. 1 shows the inner circuit of the prototype module. Sensor and circuit modules are closely arranged and put in a compact vacuum-insulating cylindrical housing having the height of 24 cm and the diameter of 22 cm. Each of camera heads will be fixed on robot arms and be able to adjust the positions and the directions. Performance evaluation test was made for the prototype module with a sealed Ba-133 radiation source. We confirmed that the imaging result is consistent with the source positioning. The angular resolution measure, abbreviated as ARM, was estimated to be 4.5 degree. The result of the test was compared with a Monte Carlo simulation study. We will report the details of the prototype module and the result of the performance evaluation test. The expecting three-dimensional performance will also be reported.

Estimating tumor/non-tumor uptake from radiolabeled monoclonal antibodies based on scintigraphic imaging

M. Salouti[a], H. Rajabi[b]

[a]Dept. of Biology, School of Sciences, Islamic Azad University, Zanjan Branch
[b]Dept. of Medical Physics, School of Medical Sciences, Tarbiat Modarres University,

Introduction: A biodistribution study in animal models bearing tumors is one of the most important procedures in evaluation of fractional uptake of radiopharmaceuticals in the tumor and non-tumor organs. The aim of this study was to develop a new soft ware method to determine activities that accumulated in the main organs as well as tumor without killing the animals based on scintigraphy images.
Material and Methods: The ^{99m}Tc labeled MAb PR81 was injected to 30 BALB/c mice with xenograft breast tumor. The anterior and posterior images of mice were taken 16 hours using a double head gamma camera. The images were transformed to PC after converting them to interfile format. Then the anterior and posterior images of each mouse were conjugated using the designed software. After that with drawing ROI around each organ as well as tumor, the counts were obtained considering calibration and background contribution. Meanwhile, the mice were killed, the organs dissected and were counted individually using a well counter. Finally, the measurements obtained by the both ways were compared.
Results: The comparison of the results obtained by both procedures showed that there is a significant difference between the absolute count of the same organs but with a linear relation ship between the main organs.
Discussion and Conclusion: The results show that although the new method cannot be replaced with the invasive one to estimate the absolute activity of each organ mainly due to overlapping of the organs, but it can be used to compare the relative activity of tumor and main organs in relation to each other in order to evaluate the quality of biologic radiophamaceuticals for targeting tumor as a basic parameter.
Keywords: Scintigraphic Imaging, Biodistribution, Radiopharmaceutical

International conference on imaging techniques in subatomic physics, astrophysics, medicine, biology and industry, June 2010.

Position correction with depth of interaction information for a small animal PET system.

M. Carles[1], Ch. W. Lerche[2], F. Sánchez[1], F. Mora[2] ,and J. M. Benlloch[1]

[1] Instituto de Física Corpuscular (CSIC-Univ.Valencia), Apdo. 22085, 46071 Valencia, Spain.
[2] I3M, Universidad Politécnica de Valencia, Camino de Vera s/n, 46020 Valencia, Spain.

One of the most important degrading factors for Positron Emission Tomography (PET) is the depth of interaction (DOI) problem. A Parallax error is introduced in γ - ray imaging whenever the thickness of the absorbing material is finite, the incidence direction of the γ - ray is oblique, and the DOI is not measured. Without depth of interaction detection, uncertainties in the parameterization of the line of response (LOR) are introduced.

In this work we study the effects on the spatial resolution for a small animal PET scanner when DOI information is included.

The method for measuring the depth of interaction is based, on one hand, on the correlation between the width of the scintillation light distribution in monolithic scintillation crystals and the DOI [1], and, on the other hand, on a small modification of the widely applied charge dividing circuits [2,3,4]. The modification of these circuits consists in adding an analogue summation circuit that allows measuring the standard deviation of the scintillation light distribution.

The PET scanner, where the additional DOI functionality was implemented, consists in eight identical modules forming an octagon with an aperture of 111 mm. Each module consists of a single monolithic LYSO scintillation crystal with dimensions 40x40x9.8 mm^3 with flat-topped pyramidal shape, and a position sensitive photomultiplier tube (PSPMT). The photomultiplier tube is of type H8500 from Hamamatsu Photonics K.K and has a sensitive area of 49x49 mm^2 and therefore matches exactly the dimensions of the larger basis of the LYSO block. All sides of the LYSO crystals, except the one coupled with optical grease to the PSPMT have been black painted. The particular pyramidal shape of the crystal reduces the image compression near their edges and therefore enhances the spatial resolution in this region. Each module also contains the DOI enhanced charge division read out, preamplifier and the high voltage supply for the PSPMT.

For a Na^{22} point source displaced along the axis of the transversal plane, we have obtained the reconstructed image with, and without, DOI information. As was reported for a small animal PET system of four modules [3], preliminary results of our study show an image quality enhancement achieved taking into account DOI information.

References.

[1] J.Karp and M. Daube – Witherspoon, *Depth-of-interaction in Na(tl) and BGO scintillation crystals using a temperature gradient*.Nucl. Instr. and Meth. A, vol.260,

[2] Christoph W.Lerche et al., *Depth of interaction for γ-ray imaging*. Nucl. Instr. And Meth., A600(2009), 624-634,

[3] Christopher W.Lerche et al., *DOI Measurement with Monolithic Scintillation Crystals: a Primary Performance Evaluation.* IEEE Nucl. Sci. Symp. & Med. Img. Conf., 4:2594-2600,Novembre 2007.

[4] Christoph W.Lerche et al., *Depth of interaction detection with enhanced position-sensitive proportional resistor network.*, Nucl. Instr. and Meth.,, A537 (2005), 326-330. pp.509-517, 1987.

Carbon translocation in a whole plant body by using positron emitting tracer imaging system (PETIS) and carbon-11-labeled carbon dioxide ($^{11}CO_2$)

Naoki Kawachi[1], Nobuo Suzui[1], Satomi Ishii[1], Sayuri Ito[1], Noriko S. Ishioka[1], Haruaki Yamazaki[1], Aya Hatano-Iwasaki[2, 3], Ken'ichi Ogawa[2, 3], Shu Fujimaki[1]

[1]Plant Nutrition and Radiotracer Imaging Research Group, Quantum Beam Science Directorate, Japan Atomic Energy Agency, [2]Plant Redox Regulation Research Group, Research Institute for Biological Sciences, Okayama, [3]Core Research for Evolutional Science and Technology (CREST), Japan Science and Technology Agency

Elucidation of carbon kinetics in a plant is important from viewpoint of environmental reduction in the amounts of atmospheric carbon dioxide (CO_2) and from an agricultural viewpoint in terms of the growth and development of the plant body. In articular photosynthetic CO_2 fixation and photoassimilate translocation are important topics for understanding the mechanisms underlying carbon kinetics. In this study, we have developed a method to investigate the carbon kinetics by using one of the most powerful radionuclide-based imaging techniques for plant study, that is, the positron emitting tracer imaging system (PETIS). Carbon-11-labeled carbon dioxide ($^{11}CO_2$) and PETIS enable video imaging of tracer dynamics of carbon fixation, photosynthesis, and translocation. Because of a large field of view (FOV) provided by the PETIS and the sufficiently small size of soybeans (G. max cv. Jack) that fit in the FOV, dynamic quantitative PETIS data of gradual changing in ^{11}C activity and ^{11}C distribution throughout the entire intact plant body after pulse-chase $^{11}CO_2$ treatment is acquired. This indicates the successful imaging of CO_2 photoassimilate translocation from the time of entry into to that of distribution of the whole plant body; further, carbon kinetics is analyzable to understand plant physiology and nutrition.

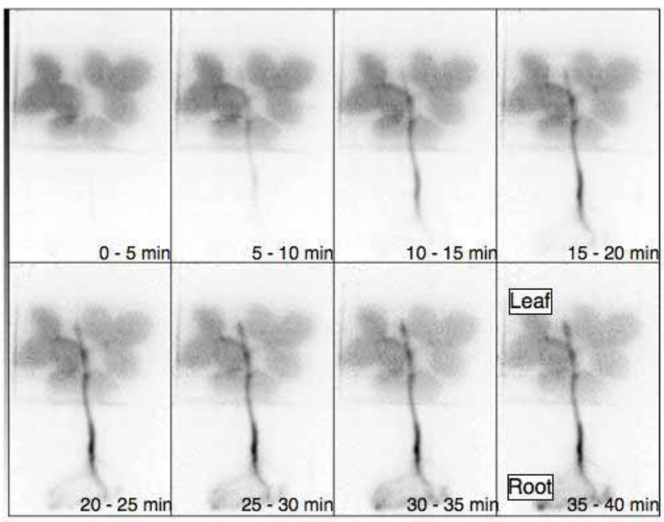

Figure. The PETIS data re-sorted in the sequence from 0–5 to 35–40 min (from left to right). All the images were corrected for ^{11}C radioactive decay (half life = 1223.1 sec).

Anatomy of plasma objects based on spectral images.

N.V.Denisova, A.V.Tupikin

Institute of Theoretical and Applied Mechanics,
630090, Novosibirsk, Russia

In the last decade, researches aimed at intensification of burning processes have steadily grown. At the same time, plasma-chemistry is currently becoming a modern technology of new materials preparations. The important characteristic of kinetic processes in plasma–chemical reactors and in flames is the spatial distribution of active particles. The emission tomography can provide information on this distribution. Using medical terminology we called it as ‘plasma anatomy’. In this paper we consider emission tomography method based on spectral images from our practical diagnostics. ‘The anatomy’ of methane plasma in plasma-chemical reactor and its evolution with 0.2 mcs time step was obtained using spectral images. Photorecording of the plasma evolution in the reactor was performed using emission spectrum from the reaction area.
Study of active particles distribution in a flame has been performed. The spectral images, integral along the flame volume, are shown in Fig.1. The spatial distributions of active radicals OH and CH in the flame are shown in Fig.2. The analysis of the obtained results has been made.

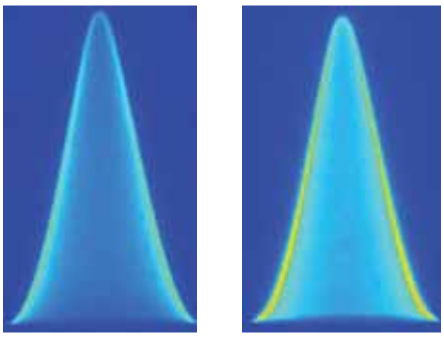

Fig. 1. Spectral flame images.
Image obtained with filter UFC5(250-400nm) (left)
Image obtained with filter FC6(290-460nm) (right)

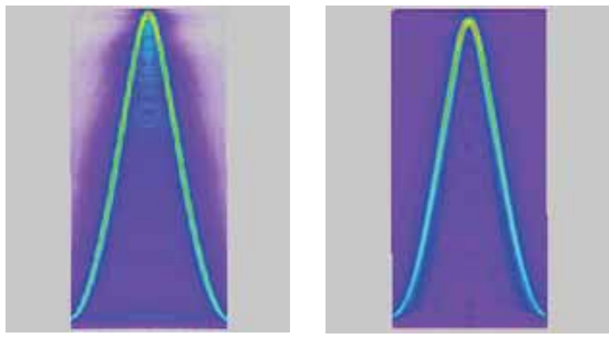

Fig.2 Spatial distribution of radical OH (left) and radical CH (right) in the flame .

This work is supported partly by the Russian Basic Research Fund, the grant №08-01-582a.

1. Denisova N. Plasma diagnostics using computed tomography method // IEEE Trans. Plasma Sci. 2009 37 4 502.
2. Denisova N., Haverlag M., Ridderhof E.J., Nimalasuriya T., Mullen J.J.A.M. van der X-ray absorption tomography of a high-pressure metal-halide lamp with a bended arc due to Lorentz-forces // J. Phys. D: Appl. Phys. 2008. V. 41. 144021. 7 pp.
3. Denisova N., Bogans E., Revalde G., Skudra A. Computer tomography imaging of emitting mercury atom spatial distributions in a capillary discharge lamp // IEEE Trans. Plasma Sci. 2008. V. 36. N. 4. P. 1188.
4. Denisova N.V., Katsnelson S.S., Pozdnyakov G.A. Tomographic diagnostics of processes in a plasma-chemical reactor AIAA paper 2007-3874.

Evaluation of Junction Termination for X-ray detectors

P. Norlin[1], C. Xu[2], M. Åslund[3], M. Bakowski[1]
[1]Acreo AB, Sweden, [2]Medical Physics Royal Institute of Technology, Sweden,
[3]Sectra Imtec AB, Sweden
mietek.bakowski@acreo.se

Modern X-ray imaging equipment makes use of a large number of detector chips in an array. Each detector contains a large number of individual detector diodes (Fig. 1). It is essential to secure low and stable values of leakage current over a lifetime of each detector for a sensitive and stable X-ray imaging. In this paper we evaluate the performance of two different junction termination (JT) designs utilizing the principle of floating rings (FR) and field plates (FP) [1,2]. A good junction termination is characterized by an even distribution of the electric field at the semiconductor surface and large tolerance to the variation of the surface charge (Fig. 2-3). Two different FR designs one containing rings and second containing rings for a fully depleted type 150 V detector are evaluated. The performance evaluation is based on the CV measurements on MOS test structures in order to establish the value and polarity of the interface charge prior to and after the irradiation and on the IV measurements of the leakage current of the large number of the individual pixel diodes (Fig. 4). The irradiation dose is selected to correspond to the typical lifetime exposure of the detector and the voltage range is up to 500V. The measurement results are compared with the simulation results obtained using simulation program AvantMedici with respect to the influence of the surface charge on the leakage current, surface electric field and maximum reverse voltage.

References

1) B. J. Baliga, ”Modern Power Devices”, John Wiley and Sons, 1987, pp.62-132.
2) K.H. Wyllie, “Floating guard rings high-voltage termination structures for radiation-tolerant silicon detectors”, Nuclear Instruments and methods in Physics Research, A409, (1998), pp. 271-274.

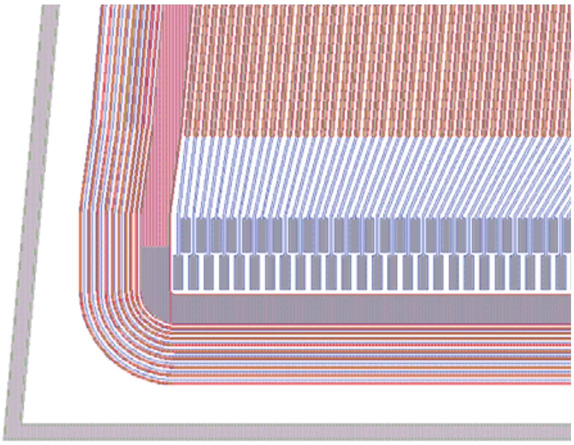

Fig. 1 Cad drawing of a chip corner showing JT with 9 FR (top view).

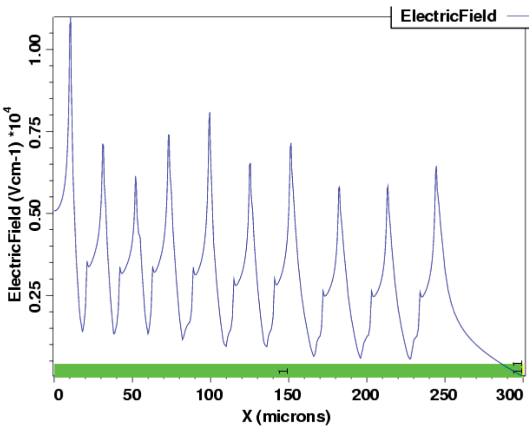

Fig. 2 Surface electric field for a JT with 9 FRs and zero surface charge.

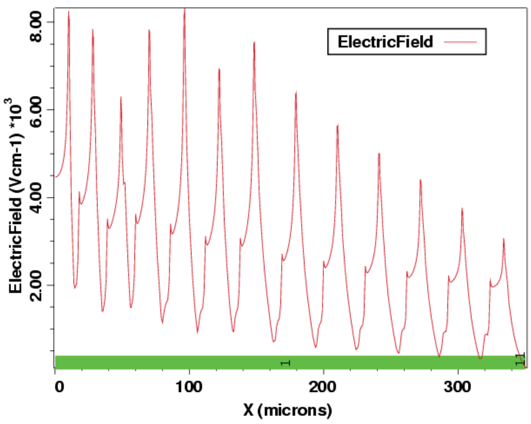

Fig. 3 Surface electric field for a JT with 12 FRs and zero surface charge

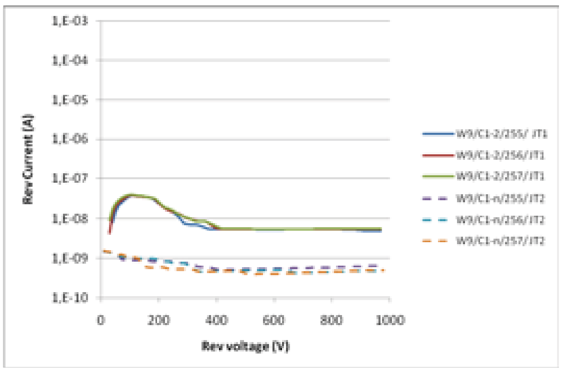

Fig. 4 Reverse I-V characteristics of diodes in a detector chip, measured before irradiation. Solid and dashed lines correspond to two different JT designs, respectively.

Bone Quality by X-ray Microtomography and Microfluorescences techniques

E.S. Sales[a], I. Lima[c,a], M. J. Anjos[b,a], J.T. Assis[c], R. T. Lopes[a]

[a] Nuclear Instrumentation Laboratory, Federal University of Rio de Janeiro

P.O. Box 68509, 21941-972 Rio de Janeiro, Brazil

[b] Physics Institute, University of Rio de Janeiro State, Rio de Janeiro, Brazil

[c] University Department of Mechanical Engineering and Energy, Rio de Janeiro State University, Nova Friburgo, RJ, Brazil.

Bone quality can be defined as the totality of features and characteristics that influence the ability of bone to resist fractures. Therefore be seen that the biological material and structure that help to determine the resistance to structural failure: bone size, thickness of cortical bone, trabecular numbers, tissue mineral content, density, porosity, and so on. The purpose of this paper was to study bone quality using X-ray microtomography and microfluorescence techniques for the measurement of bone mineral density (BMD), microarchitecture and bone mineral content (BMC). The study was done on bone samples of rats from study protocols on hyperthyroidism and aging. The results showed significant changes in the results of the architecture, BMD and BMC of the samples of aging protocol, and animals of hyperthyroidism was not found any kind of disorder, both results in the range of 95%.

Elemental Distribution Images in Prostate Tissue Samples by X-ray Fluorescence Microtomography

G. R. Pereira[a], H. S. Rocha[a], M. J. Anjos[b], I. Lima[c,a], C. A. Pérez[d], R. T. Lopes[a]

[a] Nuclear Instrumentation Laboratory, Federal University of Rio de Janeiro

P.O. Box 68509, 21941-972 Rio de Janeiro, Brazil

[b] Physics Institute, University of Rio de Janeiro State, Rio de Janeiro, Brazil

[c] University Department of Mechanical Engineering and Energy, Rio de Janeiro State University, Nova Friburgo, RJ, Brazil.

[d] Brazilian Synchrotron Light Laboratory, Campinas, Brazil

An X-ray Transmission Microtomography (CT) system combined with an X-ray Fluorescence Microtomography (XRFμCT) system was implemented in the Brazilian Synchrotron Light Laboratory (LNLS), Campinas, Brazil. The main of this work is to determine the elemental distribution in prostate samples in order to verify the concentration of some elements correlated with characteristics and pathology of each tissue observed by the transmission CT.

The experiments were performed at the X-Ray Fluorescence beamline (D09B-XRF) of the Brazilian Synchrotron Light Laboratory, Campinas, Brazil. A quasi-monochromatic beam produced by a multilayer monochromator was used as an incident beam. The sample was placed on a high precision goniometer and translation stages that allow rotating as well as translating it perpendicularly to the beam. The fluorescence photons were collected with an energy dispersive HPGe detector placed at 90º to the incident beam, while transmitted photons were detected with a fast Na(Tl) scintillation counter placed behind the sample on the beam direction.

The CT images were reconstructed using a filtered-back projection algorithm and the XRFμCT were reconstructed using a filtered-back projection algorithm with absorption corrections. The 3D fluorescence images were reconstructed using the 3D-DOCTOR software.

Three-dimensional measurements of coordinates and translations using micro X-ray point source stereoscopy

Wasil H. M. M. Salih, Joris A. M. Soons and Joris J. J. Dirckx
Laboratory of Biomedical Physics, University of Antwerp, Groenenborgerlaan 171, 2020 Antwerpen, Belgium

Abstract
In this paper we establish that a method for high-resolution measurement of three-dimensional coordinates and translations of small objects. Such a method is needed to study for instance the movements of the middle ear ossicles or other small biomechanical structures. The theory of the pinhole method is developed for a point-source X-ray projection setup using a conical beam. The method is then implemented using a micro X-ray tomography setup with a single 8μm point source. Stereo projections are obtained by rotating the object over 90° between subsequent recordings, and microscopic Tungsten beads are used as marker points. The accuracy of the method is tested on a spherical calibration object. The accuracy for measurement of three-dimensional coordinates was found to be better than 20μm. The precision for translation measurements was found to be better than 10μm along all three spatial dimensions. The method of X-ray stereoscopy can be implemented on a cone-beam setup with a point source. Our method allows high precision measurement of three-dimensional coordinates and three-dimensional motions within radio-opaque objects. Instead of full field tomographic reconstruction using many X-ray projections, high-resolution coordinate measurement can be done using just two X-ray cone beam projections.

Verification of a Readout Design for Charge Sharing Correcting in Single Photon Processing Pixel Arrays

Suliman Abdalla[1], Bengt Oelmann[1], Börje Norlin[1], Jan Thim[1], Mattias O'Nils[1], Xavier Llopart[2]
[1] Mid Sweden University, Dept. of Information Technology and Media, Sundsvall, Sweden
[2] CERN, 23 1211 Geneva, Switzerland

The Semiconductor pixel-array detectors have found many applications in the field of scientific and medical imaging. For radiation imaging applications, the hybrid pixel detector is increasingly gaining importance. In such a device, a pixel sensor chip is bonded to read-out electronics circuits. The readout is usually implemented in CMOS technology as integrating or photon-counting pixel detectors. Single photon processing pixels contain complex circuitry including analog and digital processing. This makes the pixel circuit design mainly driven by area and power consumption. The restriction of the area comes from the system requirement on the spatial resolution. The continuously ongoing downscaling of the CMOS technology makes it possible to include more advanced processing circuits in the pixels. In the Medipix2 chip [1] each pixel cell is 55 um x 55 um, working in a single photon counting mode for positive or negative input charge. Charge sharing in single photon processing imaging detectors is a problem that becomes increasingly severe as the pixel dimension shrinks. For small pixel sizes the lateral broadening of the charge will be significant and charge from a single hit may be detected in a neighbourhood of pixels. This effect limits the ability to do spectral imaging with small pixel sizes.

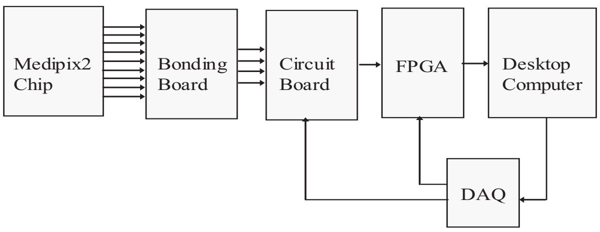

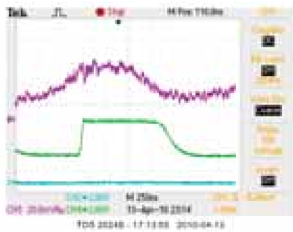

Figure 1 (a) Block diagram of the tools used in the measurements. (b) Measured signals

The objective is to study charge distribution for shared hits and to develop methods for spectrum reconstruction. This paper shows measurement results of charge sharing based on the proposed charge sharing suppression mechanism presented in [2]. The basic idea of this mechanism is to organize pixels as a group of four and to localize the detected charge that may be distributed over several pixels, to one single pixel that has larger detected charge, where all charges from the neighboring pixels are summed, and evaluate which pixel has larger signal charge to count an event. The equipment showed in Figure 1(a) includes X-ray sources, a Medipix2 chip, an FPGA and a desktop computer with LabView. This involves developing and implementing circuit architecture and mounting a Printing Circuit Board (PCB) to Medipix2 chip. Figure 1(b) shows an oscilloscope trace of the summing amplifier and discriminators outputs, the lower threshold is activated while the upper threshold is not. In the paper the ability to reconstruct the energy of photons absorbed in the border between four pixels are evaluated.

References

[1] X. Llopart, M. Campbell, R. Dinapoli, D. san Segundo and E. Pernigotti, "Medipix2, a 64k pixel readout chip with 55 μm square elements working in single photon counting mode", IEEE Transactions on Nuclear Science, vol. 49, pp. 2279-2283, October 2002.

[2] Suliman Abdalla, Hans-Erik Nilsson, and Bengt Oelmann, "Circuit Implementation of Mechanism for Charge-Sharing Suppression for Photon-Counting Pixel Arrays". Proc. of the IEEE Norchip Conference, Oulo, Findland, pp. 137- 140, 2005.

256-Slice CT Coronary Angiography in Atrial Fibrillation: The Impact of Mean Heart Rate and Heart Rate Variability on Image Quality

Wei-Yip Law[1], Liang-Kung Chen[1,2], Kun-Mu Lu[1], Greta S.P. Mok[3], Ching-Ching Yang[4] and Tung-Hsin Wu[5,*]

1 Department of Radiology, Shin Kong Wu Ho-Su Memorial Hospital, Taipei, Taiwan

2 College of Medicine, Fu Jen Catholic University, Taipei, Taiwan

3 Department of Radiological Technology, Tzu Chi college of Technology, Hualien, Taiwan

4 Department of Diagnostic Radiology & Organ Imaging, The Chinese University of Hong Kong, Shatin, N.T., Hong Kong

5 Department of Biomedical Imaging and Radiological Sciences, National Yang Ming University, Taipei, Taiwan

*Corresponding author: Tung-Hsin Wu, E-mail: tung@ym.edu.tw

Objective: To evaluate the performance of 256-slice MDCT for the visualization of the coronary arteries in a population with atrial fibrillation (AF) and to explore the impact of patients' heart rate (HR) on image quality.

Methods: Eighteen consecutive patients with AF and 18 patients in sinus rhythm were examined on a 256-slice MDCT scanner. Patients with AF were further divided into two groups: low HR (< 72 bpm) and high HR (≧ 72 bpm).Two reviewers examined images of 16 coronary artery segments for each patient based on a 4-point scale (1 = no motion artifact, 4 = not evaluative) to evaluate motion artifact.

Results: The overall image quality score for all three coronary arteries in AF was 1.7 ± 0.4 and 1.7 ± 0.3 in sinus rhythm (p<0.001). Score 1, 2 and 3 (diagnostic quality) were assigned to 100% in sinus rhythm and 99.6% in atrial fibrillation (p<0.001). Score 4 was seen only in AF group (1/245, 0.4%). The mean HR of low HR group and high HR group were 65.4 ± 8.5 bpm and 81.4 ± 6.1 bpm. There is no statistical difference with regards to heart rate variability (HRV) and image quality between the two HR groups. The optimal reconstruction phase in low HR group was mainly distributed in diastole and shifted to systole in high HR group.

Conclusion: The analysis of our initial experience shows that imaging in patients with AF is possible using 256-slice MDCT. Patients' HR does not affect image quality significantly but had impact on optimal reconstruction timing.

Reduction of Metallic Artifacts on CT-based Attenuation Correction for PET/CT Imaging

Jay Wu[1], Cheng Ting Shih[2], Shyh-Jen Wang[3,4], Bang-Hung Yang[3,4], Chih-Hao Chen[3] and Tung Hsin Wu[4,*]

[1] Institute of Radiological science, Central Taiwan University of Science and Technology, Taichung, Taiwan

[2] Department of Biomedical Engineering and Environmental Sciences, National Tsing-Hua University, Hsinchu, Taiwan

[3] Department of Nuclear Medicine, Taipei Veterans General Hospital, Taipei, Taiwan

[4] Department of Biomedical Imaging and Radiological Sciences, National Yang-Ming University, Taipei, Taiwan

[*]Corresponding author: Tung-Hsin Wu, E-mail: tung@ym.edu.tw

Abstract

The quantification ability of positron emission tomography (PET) allows its widely usage for cancer staging in clinical practice. The standard uptake values (SUV) can be calculated by the pixel values of regions of interest (ROI) after some physical corrections are performed, such as scatter correction and attenuation correction (AC). For the PET/CT modality, CT images are conveniently applied for attenuation correction. However, if they are contaminated by metal artifacts, quantitative errors may occur in the PET images. In this study, we applied a modified metal artifact reduction (MAR) algorithm and evaluated its effectiveness for attenuation correction of PET. The MAR algorithm was based on the model images which were built by the *k*-means clustering with spatial information. The projection data of the original image and model image were then combined together using an exponential weighting function. The metal-artifact-free image was reconstructed using the filter back-projection method. In this study, three cases were examined. PET scans with general-CT AC and MAR-CT AC were performed as well as without AC, respectively. The SUV ratios at five pre-defined ROIs were calculated. The results demonstrated that the MAR algorithm effectively removed the bright and dark streaks and recovered the continuity and uniformity in the CT images of the three cases. For the cylindrical water phantom inserted with a lead rod, the SUV ratios between general-CT AC and MAR-CT AC were from 1.00 to 1.09. For the brain scan with dental fillings, the SUV ratios were from 0.93 to 1.37. For the lower limb scan with metal implants, the SUV ratios were in the range of 0.78 to 0.98. We conclude that metal artifacts certainly impact the CT images and further influence the AC for PET scans. Through the MAR of CT images, the quantitative errors of PET could be reduced.

Keywords: positron emission tomography; attenuation correction; metal artifact reduction

Correction of Iodine and Barium Contrast Artifacts in PET/CT Attenuation Correction

Kuan-Yu Chang[1], Jay Wu[2], Liang-Kung Chen[3,4], Tzung-Chi Huang[5,*], Geoffrey Zhang[6]

[1]Department of Orthopedic Surgery, Mackay Memorial Hospital Taitung Branch, Taitung, Taiwan

[2] Institute of Radiological science, Central Taiwan University of Science and Technology, Taiwan

[3] Department of Radiology, Shin Kong Wu Ho-Su Memorial Hospital, Taipei, Taiwan

[4] College of Medicine, Fu Jen Catholic University, Taipei, Taiwan

[5] Department of Biomedical Imaging and Radiological Science, China Medical University, Taiwan

[6] Department of Radiation Oncology, Moffitt Cancer Center, Florida, USA

[*]Corresponding author: Tzung-Chi Huang, E-mail: tzungchi.huang@mail.cmu.edu.tw

Abstract

The photon flux of CT scan is 10^4 times greater than the germanium-68 transmission scan. Therefore, compared with germanium-based attenuation correction, CT-based attenuation correction allows decrease the overall scanning time and to create a noise-free attenuation map under standard operating condition. However, when CT relies on administration of oral or intravenous contrast agents to allow improved lesion delineation, it may cause the presence of pseudo-enhanced CT number (even streak artifacts). Thus in corrected PET image, it was observed error of the tracer uptake and easily misclassified as bone. In this study, we developed an adaptive threshold technique combining with Nagao filter for segmentation and classification of regions containing intravenous contrast agent to correct for artifacts in corrected PET images.

A Flangeless Deluxe Jaszczak phantom was used in this study. Iodine agent at concentration of 3%, 2% and 1% combined with 18F-FDG was individually filled up each cavity in the phantom. PET/CT scanner was taken with the following CT scan parameters: 140 kV, 80 mA, pitch of 0.984, slice thickness of 2.5 mm and gantry rotation time of 0.5s. Nagao Filter was applied in this study to accurately segment the artifacts in CT images. Usually, the resulted images were often unacceptable when a single threshold value was used in binary images. Adaptive threshold technique was applied for better segmentation, in which different threshold values were determined for different regions.

In standardized uptake value (SUV) measurements, 1.08, 0.05, 1.21 g/ml were measured in PET images without adaptive threshold correction, while 0.68, 0.04, 0.84 g/ml were obtained in PET images with adaptive threshold correction. Additionally, data with adaptive threshold correction was observed no significant difference as compared to that without artifacts. We concluded using adaptive threshold method for correcting intravenous artifacts in PET images yielded more accurate quantization of the lesion and normal structures.

Strategies for Reduction of Radiation Dose in Cardiac PET/CT Imaging

Nien-Yun Wu[1], Tung Hsin Wu[1], Jay Wu[2], Greta S.P. Mok[3], Ching-Ching Yang[4] and Tzung-Chi Huang[5,*]

[1] Department of Biomedical Imaging and Radiological Sciences, National Yang-Ming University, Taiwan

[2] Institute of Radiological science, Central Taiwan University of Science and Technology, Taiwan

[3] Department of Diagnostic Radiology & Organ Imaging, The Chinese University of Hong Kong, Shatin, N.T., Hong Kong

[4] Department of Radiological Technology, Tzu Chi college of Technology, Hualien, Taiwan

[5] Department of Biomedical Imaging and Radiological Science, China Medical University, Taiwan

[*]Corresponding author: Tzung-Chi Huang, E-mail: tzungchi.huang@mail.cmu.edu.tw

Introduction: Cardiac PET with ^{13}N-ammonia and ^{18}F-FDG is a powerful and quantitative tool to assess myocardial perfusion and viability. On the other hand, rapid progress in cardiac CT has enabled not only the detection and quantification of coronary artery calcification by using coronary artery calcium scoring (CTCS) but also the grading of coronary stenosis through contrast-enhanced CT coronary angiography (CTCA). However, radiation dose of these cardiac PET/CT examinations can be up to 52.36 mSv, while the proportion of CT radiation dose is about 78.6%. Therefore, in this work, we aim to reduce radiation dose in cardiac PET/CT.

Materials and methods: Firstly, to reduce radiation dose from retrospectively gated helical (RGH) CTCA, we used ECG tube current modulation (ETCM) technique for patients with heart rate (HR) higher than 65 bpm. Patients with HR less than 65 bpm were imaged using prospectively gated axial (PGA) acquisition, where the center of the data acquisition window was set at 75% of the R-R interval. Next, ultra low dose CT (ULDCT) imaging protocol (80 kV, 10 mA) was used to reduce radiation dose from CT transmission scan performed for attenuation correction. Radiation dose estimates for CT examinations were expressed by using CT dose index (CTDI).

Result: Radiation dose of RGH technique was 20 mSv. It was reduced to 10 mSv and 3.4 mSv when using ETCM and PGA techniques, respectively, which results in a dose reduction of 50-83%. Radiation dose in CT transmission scan was reduced by 96.2% from 16.98 mSv to 0.64 mSv when applying ULDCT protocol. The overall radiation dose in cardiac PET/CT examinations can thus be reduced from 41.16 mSv to less than 8.22-14.82 mSv, resulting in a radiation dose reduction of 64-80%.

Conclusion: This study demonstrated that radiation dose in cardiac PET/CT can be significantly reduced without degrading imaging quality. The proposed imaging protocol with radiation dose reduction up to 80% for an integrated cardiac PET/CT coronary artery examination should be able to provide unique insight into coronary heart disease.

Abstract

A Novel Haar-Wavelet-based Lucy-Richardson Algorithm for Positron Emission Tomography Image Restoration

Wai-Peng N. Tam[1], Jhih-Shian Lee[1], Ren-Shyan Liu [2,3], and Jyh-Cheng Chen[1,4*]

[1] Department of Biomedical Imaging & Radiological Sciences, National Yang-Ming University, No. 155, Sec. 2, Li-Nong Road, Beitou, Taipei city 112, Taiwan, ROC.

[2] National PET/Cyclotron Center, Taipei Veterans General Hospital, No. 201, Sec. 2, Shih-Pai Road, Taipei 112, Taiwan ROC

[3] National Yang-Ming University Medical School , No. 155, Sec. 2, Li-Nong Road, Baitou, Taipei city 112, Taiwan, ROC.

[4] Department of Education and Research, Taipei City Hospital, 145 Zheng Zhou Road, Taipei City, Taiwan, ROC.

Purpose: Two major technical limitations for positron emission tomography (PET) images are its low spatial resolution and signal to noise ratio (SNR). Noise will usually be enhanced after image restoration. This often results in images with low SNR regardless of the improved resolution. Images with poor SNR can lead to misdiagnoses. An ideal restoration method should enable us to achieve both high resolution and SNR. Therefore, the Haar-wavelet-based Lucy-Richardson algorithm (HALU) was developed in this study for PET image restoration.

Methods: The HALU algorithm is based on two speculations: (1) In regard to the linearity of Haar wavelets, we proved that the blurring system matrix in the image domain is the same as that in the wavelet domain. (2) Image signals and noise are Poisson distributed. The low-frequency Haar wavelet coefficients are also Poisson distributed. Based on these, we decomposed the PET images into the wavelet domain using Haar wavelets and restored each of the low-frequency subbands using the Lucy-Richardson algorithm (LR). Sequentially, the restored image was reconstructed from the restored wavelet coefficients. We also make comparisons between our method and the LR algorithm using the coefficient of variation (CV), contrast recovery coefficient (CRC) and resolution.

Results: The CVs of the original image, the LR algorithm and the HALU algorithm are 0.15, 0.14, and 0.13. The corresponding CRCs are 0.59, 0.67, and 0.70. And the subsequent resolutions are 2.33 mm, 2.11 mm, and 2.07mm, respectively.

Conclusion: The resolution of the restored image using the HALU algorithm is better with reduced noise than the original image. The CRC of the HALU restored image also shows improvements compared with the original image. The results showed that PET images can be restored with better contrast, resolution, and reduced noise using the HALU algorithm, while poising the trade-offs between denoising and deblurring.

Approach for 3D Dose Verification by Utilizing Autoactivation

Yasunori Nakajima[1)], Yuki Tsuruta[1)], Shinji Sato[1)], Taku Inaniwa[1)], Eiji Yoshida[1)], Taiga Yamaya[1)], Lembit Sihver[3)], Toshiyuki Kohno[1)]

Tokyo Institute of Technology[1)], National Institute of Radiological Sciences[2)], Chalmers University of Technology[3)],

Back Ground and Purpose

Heavy-ion therapy has been achieved successfully with the advantage of dose concentration on tumor. However, it is important to evaluate the deposited dose distribution after irradiation to improve the treatment quality. We have been proposed the method by utilizing autoactivation. Verification of 1 dimensional (1D) dose distribution along with beam axis and perpendicular to the beam axis had been achieved through our previous works. In this study, we extend our method to 3D by detecting annihilation γ-ray with a PET scanner.

Method

In spot-scanning irradiation method, pencil-like beams are delivered to the tumor position $x_{\mathbf{d}}$, $y_{\mathbf{d}}$ by scanning magnets. Range shifters of thickness S_n are inserted to adjust the depth $z_{\mathbf{d}}$ of dose spot. Particles of necessary amount are delivered to each position $x_{\rm d}$, $y_{\rm d}$, $z_{\rm d}$. The positron emitters produced through fragmentation reactions are distributed in a irradiated patient's body. Annihilation γ-rays are emitted from them. Since the distribution of annihilation γ-rays co-relates with the position of the field irradiated with incident particles, dose distribution can be estimated from the detected distribution. The annihilation γ-rays are detected with a PET scanner. The likelihood of the distribution between measured $A_{\rm m}(x,y,z)$ and calculated $A_{\rm c}(x,y,z)$ by the 3D particle transportation code is evaluated. The calculation is carried out with changing the value of E and S_n and determine the values $E_{\rm est}$ and $S_{\rm n,est}$ that maximize the likelihood. By using determined values, dose distribution in the target is calculated.

The 3D particle transportation code that calculates 3D distribution of annihilation γ-rays and dose in the target has developed for this method.

Experiment and Results

Irradiation experiment was carried out at HIMAC, NIRS. Uniform PMMA target was irradiated with beams of ^{12}C 350 MeV/u. Field shape of irradiation was simple cube 4*4*4 cm^3. The annihilation γ-rays were measured with a PET scanner for 10 minutes begun from 5 minutes after the irradiation. The values $E_{\rm est}$ and $S_{\rm n,est}$ that maximize the likelihood between $A_{\rm m}(x,y,z)$ and $A_{\rm c}(x,y,z)$ were determined. Only E and S_N which is the sum of the range shifters thickness were the free parameters (Not with $E_{xd,yd}$,$S_{N,xd,yd}$) for uniform target. The thickness of each range shifter S_n was calculated to keep the same ratio as the ratio of the variation of S_N from the actual value to estimated one. In figure 2, solid line shows the depth-dose distribution at the center of the irradiation field calculated with the $E_{\rm est}$ and $S_{\rm n,est}$. Plots by square show the dose distribution converted to the scale in PMMA target from the dose distribution measured with an ionization chamber in water.

Conclusion

3D dose distribution in the case of simple cube shape irradiation by ^{12}C to the uniform target was estimated for the validation of our method. The dose distribution estimated and measured is in good agreement in the distribution edge of deeper side. However, there was a discrepancy in shallower side edge because of the less prominent peak distribution of annihilation γ-rays.

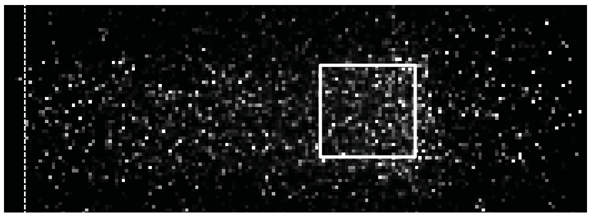

Figure 1 Annihilation γ-ray distribution measured with PET for cubic shape irradiation.

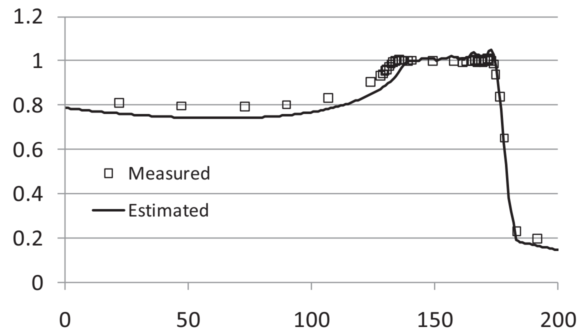

Figure 2 Depth-dose distribution at the center of irradiation field